ANTICANCER EFFICACY AND MOLECULAR THERAPEUTIC MECHANISM OF THYMOQUINONE-LOADED CALCIUM CARBONATE NANOPARTICLES COMBINED WITH 5-FLUOROURACIL AGAINST COLON CANCER

By

DENG XI

Thesis Submitted to the School of Graduate Studies, Universiti Putra Malaysia, in Fulfilment of the Requirements for the Degree of Doctor of Philosophy

December 2024

IB 2024 9

DEDICATION

This thesis is dedicated to:

Myself, who is about to turn thirty

Abstract of thesis presented to the Senate of Universiti Putra Malaysia in fulfilment of the requirement for the degree of Doctor of Philosophy

ANTICANCER EFFICACY AND MOLECULAR THERAPEUTIC MECHANISM OF THYMOQUINONE-LOADED CALCIUM CARBONATE NANOPARTICLES COMBINED WITH 5-FLUOROURACIL AGAINST COLON CANCER

By

DENG XI

December 2024

Chairman : Professor Md Zuki bin Abu Bakar @ Zakaria, PhD
Institute : Bioscience

Colon cancer ranks as the third most prevalent cancer worldwide, contributing to significant morbidity and mortality. The adverse side effects and chemoresistance associated with the primary chemotherapeutic agent, 5-fluorouracil (5-FU), have necessitated the exploration of improved therapeutic strategies. Thymoquinone (TQ) derived from *Nigella sativa*, a bioactive compound with established anti-colon cancer properties, presents a promising adjunct to 5-FU. The encapsulation of chemotherapeutic agents and phytochemicals into nano delivery systems represents a pivotal advancement, enhancing solubility and bioavailability and minimizing toxic side effects. This study aimed to develop cockle shell-derived calcium carbonate nanoparticles ($CaCO_3$np) as a delivery system for 5-FU and TQ and to evaluate the therapeutic potential of these formulations in combination therapies for colon cancer. Using a mechanical ball milling method, porous $CaCO_3$np was synthesized, and the formulations of 5-FU-loaded $CaCO_3$np (5FU-$CaCO_3$np) and TQ-loaded $CaCO_3$np

(TQ-$CaCO_3$np) were optimized by using a high-speed homogenizer for efficient loading of 5-FU and TQ. The resulting nanoparticles were characterized by their high purity, stable aragonite phase, and particle size ranging from 80 to 140 nm. The encapsulation process preserved the chemical integrity of both 5-FU and TQ, and the nanoparticles demonstrated pronounced biocompatibility and pH-sensitive sustained release profiles. *In vitro* studies revealed that TQ-$CaCO_3$np combined with 5-FU exhibited a superior synergistic effect compared to the reverse combination (5FU-$CaCO_3$np combined with TQ). This combination effectively inhibited CT26 colon cancer cell proliferation, induced apoptosis, caused G0/G1 cell cycle arrest, and suppressed the growth of CT26 spheroids. *In vivo* studies further validated the enhanced anticancer efficacy of the TQ-$CaCO_3$np and 5-FU combination in CT26 tumour-bearing mic, demonstrating significant tumour growth inhibition and reduced systemic toxicity of 5-FU. Proteomic and metabolomic analyses provided insights into the molecular mechanisms underlying the observed synergy, identifying the key pathways (biosynthesis of amino acids, 2-oxocarboxylic acid metabolism, and HIF-1 signalling pathway) and a series of key targets (Aco2, Gapdh, Psph, Pdha1, Pdhb, Rps6, alanine, glutamate, proline, glutamine, threonine, adenosine 5'-triphosphate, lactate, leucine, and isoleucine) modulated by the combination therapy. Overall, this study demonstrated that TQ-$CaCO_3$np, with its excellent biocompatibility, pH sensitivity, and sustained release properties, holds significant promise in enhancing the efficacy of 5-FU. These findings pave the way for further clinical applications, offering a novel and potentially effective approach to colon cancer treatment.

Keywords: Anticancer efficacy; Colon cancer; 5-Fluorouracil; Molecular therapeutic mechanism; Thymoquinone-loaded calcium carbonate nanoparticles

SDG: GOAL 3: Good Health and Well-being

Abstrak tesis yang dikemukakan kepada Senat Universiti Putra Malaysia
sebagai memenuhi keperluan untuk ijazah Doktor Falsafah

KEBERKESANAN ANTIKANSER DAN MEKANISME TERAPEUTIK MOLEKUL NANOPARTIKEL KALSIUM KARBONAT BERMUAT TIMOQUINON DIGABUNGKAN DENGAN 5-FLUOROURACIL TERHADAP KANSER KOLON

Oleh

DENG XI

Disember 2024

Pengerusi : Profesor Md Zuki bin Abu Bakar @ Zakaria, PhD
Institut : Biosains

Kanser kolon merupakan kanser ketiga paling lazim di dunia, menyumbang kepada morbiditi dan mortaliti yang signifikan. Kesan sampingan buruk dan kemoresistan yang berkaitan dengan agen kemoterapi utama, 5-fluorourasil (5-FU), telah mendorong eksplorasi strategi terapeutik yang lebih baik. Thymoquinone (TQ) yang berasal daripada *Nigella sativa* menunjukkan potensi sebagai tambahan kepada 5-FU. Pengkapsulan agen kemoterapi dan fitokimia ke dalam sistem penghantaran nano merupakan kemajuan penting, meningkatkan keterlarutan dan bioavailabiliti serta mengurangkan kesan sampingan toksik. Kajian ini bertujuan untuk membangunkan nanopartikel kalsium karbonat ($CaCO_3$np) sebagai sistem penghantaran untuk 5-FU dan TQ, serta menilai potensi terapeutik formulasi ini dalam terapi kombinasi untuk kanser kolon. Dengan menggunakan kaedah pengilangan mekanikal bola, $CaCO_3$np berliang telah disintesis, manakala formulasi $CaCO_3$np yang dimuatkan dengan 5-FU (5FU-$CaCO_3$np) dan TQ (TQ-$CaCO_3$np) dioptimumkan menggunakan penghomogen kelajuan tinggi untuk pemuatan 5-FU dan TQ yang efisien. Nanopartikel yang

dihasilkan dicirikan oleh tahap ketulenan yang tinggi, fasa aragonit yang stabil, dan saiz partikel dalam lingkungan 80 hingga 140 nm. Proses pengkapsulan ini mengekalkan integriti kimia 5-FU dan TQ, manakala nanopartikel menunjukkan biokeserasian yang baik dan profil pelepasan berterusan yang peka terhadap pH. Kajian *in vitro* mendedahkan bahawa TQ-$CaCO_3$np yang digabungkan dengan 5-FU menunjukkan kesan sinergistik yang lebih baik berbanding kombinasi terbalik (5FU-$CaCO_3$np digabungkan dengan TQ). Kombinasi ini berkesan menghalang proliferasi sel kanser kolon CT26, mendorong apoptosis, menyebabkan perencatan kitaran sel pada fasa G0/G1, dan menekan pertumbuhan sferoid CT26. Kajian *in vivo* turut mengesahkan keberkesanan antikanser yang dipertingkatkan oleh kombinasi TQ-$CaCO_3$np dan 5-FU pada tikus yang membawa tumor CT26, dengan menunjukkan pengurangan ketara dalam pertumbuhan tumor dan ketoksikan sistemik 5-FU. Analisis proteomik dan metabolomik memberikan gambaran tentang mekanisme molekul, dengan mengenal pasti laluan utama (biosintesis asid amino, metabolisme asid 2-oksokarboksilik, dan laluan isyarat HIF-1) serta beberapa sasaran utama (Aco2, Gapdh, Psph, Pdha1, Pdhb, Rps6, alanin, glutamat, prolin, glutamin, treonin, adenosina 5'-trifosfat, laktat, leusin, dan isoleusin) yang dimodulasi oleh terapi kombinasi tersebut. Secara keseluruhannya, kajian ini menunjukkan bahawa TQ-$CaCO_3$np, dengan biokeserasian yang cemerlang, sensitiviti terhadap pH, dan sifat pelepasan berterusan, mempunyai potensi besar untuk meningkatkan keberkesanan 5-FU. Penemuan ini membuka jalan untuk aplikasi klinikal selanjutnya, menawarkan pendekatan baharu dan berpotensi berkesan untuk rawatan kanser kolon.

Kata kunci: Keberkesanan antikanser; Kanser kolon; 5-Fluorourasil; Mekanisme terapeutik molekul; Nanopartikel kalsium karbonat bermuatan thymoquinone

SDG: MATLAMAT 3: Kesihatan dan Kesejahteraan yang Baik

ACKNOWLEDGEMENTS

As my PhD journey comes to an end, my heart is filled with immense gratitude. Looking back on this long and fulfilling journey of pursuing a PhD, every step has been supported by the care and help of many people. Without their support and encouragement, I would not have been able to complete this academic journey successfully.

First and foremost, I would like to extend my highest respect and sincerest thanks to my supervisor, Professor Dr. Md Zuki bin Abu Bakar. At every stage, he provided meticulous guidance and selfless assistance. Whenever I encountered difficulties and challenges, he was always patient, listened attentively, and provided detailed analysis. His teachings not only benefited me greatly in academics but also set an example for me in how to conduct myself in life.

Secondly, I would like to thank my co-supervisors Professor Dr. Norhaizan binti Mohd Esa, Associate Professor Dr. Ahmad Faizal bin Abdull Razis, Dr. Norsharina binti Ismail, and Dr. Chan Kim Wei for their help with the smooth completion of my PhD. I would also like to thank Associate Professor Dr. Chia Suet Lin for his great help and encouragement during my doctoral studies. Further gratitude I would like to extend is towards Mr. Salman and Ms. Najwa, who helped me during my time at the NaturMeds laboratory.

Additionally, I would like to extend thanks to my friends Zhongming Yang, Zanna, and Tahil. I appreciate the companionship, support, and encouragement they provided throughout my PhD journey.

I also want to thank my parents. Their selfless love and dedication have provided me with a solid foundation. As I pursued my academic dreams, they always gave me the greatest understanding, encouragement, and support. They provided enough financial support to cover all my expenses abroad. Without them, I would not have been able to successfully complete my studies.

Finally, I want to thank myself. I am grateful for the countless days and nights of silent effort, for not easily giving up when faced with difficulties, and for having the courage to explore the unknown and challenge myself. It is this persistence and effort that have allowed me to reach this point and complete my PhD journey. I believe that in the days ahead, I will continue to uphold this spirit, moving forward and creating more possibilities on the academic path.

This thesis was submitted to the Senate of Universiti Putra Malaysia and has been accepted as fulfilment of the requirement for the degree of Doctor of Philosophy. The members of the Supervisory Committee were as follows:

Md Zuki bin Abu Bakar @ Zakaria, PhD
Professor
Faculty of Veterinary Medicine
Universiti Putra Malaysia
(Chairman)

Norhaizan binti Mohd Esa, PhD
Professor
Faculty of Medicine and Health Sciences
Universiti Putra Malaysia
(Member)

Ahmad Faizal bin Abdull Razis, PhD
Associate Professor
Faculty of Food Science and Technology
Universiti Putra Malaysia
(Member)

Norsharina binti Ismail, PhD
Senior Research Officer
Institute of Bioscience
Universiti Putra Malaysia
(Member)

Chan Kim Wei, PhD
Senior Research Officer
Institute of Bioscience
Universiti Putra Malaysia
(Member)

ZALILAH MOHD SHARIFF, PhD
Professor and Dean
School of Graduate Studies
Universiti Putra Malaysia

Date: 13 March 2025

TABLE OF CONTENTS

LIST OF TABLES

LIST OF FIGURES

LIST OF ABBREVIATIONS

5-FU	5-fluorouracil
5FU-$CaCO_3$np	5-fluorouracil-loaded calcium carbonate nanoparticles
5-FU/LV	5-fluorouracil and leucovorin
Ace	acetate
ACF	aberrant crypts foci
Ala	alanine
ALP	alanine phosphatase
ALT	alanine aminotransferase
AO	acridine orange
APC	adenomatous polyposis coli
AST	aspartate aminotransferase
ATP	adenosine 5'-triphosphate
Bcl-2	B-cell lymphoma 2
$CaCO_3$	calcium carbonate
$CaCO_3$np	cockle shell-derived calcium carbonate nanoparticles
CI	combination index
c-MYC	cellular Myc
COX-2	cyclooxygenase 2
Cr	creatine
ddH_2O	deionized water
DMSO	dimethylsulfoxide
DOX	doxorubicin
EDX	energy dispersion X-ray
EE	encapsulation efficiency
EGFR	epidermal growth factor receptor
Elisa	enzyme-linked immunosorbent assay
EMT	epithelial-mesenchymal transition
EP	prostaglandin E2 receptor
FDA	U.S. Food and Drug Administration

FESEM	field emission scanning electron microscopy
FOLFIRI	irinotecan, 5-fluorouracil, and leucovorin
FOLFOX	oxaliplatin, 5-fluorouracil, and leucovorin
FOLFOXIRI	irinotecan, oxaliplatin, 5-fluorouracil, and leucovorin
For	formate
FTIR	Fourier transform infrared spectroscopy
G	glycerol
Gln	glutamine
Glu	glutamate
Gly	glycine
GO	Gene Ontology
GSH	glutathione
H&E	hematoxylin and eosin
HRTEM	high-resolution transmission electron microscopy
IC_{50}	half maximal inhibitory concentration
ICAM-1	intercellular adhesion molecule 1
Ile	isoleucine
ILs	interleukins
iNOS	inducible nitric oxide synthase
JAK2	Janus kinase 2
KEGG	Kyoto Encyclopedia of Genes and Genomes
Kras/Braf/MEK/MAPK	Kirsten rat sarcoma virus/B-raf/mitogen-activated protein kinase kinase/mitogen-activated protein kinase
Lac	lactate
Leu	leucine
LC	loading content
LC_{50}	lethal concentration 50
Mal	malate
MMPs	matrix metallopeptidases
MTT	3-(4,5-dimethylthiazol-2-yl)-2,5-diphenyltetrazolium bromide)
Myo	myo-inositol
NAG	N-acetyl glycoprotein
NF-κB	nuclear factor-κB
OPLS-DA	orthogonal partial least squares discriminant analysis

PBS	phosphate buffered saline
PC	phosphocholine
PCr	phosphocreatine
PGE2	prostaglandin E2
PI	propidium iodide
PI3K	phosphatidylinositol-3-kinase
PPAR-γ	peroxisome proliferator-activated receptor-γ
Pro	proline
ROS	reactive oxygen species
Ser	serine
Suc	succinate
Tau	taurine
TGF-β	transforming growth factor β
Thr	threonine
TNF-α	tumor necrosis factor-α
TQ	thymoquinone
TQ-$CaCO_3$np	thymoquinone-loaded cockle shell-derived calcium carbonate nanoparticles
UDP-GlcA	UDP-glucuronate
Uk	unknown
UV-Vis	ultraviolet-visible
VEGF	vascular endothelial growth factor
W/O	water-in-oil
XELOX	capecitabine and oxaliplatin
XRD	X-ray diffraction

CHAPTER 1

INTRODUCTION

1.1 Background and problem statement

According to the latest global cancer statistics in the *GLOBOCAN* database, colon cancer remains one of the major causes of morbidity and mortality worldwide, which is largely attributed to a relatively higher intake of animal-source foods and an increasingly sedentary lifestyle (Bray et al. 2024). Given a constant incidence rate, the expanding and aging population will lead to a significant rise in cases of colon cancer, imposing a substantial burden on society. 5-Fluorouracil (5-FU) is one of the commonly used chemotherapy drugs in the treatment of colon cancer. As an anti-metabolite drug, 5-FU can inhibit thymidylate synthase and incorporate its metabolites into RNA and DNA against colon cancer (Deng et al. 2024). However, insufficient accumulation of 5-FU in tumors due to non-specificity and a low plasma half-life, as well as limited response rates (10–15%), results in high-dosage uses of 5-FU, thereby leading to severe toxic side effects such as nausea, diarrhea, fever, myocardial ischemia, and neutropenia (Christensen et al. 2019; Vodenkova et al. 2020). Therefore, there is an urgent need to explore new approach to enhance the anti-colon cancer of 5-FU while reducing its toxic side effects, thereby improving the life quality of patients.

Nanotechnology advancements have made nanoparticle-based drug delivery systems a promising candidate for cancer treatment. The ideal anti-cancer drug delivery system should have the ability of favorable sustained release and pronounced biocompatibility with simple and economical synthesis methods (Senapati et al. 2018; Shi et al. 2017).

Thus, it can deliver the drugs to target sites to enhance the anti-cancer efficacy of drugs and reduce their side effects, with no or low toxicity to normal tissues and cells. Calcium carbonate nanoparticles have been widely studied as nanocarriers of drugs against cancer due to their excellent biocompatibility, pH responsiveness, and biodegradability. Calcium carbonate has been approved for clinical use by the U.S. Food and Drug Administration (FDA). Additionally, calcium carbonate nanoparticles showed safety on the normal breast cell line MCF10A, fibroblasts NIH3T3, normal tissues in C57BL/6 mice as well as hematological and biochemical levels in Kunming mice, and satisfactory blood compatibility (Bastos et al. 2023; Yakubova et al. 2023; Yu et al. 2023; Zhou et al. 2023). Moreover, calcium carbonate nanoparticles exhibited remarkable pH-controlled drug release, with lower release at pH 7.4 in the blood and healthy tissue environment but more rapid release in the acidic tumor environment (Huang et al. 2020a; Ibiyeye, Idris & Zuki 2020; Xu et al. 2023a; Yang et al. 2016; Zhao et al. 2023). Meanwhile, calcium carbonate nanoparticles can decompose into Ca^{2+} and CO_2 under acidic conditions, facilitating tumor-targeted delivery (Dong et al. 2020). Cockle shells, abundant in coastal areas, are a natural source of calcium carbonate that is low-cost and easily available. Besides, cockle shells consist of good-quality calcium carbonate in aragonite polymorph form, of which aragonite is a stable phase of calcium carbonate (Chemmalar et al. 2021; Isa et al. 2016). Furthermore, compared with down-top methods such as precipitation, emulsion, and polymerization, mechanical ball milling (top-down approach) can synthesize large-scale cockle shell-derived calcium carbonate nanoparticles ($CaCO_3$np) by a simple operation while maintaining their unique features (Islam et al. 2013).

Natural compound thymoquinone (TQ), primary active ingredient of natural product *Nigella sativa* seeds, exhibited chemopreventive or chemotherapeutic effects on colon

cancer and other cancers through modulating reactive oxygen species production and cellular proliferation, autophagy, apoptosis, invasion, as well as metastasis (Homayoonfal, Asemi & Yousefi 2022; Jrah-Harzallah et al. 2013; Zhu et al. 2016b). Nevertheless, the high hydrophobic property of TQ contributes to its poor solubility and low bioavailability, leading to limited therapeutic effects (Alkharfy et al. 2015; Salmani et al. 2014). To improve the anticancer efficacy of 5-FU and TQ while reducing toxic side effects, various kinds of nanocarriers have been applied to deliver them to target cancerous cells. For example, 5-FU-loaded lactoferrin nanoparticles were synthesized for malignant melanoma, whereas 5-FU was loaded into the mesoporous silica-based hybrid nanoparticles to enhance efficacy against colon cancer (Kumari & Kondapi 2017; Pan et al. 2017). As for TQ, PEGylated-TQ nanoparticles and TQ-loaded poly lactic-co-glycolic acid nanoparticles were prepared for breast cancer and malignant melanoma, respectively (Bhattacharya et al. 2015; Ibrahim, Rosli & Doolaanea 2020). However, 5-FU or TQ-loaded calcium carbonate nanoparticles have been relatively less explored, although calcium carbonate nanocarrier-based nanomedicines and loading 5-FU or TQ into different nanocarriers have been extensively studied.

Moreover, combining chemotherapeutic drugs and natural compounds has become a novel multi-targeted approach to cancer treatment, enhancing the effectiveness of chemotherapy drugs and mitigating their toxic side effects (Rejhová et al. 2018). TQ and 5-FU have shown promising anticancer properties in the treatment of triple-negative breast cancer and gastric cancer (Lei et al. 2012; Zheng et al. 2021). Importantly, Kensara et al. (2016b) demonstrated that 5-FU combined with TQ was more effective than the individual agents in colorectal cancer rats, with a synergistic

effect twice that of the individual therapies. However, no literature has investigated the combinatorial use of 5-FU-loaded nanoparticles and TQ and the combinatorial use of TQ-loaded nanoparticles and 5-FU for colon cancer treatment. Furthermore, the underlying mechanisms of TQ in combination with 5-FU against colon cancer have not been comprehensively investigated.

Hence, this study begins with synthesizing the optimal 5-FU-loaded $CaCO_3$np (5FU-$CaCO_3$np) and TQ-loaded $CaCO_3$np (TQ-$CaCO_3$np) and evaluates the synergistic effects of 5FU-$CaCO_3$np in combination with TQ and TQ-$CaCO_3$np in combination with 5-FU, followed by analysing the anti-colon cancer efficacy of the combination with superior synergism and elucidating its molecular therapeutic mechanism. The *in vitro* anti-colon cancer effect was proven on the Murine colon cancer CT26 cell line, while the *in vivo* anti-colon cancer efficacy was evaluated in CT26 tumour-bearing BALB/c mice. Furthermore, label-free proteomics and NMR-based metabolomics were performed to elucidate the therapeutic mechanism of the combination therapy against colon cancer.

1.2 Hypotheses

- The combination of 5FU-$CaCO_3$np and TQ and the combination of TQ-$CaCO_3$np and 5-FU enhance the anticancer effects of the individual treatments against colon cancer *in vitro* and *in vivo*.
- The targeted nano system demonstrates improved specificity for colon cancer cells, thereby reducing the cytotoxicity of 5-FU and TQ on normal cells.

1.3 Objectives

1.3.1 Main objective

The main objective of this study is to evaluate the synergistic effects of 5FU-$CaCO_3$np in combination with TQ and TQ-$CaCO_3$np in combination with 5-FU against colon cancer and elucidate the molecular therapeutic mechanism of the combination with superior synergism.

1.3.2 Specific objectives

- To prepare $CaCO_3$np, 5FU-$CaCO_3$np, and TQ-$CaCO_3$np and characterize their physicochemical properties and biocompatibility.
- To compare the synergistic effect of 5FU-$CaCO_3$np in combination with TQ and TQ-$CaCO_3$np in combination with 5-FU and evaluate the efficacy of the combination with superior synergism against colon cancer CT26 cells.
- To determine the anti-tumor efficacy of the combination with superior synergism in CT26 tumor-bearing BALB/c mice.
- To elucidate the molecular therapeutic mechanism of combination therapy in colon cancer by integrating proteomic and metabolomic analyses.

CHAPTER 2

LITERATURE REVIEW

2.1 Epidemiology of colon cancer

Based on the *GLOBOCAN* database (World Health Organization 2024), there were 1.1 million new colon cancer cases and 538,167 deaths in 2022, accounting for around one-sixth of the total cancer cases and deaths in the world. As a whole, colon cancer ranked fourth in incidence rate and fifth in terms of mortality among various cancers, as shown in Figure 2.1.

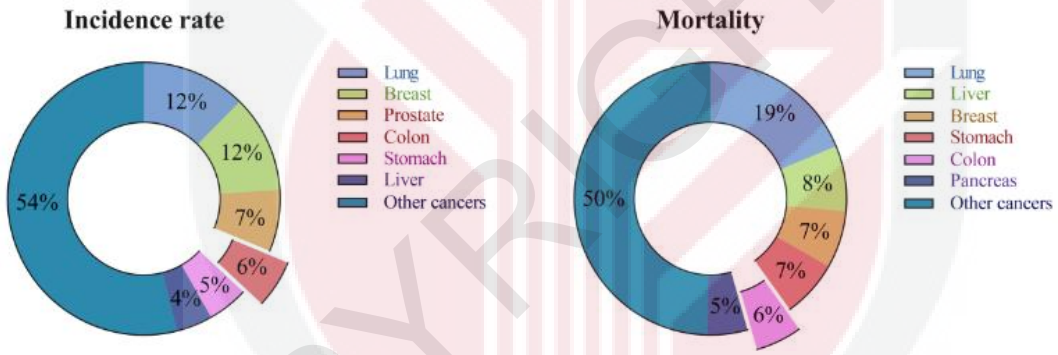

Figure 2.1: Incidence rate and mortality for top 6 cancers in 2022 worldwide (World Health Organization 2024).

In 2022, Asia and Europe were the regions with the highest number of new cases and deaths, relative to Africa, Oceania, Northern America, Latin America, and the Caribbean, probably due to the disparities in lifestyle and diet program (Figure 2.2) (Bray et al. 2024). A relatively high intake of animal-based foods, an increasingly sedentary lifestyle, alcohol consumption, smoking, the consumption of red or processed meats, and obesity increase the overall risk of developing colon cancer (Deng et al., 2024). In addition, the new cases and deaths of colon cancer among males are higher than among females (Figure 2.2). In 2022, 609,228 and 533,058 males and

females were diagnosed with colon cancer, respectively, while the deaths of colon cancer among males and females worldwide were 283,784 and 254,383, respectively (World Health Organization 2024). Moreover, colon cancer occurred predominantly in individuals between 45 and 84 years old, with 419,935 mortalities reported worldwide (Figure 2.2) (World Health Organization 2024). Furthermore, due to population growth and aging, the incidence rate and mortality of colon cancer are likely to increase over the next few decades (Bray et al. 2024). Overall, colon cancer poses a major challenge to public health. Preventive and therapeutic measures should be taken to control this dreadful disease.

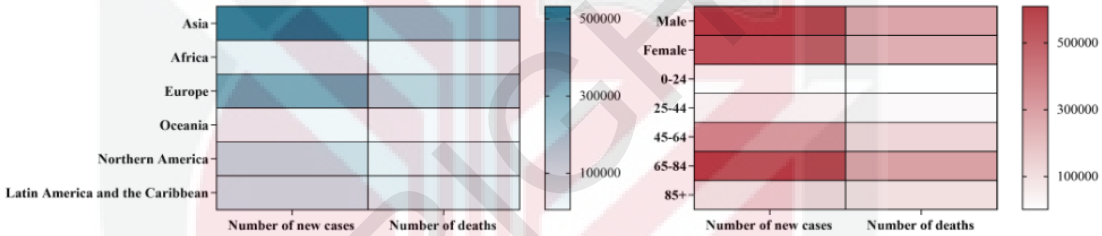

Figure 2.2: Number of new cases and deaths by regions, sex, and ages for colon cancer in 2022 (World Health Organization 2024).

2.2 Pathophysiology of colon cancer

Colon cancer is one of the common malignant tumors in the digestive tract. In our body, the digestive tract starts from the mouth and ends in the large intestine. The large intestine consists of cecum, colon, rectum, and anal canal (Bhaskaran & Kumar 2021). The colon is further divided into four parts, including ascending colon, descending colon, transverse colon and sigmoid colon (Tiwari et al. 2020). Moreover, each segment is composed of serosa, muscularis externa, submucosa, and mucosa (Hani et al. 2021), which is shown in Figure 2.3. Colon cancer generally refers to the malignant

lesions of the colon mucosal epithelium under the action of various carcinogenic factors such as environment or genetics (O'Keefe 2016).

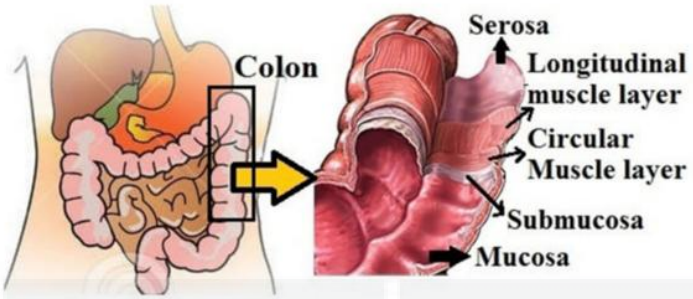

Figure 2.3: Anatomy of the colon (Hani et al. 2021).

2.2.1 Histopathology of colon cancer

Based on the histopathological features, colon cancer can be classified into four different stages, from Stage 0 to Stage IV (Figure 2.4). In the initial stage, polyps form and develop in the mucosal lining of the colon (Bhaskaran & Kumar 2021). Stage I implies that the polyps have converted into tumors and invaded the inner lining of the colon (Tiwari et al. 2020). In this stage, surgery is the main treatment, and the survival rate can reach 95%. The second stage is characterized by cancer that has spread beyond the colon but has not metastasized to the lymph nodes (Wahab et al. 2021). Resection surgery is the only choice for the treatment of colon cancer at this stage, and the survival rate is 85%. In the third stage, the cancer cells have spread to the entire colon wall and the surrounding lymph nodes (Gulbake et al. 2016). In addition to surgery, chemotherapy and other drugs are needed in this stage, and the survival rate is 30-60%. Stage IV means the cancer has spread to the other organs of the body, such as the intestine, lungs, and liver (Wahab et al. 2021). In this stage of colon cancer, the survival rate is only 3% (Mishra & Chaurasia 2017).

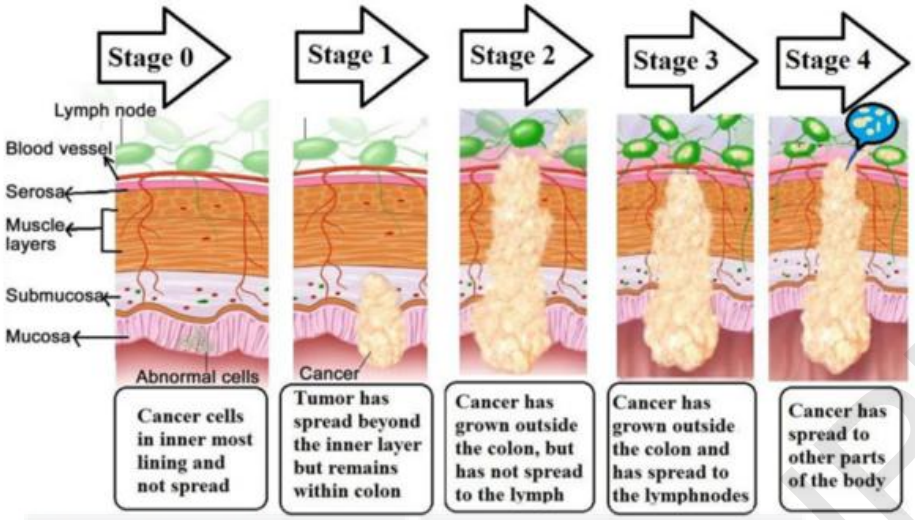

Figure 2.4: Different stages of colon cancer (Hani et al. 2021)**.**

2.2.2 Pathogenesis of colon cancer

Colon cancer refers to the malignant lesions of the colon mucosal epithelium under the actions of various carcinogenic factors. Approximately 70% of colon cancer cases are sporadic, influenced by dietary and environmental factors, such as obesity, sedentary lifestyle, low fiber-high fat diet, alcohol abuse, and cigarette smoking (Afrin et al. 2020; O'Keefe 2016). Colon cancer cases attributed to family history are approximately 25%, while inherited cases account for the remaining 5% (Lynch syndrome or hereditary non-polyposis colon cancer, serrated polyposis syndrome, familial adenomatous polyposis, MUTYH-associated polyposis, and hamartomatous polyposis) (Bogaert & Prenen 2014; Mao et al. 2021). In addition, inflammatory bowel diseases, such as ulcerative colitis and Crohn's disease are also risk factors for colon cancer (Piotrowska et al. 2021). In 1990, Fearon and Vogelstein proposed the hypothesis of the adenoma-carcinoma sequence in colon cancer pathogenesis, which is still applicable to date for the majority of colon cancer cases. According to their model, colon cancer formation begins with the transformation from normal epithelium to benign adenoma, and due to

the continuous accumulation of genetic and epigenetic alterations, the adenoma transforms into adenocarcinoma, finally resulting in metastasis of malignant tumors (Fearon & Vogelstein 1990).

The capabilities of colon cancer cells to survive, grow, and disseminate are underpinned by chronic inflammation and genomic instability. Genetic factors and chronic inflammation possibly induced by dietary and environmental factors play inseparable roles in the initial phase of colon cancer progression (Figure 2.5). During the process, nuclear factor-κB (NF-κB) is activated and results in regulation of a series of pro-inflammatory mediators and cytokines, including inducible nitric oxide synthase (iNOS), cyclooxygenase 2 (COX-2), prostaglandin E2 (PGE2), tumor necrosis factor-α (TNF-α), and interleukins (ILs) (Guo et al. 2024). In the transformation from normal epithelium to early adenoma or aberrant crypts foci (ACF), adenomatous polyposis coli (APC) mutation is the first step, which will promote the dysregulation of β-catenin, thereby activating the Wnt pathway (Testa et al. 2018). Subsequently, activation of the Wnt pathway stimulates the transcription of downstream genes, such as the cyclin D1 gene and cellular Myc (c-MYC) proto-oncogen, leading to cancer cell proliferation (Jha et al. 2023; Zhan et al. 2017). The activation of the epidermal growth factor receptor (EGFR) pathway plays a vital role in colon cancer development from early adenoma or ACF to intermediate adenoma. It is not only results in the activation of Kirsten rat sarcoma virus/B-raf/mitogen-activated protein kinase kinase/mitogen-activated protein kinase (Kras/Braf/MEK/MAPK) pathway but also leads to the activation of phosphatidylinositol-3-kinase/Akt (PI3K/Akt) pathway, thereby suppressing cell apoptosis and inducing cell survival and proliferation (Tang et al. 2024).

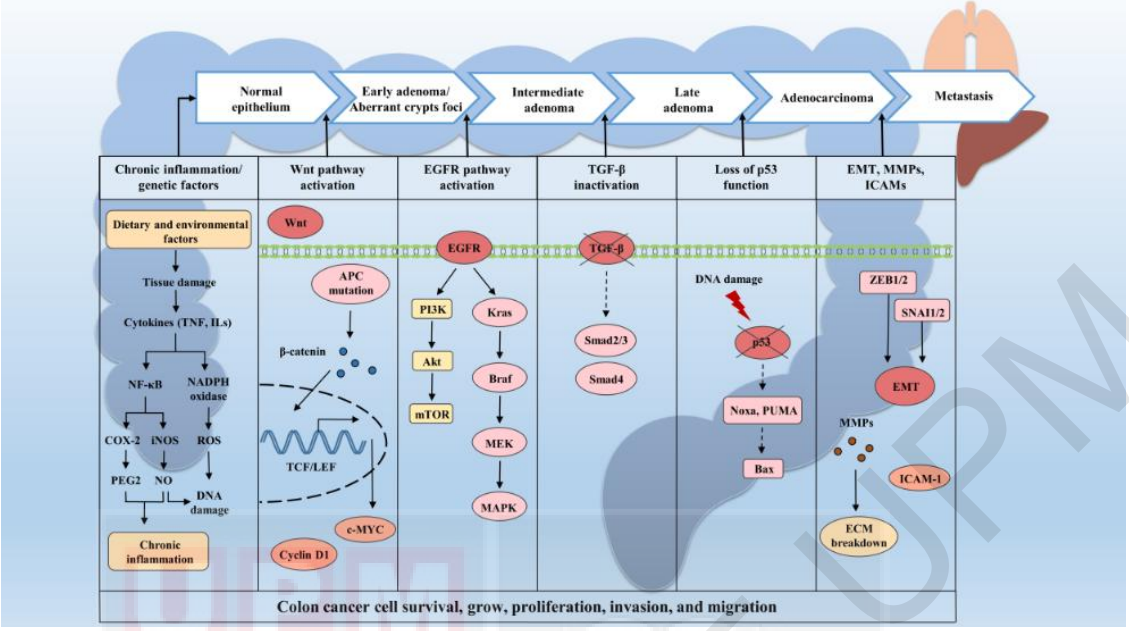

Figure 2.5: Signaling pathways in stages of colon cancer pathogenesis (Deng et al., 2024).

Inactivation of transforming growth factor β (TGF-β), a tumor suppressor, leads to the transformation of intermediate adenoma to late adenoma (Koveitypour et al. 2019). TGF-β bound to specific TGF-β receptors will trigger the suppressor of mothers against decapentaplegic (Smad) signaling pathway, resulting in transcriptions of active target genes, reduction of cell proliferation, and induction of cell apoptosis (Farooqi et al. 2019; Jung, Staudacher & Beauchamp 2017). p53 is a well-known tumor suppressor that repairs DNA damage and induces cell apoptosis (Abuetabh et al. 2022). The loss of p53 causes an uncontrolled cell cycle and cell proliferation, leading to the progression of late adenoma to adenocarcinoma/malignant tumor (Malki et al. 2020). The final stage of colon cancer is represented by the adenocarcinoma metastasis to other parts of the body, such as the liver and lung, via epithelial-mesenchymal transition (EMT) which is a dedifferentiation program, making polarized and stationary epithelial cells biochemically change to induce cell migration and invasion (Alam, Almoyad & Huq 2018). In addition, the expression of matrix metallopeptidases

(MMPs) and intercellular adhesion molecule 1 (ICAM-1) is also related to colon cancer metastasis (Maeda et al. 2002; Said, Raufman & Xie 2014).

2.3 Chemotherapies for colon cancer treatment

Based on the stages of colon cancer and the characteristics of patients, standard and conventional treatment of colon cancer mainly consists of surgery, radiation, and chemotherapy (Brouwer et al. 2018). However, there are some risks of surgery, such as serious blood loss, infection, and severe tissue damage caused by colectomy, resulting in anastomotic leakage (Chiu et al. 2019; Kirchhoff, Clavien & Hahnloser 2010). Moreover, there is a high risk of fecal and urinary incontinence after radiation treatment (Miguel et al. 2020; Pan et al. 2018). Consequently, chemotherapy plays a vital role in the treatment of colon cancer. According to the National Cancer Institute (2020), 5 chemotherapeutic drugs have been approved by the FDA for the treatment of colon cancer, i.e., 3 intravenous drugs (irinotecan hydrochloride, oxaliplatin, and 5-fluorouracil) and 2 oral drugs (capecitabine, and combination of trifluridine and tipiracil hydrochloride). 5-Fluorouracil has been the mainstay against colon cancer for many years (He et al. 2019).

2.3.1 5-Fluorouracil

5-FU was synthesized and patented in the 1950s. At that time, experiments showed that it was possible to specifically target the intracellular uracil metabolic pathway (Grivicich et al. 2001). Since 1957, it has been the key to the treatment of colorectal cancer, gastric cancer, and breast cancer (Vodenkova et al. 2020). 5-FU is a heterocyclic aromatic organic compound. It is an analog of uracil because its structure is similar to that of DNA and RNA, except that there is a fluorine atom at the C-5

position instead of hydrogen (Arthur-Baidoo et al. 2022). Because of this structure, 5-FU can interfere with nucleoside metabolism and incorporate DNA and RNA, resulting in cytotoxicity and cell death (Arthur-Baidoo et al. 2022; Sethy & Kundu 2021). 5-FU can also act as an inhibitor of TS, leading to thymine-less cell death (Vodenkova et al. 2020). These are the two main antitumor mechanisms of 5-FU.

However, 5-FU also has many disadvantages, such as nonspecific targeting, poor solubility, reduced permeability, dose-dependent toxicity on normal tissues, and minimal tumor accumulation, which greatly limits its clinical application (Wahab et al. 2021). The most common toxic effects of 5-FU are mucositis, diarrhea, myelosuppression, and peripheral venous thrombophlebitis (Vodenkova et al. 2020). Although the frequency of various cardiotoxicity of 5-FU is low, it is usually more serious (Yuan et al. 2019). As a single agent against colon cancer, 5-FU has an overall response rate of only 10%-15% (Wathoni et al. 2020). Therefore, researchers moved forward and found a better therapy for the treatment of colon cancer, which is combination of the chemotherapeutic drugs.

2.3.2 Combination of chemotherapeutic drugs

The combination of chemotherapeutic drugs is the administration of two or more drugs, which is used to increase antitumor efficacy (Wathoni et al. 2020). The early standard combination chemotherapy regimen is the combination of 5-FU and leucovorin (5-FU/LV), which is mainly used in Stage II and Stage III of colon cancer, since leucovorin can stabilize FDUMP and thymidylate synthase complex, thereby enhancing the cytotoxicity of 5-FU (Kotelevets et al. 2016). Afterward, studies have proved that the survival of Stage III patients can be improved after the addition of

oxaliplatin to 5-FU/LV (FOLFOX) compared with 5-FU/LV (Meyers et al. 2017). Capecitabine, an oral prodrug of 5-FU, is also used to combine with oxaliplatin (XELOX). It has been reported that XELOX has similar efficacy and safety to FOLFOX and can be used as an alternative to FOLFOX (Brandi et al. 2016). In addition, irinotecan combined with 5-FU/LV (FOLFIRI) or FOLFOX (FOLFOXIRI) is more used for metastatic colon cancer due to a better response rate and progression-free survival compared with monotherapy (Duarte & Vale 2022b; Kotelevets et al. 2016).

2.3.3 Limitations of chemotherapies against colon cancer

Chemotherapeutic drugs mainly act on active cells which grow and divide faster than other cells. However, due to this, while chemotherapeutic drugs act on cancer cells, some active healthy cells such as the gastrointestinal tract and hair follicle cells are also affected (Aiello et al. 2019). Therefore, chemotherapeutic drugs will produce some side effects, including fatigue, stomach pain, nervous system injury, and so on. Although many studies have supported the efficacy of combination agents by showing the improvement of overall survival of patients after the treatment, combination chemotherapy regimens still have some toxic side effects and the emergence of drug-resistant tumor cells reduces the efficacy of chemotherapy (Lee et al. 2018).

2.4 Phytochemicals for colon cancer treatment

Due to the drug resistance and toxic side effects of common chemotherapeutic drugs, researchers have begun to study phytochemicals for the treatment of colon cancer, which have the advantages of safety and more affordable (Weng & Goel 2022). In reality, phytochemicals have been studied and used as medicines to treat a variety of

diseases for many years, especially for the treatment of cancer. Some anticancer compounds extracted from plants have been well studied and applied owing to their strong anti-inflammatory and antioxidant activities since phytochemicals with a high content of antioxidants can activate different survival pathways and protect normal cells from the negative effects of anticancer therapy (Henamayee et al. 2020). Hence, phytochemicals play a significant role in the treatment of colon cancer. One of the popular phytochemicals or potential agents for the treatment of colon cancer is thymoquinone.

2.4.1 Thymoquinone

TQ (2-methyl-5-isopropyl-1, 4-benzoquinone, Figure 2.6) is a phytochemical compound isolated from black cumin (*Nigella sativa*), widely used as a condiment in many countries (Abbas et al. 2024). In traditional medicine, TQ was used as an antitumor, antioxidant, analgesic, and anti-inflammatory agent (Almajali et al. 2021).

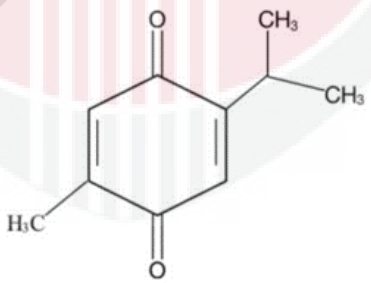

Figure 2.6: Structural formula of thymoquinone (TQ).

Since the study report in 2003 noted that TQ induced apoptosis of cancer cells, TQ has attracted more attention in cancer treatment (Zhang, Bai & Yang 2016a). Reports point that TQ can be used to treat various cancers, such as breast, liver, colon, and brain

cancers (Abbas et al. 2024; Chen et al. 2017). TQ plays an antitumor role through various mechanisms, particularly by showing the selective regulation of active species and free radical agents, interfering with DNA, immunomodulation, and regulating a variety of potential targets and their signaling pathways (Khan et al. 2017; Taha et al. 2016). The potential targets include NF-κB, peroxisome proliferator-activated receptor-γ (PPAR-γ), p53, p73, and reactive oxygen species (ROS) (Phua et al. 2021).

In the treatment of colon cancer, TQ can block signal transducer and activator of transcription 3 (STAT3) signal by inhibiting Janus kinase 2 (JAK2)- and Src-mediated epidermal growth factor receptor (EGFR) tyrosine kinase phosphorylation, thereby inducing apoptosis in HCT116 colon cancer cells (Abbas et al. 2024). In addition, Zhang et al. (2016a) found that 20, 40, and 60 μM of TQ could reduce the phosphorylation level of p65 in the nucleus and reduce the expression levels of c-MYC, B-cell lymphoma 2 (Bcl-2), and vascular endothelial growth factor (VEGF) in COLO205 and HCT116 cells, which indicated TQ could inhibit NF-κB activation. Moreover, 20 μM of TQ can suppress the proliferation and migration of LoVo human colon cancer cells by inhibiting p-PI3K, p-Akt, p-GSK3β, β-catenin, and COX-2 expression, which can reduce the level of PGE2 and the activation of prostaglandin E2 receptor (EP)2 and EP4 (Hsu et al. 2017). In general, TQ is a promising natural product-based drug against colon cancer.

2.4.2 Combination of phytochemicals with chemotherapeutic drugs

The combination of chemotherapeutic drugs and phytochemicals has become one of the new approaches to treat cancer. It has been reported that sulforaphane can improve the anticancer activity of 5-FU which is the most effective agent in the HT-29 colon

cancer cell line, and the combination of sulforaphane and 5-FU can induce HT-29 colon cell death through receptor-mediated apoptosis (Milczarek et al. 2018). Kensara et al. (2016a) note that 5-FU combined with TQ is more effective than treatment with individual agents, and its synergistic effect is twice that of alone treatments. Furthermore, another phytochemical, resveratrol, can make HT-29 and SW620 colon cell lines sensitive to cytotoxic oxidative stress induced by 5-FU by suppressing their endogenous antioxidant capacity (Santandreu et al. 2011). Another study suggested that the combination of 15 μM of resveratrol and 0.5 μM of 5-FU significantly could inhibit cell proliferation, migration, and S-phase cell cycle arrest, resulting in HCT-116 cell apoptosis (Redondo-Blanco et al. 2017).

2.4.3 Limitations of phytochemicals against colon cancer

Compared with conventional chemotherapeutic drugs, phytochemicals are more easily available and cost-effective with fewer side effects. However, several obstacles to the clinical use of phytochemicals as therapeutic agents for colon cancer need to be considered, including poor water solubility and poor ability to absorb or convert into conjugates (Rejhová et al. 2018). Thus, to improve bioavailability of phytochemicals, nanocarriers have been used (Butt, Nisar & Mughal 2018; Rathore et al. 2020).

2.5 Nanotechnology-based novel drug delivery systems

Nanotechnology is a rapidly emerging technology, which plays a vital role in medicine, particularly in drug delivery targeting pathological sites (Pavitra et al. 2021). Nanoparticles are a class of material in nanotechnology, which contain substances with a particle size of approximately 10-200 nm (Sahu et al. 2021). Nanoparticles consist

of the surface layer, shell layer, and the core. The surface layer can be functionalized by various small molecules, metal ions, surfactants, and polymers (Heinz et al. 2017; Naeem et al. 2020). Unlike the core, the shell layer is a chemically diverse material, and the core is the central part of nanoparticles, which is normally called nanoparticles themselves (Heinz et al. 2017).

The use of nanoparticles to treat cancer is part of novel drug delivery systems (Wahab et al. 2021). Novel drug delivery systems can deliver anticancer drugs to tumor sites through passive or active targeting strategies, thereby improving drug efficacy and reducing adverse reactions due to the unique physicochemical and pharmacokinetic properties of nanoparticles (Banerjee et al. 2017). In passive targeting, nanocarriers exploit the physiopathologic characteristics of tumors, such as the tumor vascular system, to passively localize their loaded anticancer drugs in tumor tissues (Khan et al. 2018). The tumor vasculature becomes highly defective with poor lymphatic drainage, resulting in the enhanced permeation and retention effect (Bahrami et al. 2017). By enabling nanocarriers to circulate for extended periods and repeatedly pass through the tumor microenvironment, the anticancer activity of drug-loaded nanocarriers is increased (Jin et al. 2020). Active targeting aims to overcome the non-selectivity limitation of passive targeting by modifying the surface of the nanocarrier with targeting moieties that recognize specific receptors or antigens associated with tumors (Bahrami et al. 2017). Consequently, active targeting allows drugs to be selectively delivered to the site of action, reducing drug uptake by normal cells and tissues (Rosenblum et al. 2018).

In addition, based on the chemical properties, nanoparticles can be classified into organic, inorganic and carbon-based nanoparticles (Sahu et al. 2021). Amongst them,

organic-based nanoparticles are the most common, including polymersomes, dendrimers, and liposomes, which are made up of organic material (Khalid et al. 2020). Polymeric nanoparticles are derived from polymers, including natural, semi-synthetic, and synthetic polymeric nanoparticles (Guo et al. 2016). Polymersomes are a class of polymeric nanoparticles, that are formed by self-assembled amphiphilic block copolymers and normally appear as hollow spheres (Araste et al. 2021). Due to the limitation of doxorubicin (DOX) in the treatment of colon cancer, researchers prepared PEG-PLGA polymersome of DOX, and the research showed the advantages of polymeric nanoparticles in improving targeting and bioavailability, avoiding off-site targeting, and having sustained effects (Alibolandi et al. 2017). Moreover, liposomes are lipidic vesicles composed of a lipophilic bilayer and a hydrophilic core and are ideal for direct administration into the systemic circulation owing to their biodegradability and non-immunogenicity properties (Bhaskaran & Kumar 2021; Senapati et al. 2018). In the treatment of colon cancer, the combination of folic acid as a targeting agent and liposomes encapsulated with 5-FU has been proven to help reduce the dose of 5-FU and obtain the best antitumor activity (Handali et al. 2018). Furthermore, dendrimers are another class of polymeric nanoparticles, composed of repeatedly highly branched star-like polymeric molecules with 3D geometry (Criado et al. 2022). In some aspects, dendrimers are better than liposomes because of dendrimers' higher solubility, smaller size, and greater drug encapsulation capacity (Chis et al. 2020; Wang et al. 2022). Xie et al. (2015) make the point that dendrimers can be applied in HT29 colon cancer cells and conjugated polyamidoamine dendrimers can be used to capture colorectal CTCs.

Inorganic nanoparticles are mainly composed of metal-based nanoparticles, metal

oxide-based nanoparticles, quantum dots, and ceramic nanoparticles, such as gold and Mesoporous silica nanoparticles (Babaei et al. 2020; Bhaskaran & Kumar 2021; Wahab et al. 2021). Gold nanoparticles (Au nanoparticles), a class of metal-based nanoparticles, are characterized by their unique chemical behavior and surface properties, strong optical absorption, and high electron density, and Au nanoparticles can be easily surface modified to make them suitable for drug delivery and accurate targeting (Farooq et al. 2018; Jazayeri et al. 2016). In a recent study, Au nanoparticles were prepared and chemically modified with PEG, combined with adriamycin and kaempferol in the treatment of colon cancer, which was efficient to induce cytotoxic effect and apoptosis in cancer cells without severe side effects (Meena, Vimala & Kannan 2022). The synthesis of metal oxide-based nanoparticles is essentially owing to nanoparticles' improvement of reactivity and efficiency (Nikolova & Chavali 2020). Moreover, mesoporous silica nanoparticles (Ms nanoparticles) have a variety of attractive properties, such as large surface area, stability at different pH values, adjustable pore size and shape, and ease of manufacture on a large scale, which make them suitable for drug delivery (Janjua et al. 2023; Niroumand et al. 2023). In another study on the treatment of colon cancer, researchers wrapped Ms nanoparticles with bilirubin and loaded DOX into these bovine serum albumin functionalized Ms nanoparticles, and the results revealed that the formula could improve the tumoricidal performance of mouse MC-38 and human HCT-116 cells and reduce the side effects of DOX (Srivastava et al. 2017).

Carbon-based nanoparticles are mainly composed of carbon particles, such as carbon nanotubes and graphene (Sahu et al. 2021). Carbon nanotubes are hollow cylindrical tubes made of carbon graphite nanomaterials with a diameter in the nanometer range (Maheswaran & Shanmugavel 2022). They have excellent thermal, electrical, and

mechanical properties, required size distribution, ideal surface charge, and surface chemical functions (Eatemadi et al. 2014). It has been reported that folic acid-conjugated multi-walled carbon nanotubes were developed to reduce DOX-related side effects and improve the efficacy of DOX (Yan et al. 2018). Furthermore, graphene is composed of carbon atoms closely arranged in a honeycomb structure, which has good colloidal stability, surface functionalization, and high encapsulation (Bhaskaran & Kumar 2021). Al-Ani et al. (2020) note that the graphene composite made of curcumin combined with graphene and gold nanoparticles can improve the bioavailability of curcumin, and help target cells better internalize and absorb curcumin in the treatment of colon cancer.

At present, novel drug delivery systems have been proven to be an effective approach for the treatment and management of colon cancer (Hani et al. 2021). Although the field of nanomedicine is booming, nanotechnology for cancer treatment is still in the primary stage of development (Bhaskaran & Kumar 2021). The number of nano formulations approved for clinical use in the treatment of colon cancer is still small. Therefore, the development of appropriate nano therapies for the treatment of colon cancer remains a challenge.

2.6 Calcium carbonate nanoparticles

2.6.1 Polymorphs of calcium carbonate

Calcium carbonate ($CaCO_3$) is a polymorphic material abundant in nature, found in lakes, oceans, shells, animal bones, and stalactites (Vergaro et al. 2019). $CaCO_3$ has six crystal forms, including monohydrocalcite, ikaite, amorphous $CaCO_3$, calcite,

aragonite, and vaterite (Lauth, Maas & Rezwan 2017). Anhydrous $CaCO_3$ has three polymorphs: calcite, aragonite, and vaterite (Lauth, Maas & Rezwan 2017). Under standard conditions of pressure and temperature, calcite is the stable phase, whereas vaterite and aragonite are metastable forms that easily transform into stable phases (Popova et al. 2021). Among these, calcite is the most thermodynamically stable and the least soluble in water, followed by aragonite (Kezuka et al. 2017). Vaterite is the most unstable and soluble in water (Boulos et al. 2014).

2.6.2 Synthesis methods of calcium carbonate nanoparticles

$CaCO_3$ is a low-cost material with a high specific surface area, excellent safety, pH sensitivity, biodegradability, and biocompatibility, making $CaCO_3$ nanoparticles a highly active research field in cancer treatment (Borrego-Sánchez et al. 2019; Shi et al. 2015). Unlike other popular drug delivery agents, such as metal nanoparticles, synthetic copolymers, and cationic lipids, calcium carbonate does not have potential safety issues and is already marketed as an FDA-approved antacid, digestive, antidiarrheal, and weight control drug, facilitating the approval and implementation of novel $CaCO_3$ nanoparticles-based drug formulations (Trushina et al. 2022). Furthermore, the intrinsic pH sensitivity of $CaCO_3$ nanoparticles allows for a targeted release mechanism, where the nanoparticles remain stable at physiological pH but rapidly dissolve in the acidic environment typically found in tumor tissues (Hamidu et al. 2019; Ibiyeye, Idris & Zuki 2020; Zhao et al. 2022). This characteristic enhances the precision of drug delivery, minimizing the impact on healthy tissues and reducing side effects.

Currently, common methods for synthesizing $CaCO_3$ nanoparticles include the

solution precipitation method, microemulsion method, gas diffusion method, flame synthesis method, biomineralization method, and mechanical ball milling method (Table 2.1).

Table 2.1: Common synthesis methods of $CaCO_3$ nanoparticles.

Method	Content	Advantage	Disadvantage	Reference
Solution precipitation	Mixing calcium and carbonate supersaturated solutions to utilize the reaction of Ca^{2+} and CO_3^{2-} in the solution	Simple and affordable to operate	Various reaction conditions need to be controlled	(Persano et al. 2022; Yang et al. 2021)
Microemulsion	Mixing "calcium microemulsion" and "carbonate microemulsion" formed by Ca^{2+} and CO_3^{2-} aqueous phases and organic phases respectively	Adjustable size and morphology	Difficult to separate phases and lack of homogeneity	(Pai & Pillai 2008; Wu, Ding & Xue 2008)
Gas diffusion	Diffusion of CO_2 and NH_3 produced by the decomposition of $(NH_4)_2CO_3$ or NH_4HCO_3 into the ethanol solution containing calcium salts	Controllable reaction speed and high purity of nanoparticles	Complex setup	(Chuzeville et al. 2022; Ju et al. 2022; Xu et al. 2023a)
Flame synthesis	Flame burning of calcium-rich precursor materials	High production rates and suitable for industrial-scale production	Safety concerns with high-temperature flames and combustible materials	(Huber et al. 2005)
Biomineralization	Leveraging biological molecules and processes to mimic the natural formation of minerals in living organisms	High environmental compatibility and biocompatibility	Slow reaction rate	(Caicedo-Pineda et al. 2018; Zheng et al. 2023)
Mechanical ball milling	Solid-state technique involving repeated fracturing and welding of powder particles using grinding balls in a rotating cylindrical container	Excellent scalability and cost-effectiveness	Impurity of nanoparticles	(Chemmalar et al. 2021; Sargheini et al. 2012)

The solution precipitation method involves mixing calcium and carbonate supersaturated solutions, leveraging the reaction between Ca^{2+} and CO_3^{2-} in the solution to obtain $CaCO_3$ nanoparticles. This method does not require surfactants, reducing the production cost of $CaCO_3$ nanoparticles. Synthesis parameters such as pH, temperature, ion concentration, stirring speed, solvent type, and additives are used to control the size, shape, and phase of $CaCO_3$ nanoparticles. For example, Yang et al. (2021) used $CaCl_2$ and Na_2CO_3 as raw materials and $Ca(OH)_2$ as an additive, finding that higher pH values of the reaction system resulted in the smaller size of $CaCO_3$ nanoparticles. Persano et al. (2022) studied the effects of different synthesis parameters, such as salt concentration and stirring speed, on the size of $CaCO_3$ nanoparticles. They found that increased stirring speed and high salt concentration led to smaller nanoparticles die to higher supersaturation (Persano et al. 2022).

The microemulsion method, first proposed by TP Hoar and JH Shulman in 1943, involves a mixture of oil, water, surfactant (Tween 20 or Tween 80), and co-surfactant (hexadecane or cetyl alcohol), including reverse microemulsion (water-in-oil, W/O) and double emulsion methods (Hoar & Schulman 1943). The reverse microemulsion method uses W/O microemulsion droplets as nanoreactors, encapsulating Ca^{2+} or CO_3^{2-} ions in micelles. When "calcium microemulsions" and "carbonate microemulsions" two microemulsions are mixed, micelles collide, allowing reactants to mix and form $CaCO_3$ nanoparticles (Pai & Pillai 2008). The double emulsion method is similar but involves mixing a W/O "calcium microemulsion" with a water phase (containing CO_3^{2-}), forming a W/OW double emulsion, where Ca^{2+} reacts with CO_3^{2-} to generate $CaCO_3$ nanoparticles (Wu, Ding & Xue 2008).

The gas diffusion method involves the thermal decomposition of $(NH_4)_2CO_3$ or NH_4HCO_3 to produce CO_2 and NH_3, which diffuse into an ethanol solution containing calcium salt to form a precipitate, or passing CO_2 gas into the calcium salt ethanol solution under normal pressure to synthesize $CaCO_3$ nanoparticles. Chuzeville et al. (2022) used this method to synthesize stable, uniform spherical nanoparticles below 150 nm, with ethanol inhibiting spontaneous aggregation and crystallization. This method can control the size, morphology, and polymorphism of the prepared $CaCO_3$ nanoparticles by changing additives, temperature, and Ca^{2+} concentrations. Ju et al. (2022) synthesized stable amorphous $CaCO_3$ nanoparticles in an ethanol-water binary system, finding that continuous addition of ammonia water decreased the sizes of $CaCO_3$ nanoparticles. In another study, Xu et al. (2023a) synthesized $CaCO_3$ nanoparticles by adding $Ca(OH)_2$ and CO_2 to the methanol-water system, observing that increased water content led to the transformation of amorphous calcium carbonate to metastable vaterite crystals.

The flame synthesis method uses high-temperature flames to form $CaCO_3$ nanoparticles from calcium-rich precursor materials. Huber et al. (2005) fed calcium 2-ethylhexanoate into a methane-oxygen flame, producing $CaCO_3$ nanoparticles with varying surface structures and crystallinity. This method facilitates industrial-scale production due to its high production rates, but it is seldom used in laboratories for biomedicine due to safety concerns with the high-temperature flames and combustible materials.

The biomineralization method uses biomolecules such as proteins, peptides, enzymes, and microbes to synthesize $CaCO_3$ nanoparticles. Zheng et al. (2023) used *Bacillus mucilaginosus* and *Bacillus alcalophilus* to prepare uniformly dispersed rhombohedral

calcite and spherical vaterite $CaCO_3$ nanoparticles, respectively, with *Bacillus mucilaginosus* promoting $CaCO_3$ generation through microbial enzymatic action and *Bacillus alcalophilus* controlling $CaCO_3$ precipitation through microbial metabolic decomposition. Caicedo-Pineda et al. (2018) demonstrated the use of *Bacillus cereus* to synthesize $CaCO_3$ nanoparticles by subculturing the bacteria in a medium containing 1.0% tryptone and 0.5% calcium acetate, resulting in $CaCO_3$ nanoparticles during bacterial metabolism. Moreover, it was also found that as the tryptone concentration increased and decreased, $CaCO_3$ nanoparticles with high vaterite phase and calcite phase were synthesized, respectively (Caicedo-Pineda et al. 2018). Overall, different microbial species induced the production of different $CaCO_3$ nanoparticles, revealing the diversity of biomineralization.

The mechanical ball milling method involves repeated fracturing and welding of powder particles using grinding balls in a rotating cylindrical container to produce $CaCO_3$ nanoparticles. Sargheini et al. (2012) obtained $CaCO_3$ nanoparticles by grinding a mixture of $CaCl_2$ and Na_2CO_3 powders with NaCl or KCl as the diluent in a planetary ball mill. Chemmalar et al. (2021) used environmentally friendly and resource-rich cockle shells to prepare $CaCO_3$ micron-sized powder, which was then ground in a programmable ball mill for 120 hours to obtain $CaCO_3$ nanoparticles. The synthesized spherical, porous $CaCO_3$ nanoparticles were aragonite phase and pH-sensitive, making them suitable for drug delivery (Chemmalar et al. 2021).

2.6.3 Cockle shell-derived calcium carbonate nanoparticle

The ideal choice for biomedical applications is to use natural reserves of $CaCO_3$ to synthesize $CaCO_3$ nanoparticles, such as cockle shells since they are non-toxic and

easy to obtain (Idris et al. 2019; Render et al. 2016). In Malaysia, cockle shells are commonly treated as waste due to large production and rapid annual growth, and the effective use of cockle shells can also manage the waste well (Fu et al. 2017). Moreover, aragonite has attracted more and more attention, which has been used to develop anticancer drug carriers, and bone repair and tissue engineering scaffolds (Hoque 2013; Maleki Dizaj et al. 2015). Cockle shell (*Anadara granosa*) is a rich source of biogenic aragonite (Bharatham et al. 2014). Cockle shell-derived aragonite $CaCO_3$ nanoparticles not only have the excellent properties of $CaCO_3$ nanoparticles but also is highly porous, thereby having high loading capacity (Ibiyeye, Idris & Zuki 2020).

Although there is no FDA-approved anticancer drug carrier based on $CaCO_3$np for clinical use, this material is undoubtedly promising. The potential utility of $CaCO_3$np as a drug delivery system for osteosarcoma treatment in an orthotopic rat model has been demonstrated by Fu et al. (2019). Due to the enhanced permeability and retention effect and pH sensitivity of $CaCO_3$np, $CaCO_3$np loaded with DOX increased the passive targeting of tumors, thus reducing systemic toxicity and increasing chemotherapeutic effect on tumors (Fu et al. 2019). Furthermore, the study on the effect of $CaCO_3$np (20-50nm) as carriers of cytarabine on human leukemia HL-60 cells and as antitumor treatment of SCID mice with leukemia showed that $CaCO_3$np-cytarabine was more effective than free cytarabine in inducing apoptosis (Ghaji et al. 2018). In another study, the efficacy of docetaxel (DTX)-loaded $CaCO_3$np on 4T1 cell lines was evaluated in vitro, in which $CaCO_3$np were used as drug-releasing compounds in cancer chemotherapy. The results suggested that the anticancer activities of DTX-$CaCO_3$np on 4T1 cells were equivalent to that of free DTX, but DTX-$CaCO_3$np could be better used as a substitute for free DTX owing to a slow releasing rate of $CaCO_3$np (Hammadi et al. 2017).

CHAPTER 3

SYNTHESIS, CHARACTERIZATION, AND BIOCOMPATIBILITY EVALUATION OF COCKLE SHELL-DERIVED CALCIUM CARBONATE NANOPARTICLES LOADED WITH 5-FLUOROURACIL (5FU-CACO3NP) AND THYMOQUINONE (TQ-CACO3NP)

3.1 Introduction

Nanotechnology-based drug delivery systems have gained increasing attention due to their potential to improve the efficacy and specificity of chemotherapeutic agents and phytochemicals (Pavitra et al. 2021; Wahab et al. 2021). $CaCO_3$np are particularly promising due to their biocompatibility, pH sensitivity, and ability to be functionalized with various compounds. These nanoparticles can provide a controlled release mechanism, ensuring that the drug is released in a more targeted and efficient manner, particularly in the acidic microenvironment of tumor cells (Chemmalar et al. 2021; Hamidu et al. 2019; Ibiyeye, Idris & Zuki 2020; Isa et al. 2016). In this research, we sought to utilize $CaCO_3$np as a delivery system for the hydrophilic compound 5-FU and the hydrophobic compound TQ, respectively. By loading these compounds onto $CaCO_3$np, we aimed to explore a compound delivery approach that could potentially overcome some of the limitations of conventional chemotherapies and phytochemicals, such as drug resistance, systemic toxicity, and low availability, thereby enhancing the anticancer efficacy of these compounds while reducing toxic side effects.

This chapter was to develop pH-sensitive and biocompatible $CaCO_3$np, 5FU-$CaCO_3$np,

and TQ-$CaCO_3$np, with a general concept illustrated in Figure 3.1. Purely aragonite $CaCO_3$np was synthesized by the mechanical ball milling approach. The better synthesis method of 5FU-$CaCO_3$np and TQ-$CaCO_3$np was determined by comparing loading content and encapsulation efficiency results from loading compounds using a shaking incubator and a high-speed homogenizer. The optimized 5FU-$CaCO_3$np and TQ-$CaCO_3$np were prepared following the best formulation (the weight ratio between the compound and $CaCO_3$np with the best loading results). In addition, $CaCO_3$np, 5FU-$CaCO_3$np, and TQ-$CaCO_3$np were characterized by high-resolution transmission electron microscopy (HRTEM), field emission scanning electron microscopy (FESEM), Zetasizer, energy dispersion X-ray (EDX), X-ray diffraction (XRD), and Fourier transform infrared spectroscopy (FTIR) for evaluating their physicochemical properties. *In vitro* compound release profiles of 5FU-$CaCO_3$np and TQ-$CaCO_3$np at pH 7.4, 6.5, and 5.0 were studied. Moreover, the biocompatibility of $CaCO_3$np, 5FU-$CaCO_3$np, and TQ-$CaCO_3$np were investigated by assessing their hemocompatibility, cytotoxicity on normal fibroblast NIH3T3 cell line, and toxicity on brine shrimp.

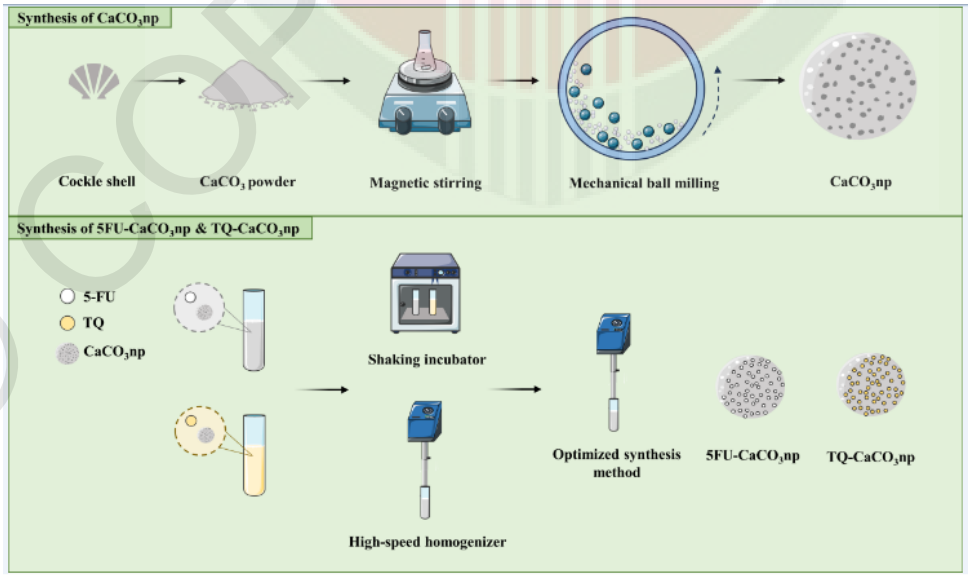

Figure 3.1: Schematic illustration of synthesis of $CaCO_3$np, 5FU-$CaCO_3$np, and TQ-$CaCO_3$np.

3.2 Materials and methods

3.2.1 Preparation of $CaCO_3$np from cockle shells

The initial step was the preparation of micro-sized calcium carbonate from cockle shells. Briefly, cockle shells were boiled for 30 min in a steel container and thoroughly washed to remove stains on the shells. Upon drying in an oven at 50°C, the shells were finely ground and then sieved using a stainless-steel laboratory test sieve with an aperture size of 75 μm to obtain micro-sized calcium carbonate powder.

For the preparation of $CaCO_3$np, 5 g of micro-sized calcium carbonate powder was mixed with 50 mL of deionized water in a flat bottom flask. The suspension was stirred with a magnetic stirrer bar at 1000 rpm for 30 min using a magnetic stirring machine, followed by adding 1.5 mL of BS-12 and stirring again at 1000 rpm for 2 h at room temperature. The obtained samples were then centrifuged three times to remove BS-12 and dried in an oven at 50°C. The dried samples were placed in a glass cylindrical jar containing ceramic balls and rolled on a programmable ball miller (BML-6″, Korea) at 200 rpm for 500 h to obtain the final $CaCO_3$np.

3.2.2 Synthesis and optimization of 5FU-$CaCO_3$np and TQ-$CaCO_3$np

Compound-loaded nanoparticles were synthesized by two methods, including using a shaking incubator and a high-speed homogenizer. Briefly, different weight ratios of compounds to $CaCO_3$np (1:2, 1:4, 1:6, 1:8, 1:10, 1:15, and 1:20 w/w) were prepared. The hydrophilic compound 5-FU in deionized water and the hydrophobic compound TQ dissolved in ethanol were mixed with $CaCO_3$np suspension, respectively. For the synthesis method using a shaking incubator, the mixtures were continuously

shaken at 200 rpm overnight in the dark at room temperature in the shaking incubator (LSI 3016R, Daihan Labtech, Korea). For the synthesis method using a high-speed homogenizer (IKA-T25 digital Ultra-Turrax, Germany), the mixtures were homogenized at the time and speed determined by single-factor experiments. Single-factor experimental design is shown in Table 3.1. Finally, 5FU-$CaCO_3$np and TQ-$CaCO_3$np were collected by centrifuging, washing, and drying, and kept at room temperature for further use.

Table 3.1: Single-factor experimental design. rpm, revolutions per minute; min, minute.

Factor	**5FU-$CaCO_3$np**		**TQ-$CaCO_3$np**	
	Speed (rpm)	**Time (min)**	**Speed (rpm)**	**Time (min)**
Speed	6000	3	6000	3
	12000	3	12000	3
	18000	3	18000	3
	24000	3	24000	3
Time	6000	1	24000	1
	6000	3	24000	3
	6000	5	24000	5
	6000	7	24000	7

The supernatant of each formulated mixture was collected for compound loading content (LC) and encapsulation efficiency (EE) analyses. The better synthesis method and the best formulation were chosen by comparing the results of LC and EE. The amount of free compound in the supernatant was evaluated using an Ultraviolet-visible (UV-Vis) spectrophotometer. The results of LC and EE were determined by calculating the difference between the total weight of the compound fed and the free compound

weight in the supernatant as the following equations:

LC (%) = (weight of compound fed – weight of free compound) / weight of nanoparticles × 100%,

EE (%) = (weight of compound fed – weight of free compound) / weight of compound fed × 100%.

3.2.3 Physicochemical characterization of nanoparticles

3.2.3.1 Electron microscopy and Zetasizer

Surface morphology and particle size of $CaCO_3$np, 5FU-$CaCO_3$np, and TQ-$CaCO_3$np were analyzed by FESEM (Nova^{TM}NanoSEM 230, USA) and HRTEM (Hitachi H-7100, Japan). The nanoparticles were suspended in 100% acetone followed by sonication for 30 min. Subsequently, a drop of the dispersion was placed on a carbon-coated copper grid, and the samples were dried at room temperature before microscopy viewing. The particle size in the HRTEM figure was measured using ImageJ software. Zeta potential and size of nanoparticles were determined using dynamic light scattering (Zetasizer Nano ZS, Malvern Instruments, UK). The dried nanoparticles were dispersed in 100% acetone for hydrodynamic size analysis and in deionized water for zeta potential analysis.

3.2.3.2 Energy dispersion X-ray spectroscopy and X-ray diffraction

Elemental compositions of $CaCO_3$np, 5FU-$CaCO_3$np, and TQ-$CaCO_3$np were determined using EDX spectroscopy, which is conjugated with FESEM. The crystalline nature and purity of $CaCO_3$np, 5FU-$CaCO_3$np, and TQ-$CaCO_3$np were determined using a Shimadzu XRD-6000 powder diffractometer on a continuous

scanning process with Cu Kα (λ = 1.5406 Å) as the X-ray source. The obtained XRD data was analyzed using Jade software, and the crystallographic model was created using Vesta software. Crystallite sizes of $CaCO_3$np, 5FU-$CaCO_3$np, and TQ-$CaCO_3$np were obtained using Scherrer's equation:

$$D = 0.9\lambda / B \times \cos\theta,$$

where D is crystallite size in angstroms, λ is X-ray wavelength (1.5406 Å), B is full-width at half maximum of peak in radian unit, and θ is peak position in radian unit.

3.2.3.3 Fourier transform infrared spectroscopy

The chemical properties of $CaCO_3$np, 5FU-$CaCO_3$np, and TQ-$CaCO_3$np were determined using FTIR (Perkin Elmer, USA) over the range of 4000 to 400 cm^{-1} at a 2 cm^{-1} resolution and averaging 64 scans.

3.2.3.4 *In vitro* compound release study

The compound release study of 5-FU and TQ was monitored in phosphate buffered saline (PBS) buffer with 1% (v/v) Tween 80 at pH 7.4, 6.5, and 5.0 using the pre-treated dialysis tubing cellulose membrane. The dialysis was conducted in an incubator shaker at 37 ± 0.5 °C and 100 rpm. At predetermined time intervals, the release medium was withdrawn and replaced with the same volume of fresh medium. The quantity of 5-FU and TQ released from compound-loaded $CaCO_3$np was detected by UV-vis spectrophotometry. The compound release data were fitted in different kinetic models, including zero-order, first-order, Higuchi, Hixson-Crowell, and Krosmeyer-Peppas models. The R^2 value was used to evaluate the best fit of the data to the kinetic models. The compound release mechanism was analyzed by the n value from the Krosmeyer-Peppas model.

3.2.4 Biocompatibility evaluation of nanoparticles

3.2.4.1 Cytotoxicity analysis

Cytotoxicity of nanoparticles was evaluated in the NIH3T3 mouse embryonic fibroblast cell line. NIH3T3 cell line was cultured with different concentrations of $CaCO_3$np (0-1000 µg/mL), 5-FU and 5FU-$CaCO_3$np (0-480 µM), and TQ and TQ-$CaCO_3$np (0-60 µM) for 96 h. After 96 h of incubation, the media was aspirated, and 20 µL of 3-(4,5-dimethylthiazol-2-yl)-2,5-diphenyltetrazolium bromide) (MTT) solution was added to each well and incubated at 37°C (5% CO_2 and 95% air) for 4 h. The solution was then removed and the purple formazan crystals were solubilized in dimethylsulfoxide (DMSO). The absorbance was measured at 570 nm with reference wavelength 630 nm using the multimode microplate reader (Synergy H1, BioTek, USA) and cell viability was determined.

3.2.4.2 Hemocompatibility analysis

The rat red blood cells (erythrocytes) were collected from plasma (1 mL) by centrifugation at 3000 rpm for hemocompatibility analysis. The erythrocytes were redispersed in the PBS to prepare a 4% solution. Dispersed blood was added to each test sample aliquot at different concentrations (62.5-4000 µg/mL) followed by incubation at 37°C. Thereafter, the test samples were recentrifuged and the supernatant was analyzed at 540 nm by microplate reader. The PBS solution and deionized water were used as negative (0% hemolysis) and positive control (100% hemolysis), respectively. The hemolysis percentage was calculated using the following equation:

$$\text{hemolysis (\%)} = [(A_{sample} - A_{negative}) / (A_{positive} - A_{negative})] \times 100\%,$$

where A_{sample}, $A_{negative}$, and $A_{positive}$ represent the absorbance of test sample, negative control, and positive control, respectively.

3.2.4.3 Toxicity analysis in brine shrimp

The toxicity was determined by measuring the survival rate of brine shrimp treated with different concentrations of nanoparticles. Briefly, sea salt (without iodine) was dissolved in deionized water as the simulated seawater, and 1 g of brine shrimp eggs (sourced from local pet shop in Kuala Lumpur, Malaysia) were put into the salt water. The eggs were then incubated with constant air and a light source (12 h light-dark cycle) at room temperature for 24 h. Once hatching, 10 active nauplii in 1 mL of salt water were transferred to each well of the 24-well plate. Different concentrations (0-1000 μg/mL) of $CaCO_3$np, 5FU-$CaCO_3$np, and TQ-$CaCO_3$np were added into the wells containing the nauplii, whereas $KMnO_4$ dissolved in simulated seawater with the same concentrations served as the positive control. The surviving nauplii were observed using light microscopy and recorded at 12, 24, 36, and 48 h. The brine shrimp survival rate was calculated using the following formula:

survival rate (%) = alive brine shrimp / total brine shrimp × 100%.

3.2.5 Statistical Analysis

Data analysis was performed with at least triplicates using the GraphPad Prism 8 and Origin 2022 software. Statistical analysis involved one-way ANOVA followed by Turkey's post-test for multiple comparisons or Student's t-test for a single comparison and two-way ANOVA followed by Dunnett's post-test. P value < 0.05 ($p<0.05$) was considered as statistical significance. Unless otherwise stated, the results were expressed as mean ± standard deviation.

3.3 Results and discussion

3.3.1 Compound loading content and encapsulation efficiency

3.3.1.1 Synthesis of compound-loaded nanoparticles using a shaking incubator

The most critical parameters for compound loading into nanoparticles are the weight percentage of the compound in the delivery system (LC) and the percentage of the encapsulated drug to its initial amount for loading (EE). Additionally, optimizing EE can reduce compound loss by minimizing the amount of left compound in the loading process, and optimal LC ensures the dose of the encapsulated compound before administration and minimizes the amount of nanocarrier, thereby reducing the potential side effects of nanocarrier (Trushina et al. 2022). Compound loading with various weight ratios (weight of compounds to weight of nanocarriers) was performed using the shaking incubator to obtain the best formulation. Figure 3.2(a) shows the highest EE (5.72%) of 5FU-$CaCO_3$np at the weight ratio 1:15, with 0.38% of LC. From Figure 3.2(b), it is observed that the highest EE in the 1:4 group (19.31%) had no significant difference from the result in the 1:6 group (17.88%) when using the shaking incubator to load TQ into $CaCO_3$np. However, the LC in the 1:4 group was significantly higher than that in the 1:6 group ($p<0.05$). Therefore, the 1:4 weight ratio of TQ to $CaCO_3$np was considered the best formulation for TQ loading.

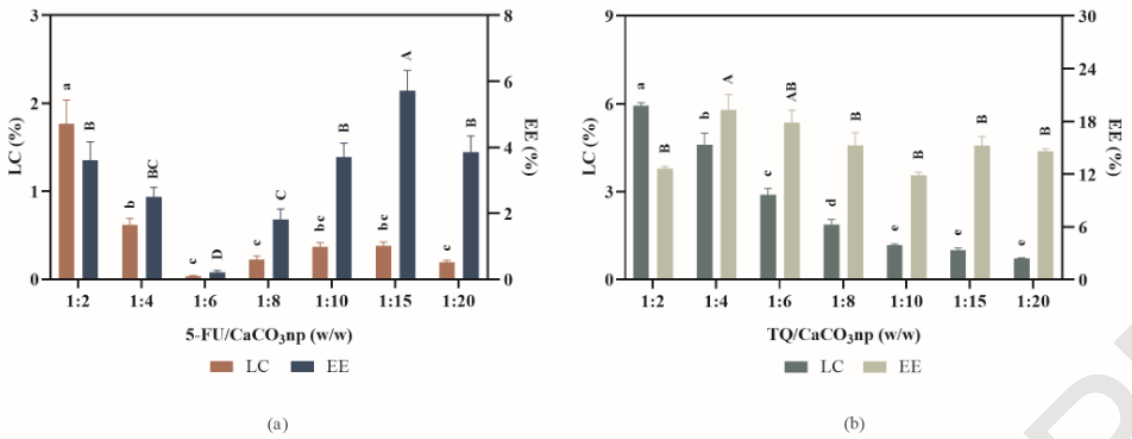

Figure 3.2: LC and EE of (a) 5-FU in 5FU-$CaCO_3$np and (b) TQ in TQ-$CaCO_3$np with different weight ratios between compounds and nanocarriers when using a shaking incubator for compound loading. The results with the different superscripts (a-e and A-D nomenclature) indicate significant differences ($p<0.05$). LC, loading content; EE, encapsulation efficiency.

It is noted that the LC and EE of 5-FU in 5FU-$CaCO_3$np and TQ in TQ-$CaCO_3$np did not increase along with the increase of weight ratios between compounds and $CaCO_3$np, indicating there should be an optimal weight ratio of compounds to $CaCO_3$np for loading compounds into $CaCO_3$np. The loading process reaches equilibrium when the optimal weight ratio is achieved, making it difficult to accommodate the additional compound molecules into $CaCO_3$np. Although the LC may continue to increase, the EE will reduce. Moreover, it is obtained that $CaCO_3$np loading TQ showed better loading results than $CaCO_3$np loading 5-FU ($p<0.05$). For one thing, it may be related to the solubility of compounds (Trushina et al. 2022). TQ in ethanol has better solubility than 5-FU in deionized water, which may contribute to a more homogenous distribution of TQ molecules in ethanol to promote better loading into $CaCO_3$np (Haq & Michniak-Kohn 2018; Zorrilla-Veloz, Stelzer & López-Mejías 2018). This also helps to explain why the best loading results of 5-FU were at a lower weight ratio (1:15 w/w), whereas TQ obtained the best loading results at a higher weight ratio (1:4 w/w). For another thing, the dispersity of $CaCO_3$np in the loading medium may be an important factor in compound loading

(Dey, Kumar & Samantaray 2017). $CaCO_3$np may disperse better in organic solvent ethanol than in water due to the stronger viscosity of ethanol, which may increase the surface area of $CaCO_3$np for compound loading, resulting in more effective interactions between TQ and $CaCO_3$np (Fang et al. 2019; Tadano et al. 2014). To increase the interactions between compounds and nanoparticles and better loading results, a high-speed homogenizer with strong thrust forces is considered a potentially effective method for compound loading.

3.3.1.2 Determination of optimized speed and time for high-speed homogenizer

Besides the weight ratios between the compound and nanocarrier, two factors will influence the loading results when the high-speed homogenizer is used for compound loading: speed and time (Sharma, Madan & Lin 2016). Based on the results in the single-factor experiments, the 6000-rpm group showed the highest LC and EE for 5-FU loading at the constant time and weight ratio in Figure 3.3(a). Even though the LC and EE of 5FU-$CaCO_3$np in the 3-min group had no significant difference with the values in the 5-min group (Figure 3.3(b)), the more effective 3-min was chosen as the time of 5-FU loading. For TQ loading, it can be seen from Figures 3.3(c) and 3.3(d) that 24000 rpm and 3 min achieved the highest LC and EE of TQ-$CaCO_3$np in the single-factor experiments, respectively, thus used as the target speed and time for TQ loading. Therefore, 6000 rpm and 3 min were used for 5-FU loading into $CaCO_3$np, whereas 24000 rpm and 3 min for TQ loading.

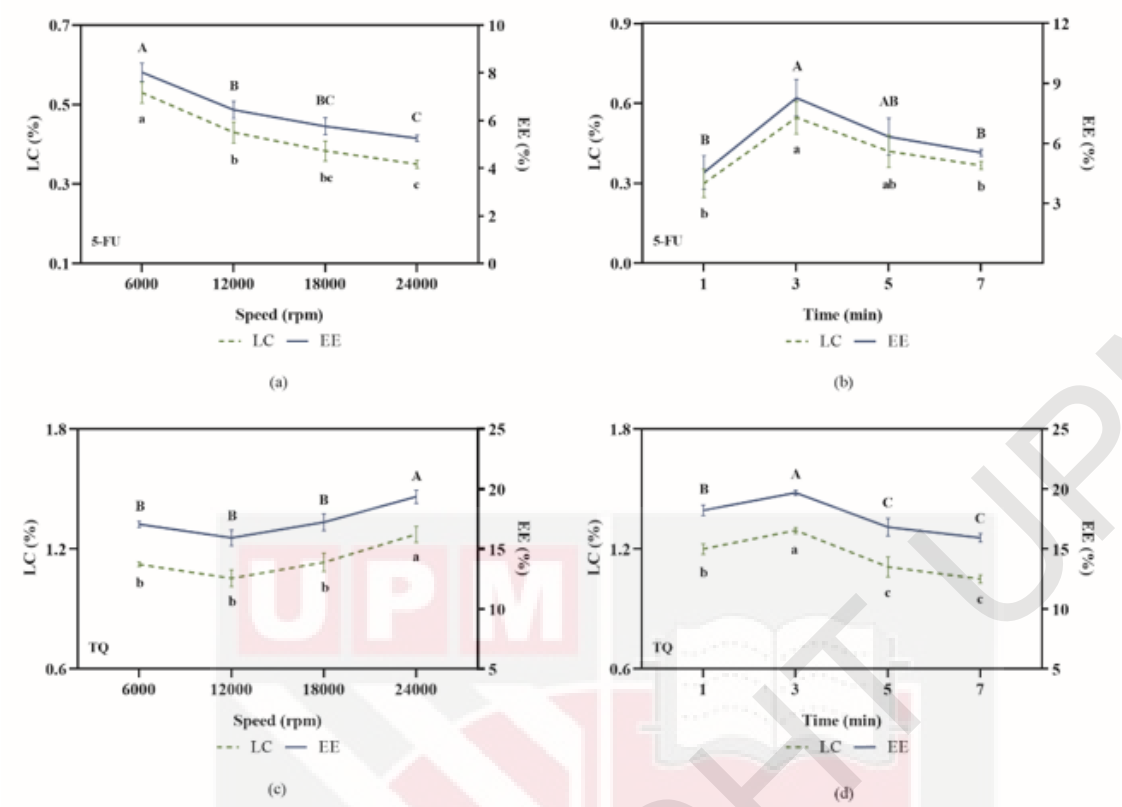

Figure 3.3: LC and EE of (a) 5-FU in 5FU-$CaCO_3$np with different speeds at the constant time and weight ratio, (b) 5-FU in 5FU-$CaCO_3$np with different time at the constant speed and weight ratio, (c) TQ in TQ-$CaCO_3$np with different speeds at the constant time and weight ratio, and (d) TQ in TQ-$CaCO_3$np with different time at the constant speed and weight ratio when using a high-speed homogenizer for compound loading. The results with the different superscripts (a-c and A-C nomenclature) indicate significant differences ($p<0.05$). LC, loading content; EE, encapsulation efficiency; rpm, revolutions per minute; min, minute.

3.3.1.3 Synthesis of compound-loaded nanoparticles using a high-speed homogenizer

After the optimized speed and time of the high-speed homogenizer were determined for compound loading, various weight ratios of the compound to $CaCO_3$np were tested at the chosen speed and time for the best formulation of compound loading. According to Figure 3.4(a), the EE of 5FU-$CaCO_3$np obtained the highest value (9.61%) at the weight ratio of 1:20 with the corresponding LC 0.48%, better than the values when using the shaking incubator ($p<0.05$), so the high-speed homogenizer operated at 6000 rpm for 3 min with the 1:20 weight ratio of 5-FU to $CaCO_3$np was chosen for loading

5-FU into $CaCO_3$np. Although it is displayed in Figure 3.4(b) that the 1:4 group achieved the highest EE of TQ-$CaCO_3$np with 8.82% of LC, the LC of the 1:2 group (13.68%) was much higher than other groups ($p<0.05$), and meanwhile, the 1:2 group still obtained high EE (27.36%). Therefore, the 1:2 weight ratio of TQ to $CaCO_3$np was considered the best formulation. Moreover, the best result produced using the high-speed homogenizer for TQ loading was better than that produced using the shaking incubator ($p<0.05$). Overall, the high-speed homogenizer was chosen as the final synthesis method for 5FU-$CaCO_3$np and TQ-$CaCO_3$np, 1:20 weight ratio of 5-FU to $CaCO_3$np at 6000 rpm for 3 min for 5-FU loading while 1:2 weight ratio of TQ to $CaCO_3$np with 24000 rpm for 3 min for TQ loading.

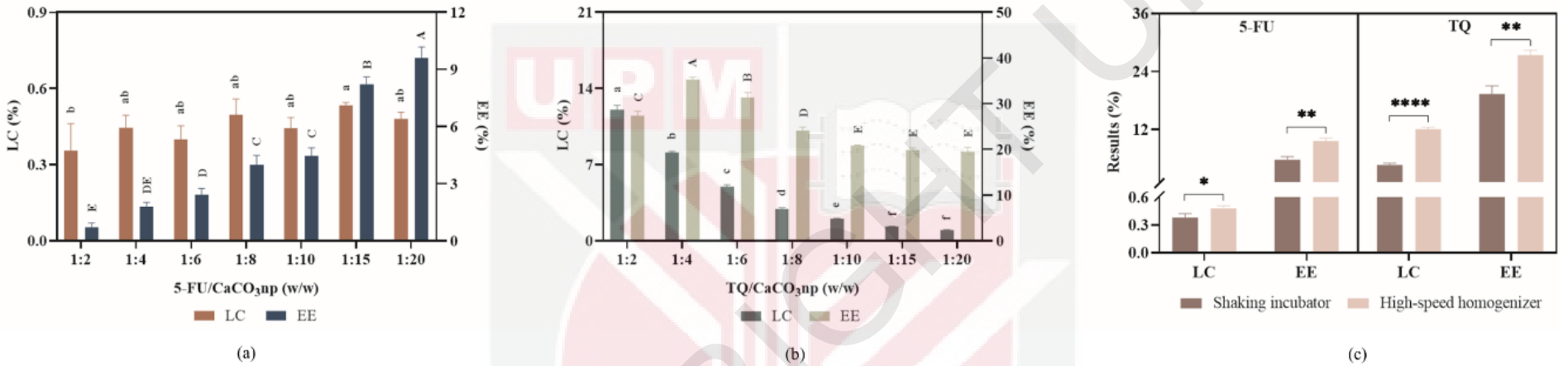

Figure 3.4: LC and EE of (a) 5-FU in 5FU-$CaCO_3$np and (b) TQ in TQ-$CaCO_3$np with different weight ratios between compounds and nanocarriers when using a high-speed homogenizer for compound loading; (c) comparison of optimized loading results between using a shaking incubator and a high-speed homogenizer. The results with the different superscripts (a-f and A-E nomenclature) indicate significant differences ($p<0.05$). LC, loading content; EE, encapsulation efficiency. *$p<0.05$, **$p<0.01$, ****$p<0.0001$.

This is the first study on 5-FU and TQ loading by using a high-speed homogenizer, with 0.48% LC and 9.61% EE of 5FU-$CaCO_3$np as well as 13.68% LC and 27.36% EE of TQ-$CaCO_3$np, better than the optimized results produced by using a shaking incubator ($p<0.05$) displayed in Figure 3.4(c). Both the hydrophobic compound TQ and the hydrophilic compound 5-FU were demonstrated to be successfully loaded into $CaCO_3$np. As with the results when using the shaking incubator for compound loading, the higher weight ratios of the compound to $CaCO_3$np did not lead to better compound loading results when using the high-speed homogenizer. For 5-FU loading into $CaCO_3$np, the lower weight ratio of 5-FU to $CaCO_3$np was, the higher EE of 5FU-$CaCO_3$np was. For TQ loading, from 1:20 to 1:4 w/w, the EE of TQ-$CaCO_3$np increased and reached the highest value at 1:4 weight ratio of TQ to $CaCO_3$np, but the EE decreased when the weight ratio increased from 1:4 to 1:2 w/w. However, the LC of TQ-$CaCO_3$np increased along with the increase in weight ratio. Additionally, TQ-$CaCO_3$np exhibited better loading results than 5FU-$CaCO_3$np when using the high-speed homogenizer for compound loading ($p<0.05$), which may be also due to the solubility of compounds and dispersity of $CaCO_3$np in different solvents (Dey, Kumar & Samantaray 2017; Trushina et al. 2022).

The synthesis method using a shaking incubator, or a high-speed homogenizer is based on the physical adsorption of compounds onto the surface or encapsulation within the nanoparticles. Compound loading using a high-speed homogenizer showed better LC and EE values than loading using a shaking incubator since compound loading using a shaking incubator is a simple shaking method, whereas using a high-speed homogenizer with strong physical forces is more efficient (Safavi et al. 2017). A high-speed homogenizer can rapidly promote the interactions between compounds and

nanoparticles by intense mechanical forces, leading to faster compound loading and improved loading results compared with gentler agitation provided by a shaking incubator. On the other hand, high-speed homogenization facilitates a more uniform dispersion of compounds and prevents nanoparticle agglomeration, contributing to a more consistent and reproducible compound-loading process (Dey, Kumar & Samantaray 2017).

3.3.2 Surface morphology and particle size

As seen in Figures 3.5(a-f), both FESEM and HRTEM images of $CaCO_3$np and HRTEM images of compound-loaded $CaCO_3$np displayed homogeneous spherical-shaped or nearly spherical-shaped porous nanoparticles. Meanwhile, HRTEM images revealed an average nanoparticle size of 77 nm before compound loading and 125 and 98 nm after loading 5-FU and TQ, respectively (Figure 3.5(g)). Moreover, the hydrodynamic size and zeta potential distribution of $CaCO_3$np and compound-loaded $CaCO_3$np are shown in Figures 3.5(h) and (i). Dynamic light scattering revealed consistent results in the hydrodynamic diameter of $CaCO_3$np and compound-loaded $CaCO_3$np with the results by HRTEM, where the average hydrodynamic diameters of $CaCO_3$np, 5FU-$CaCO_3$np, and TQ-$CaCO_3$np were 86, 133 and 139 nm, respectively. The zeta potential of $CaCO_3$np was -11.4 mV, while 5FU-$CaCO_3$np and TQ-$CaCO_3$np had a higher value of -13.2 and -17.3 mV, respectively, indicating an increase of negativity in zeta potential due to 5-FU and TQ loading.

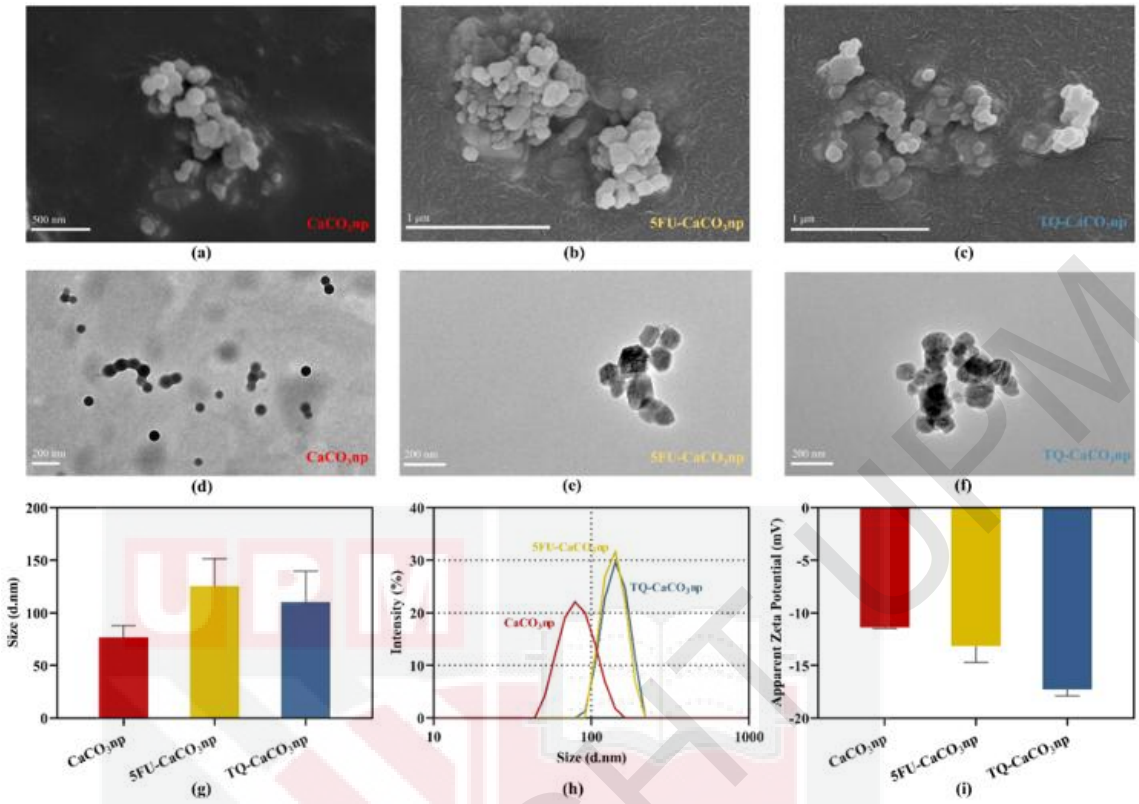

Figure 3.5: Surface morphology of (a) $CaCO_3$np in FESEM, (b) 5FU-$CaCO_3$np in FESEM, (c) TQ-$CaCO_3$n in FESEM, (d) $CaCO_3$np in HRTEM, (e) 5FU-$CaCO_3$np in HRTEM, and (f) TQ-$CaCO_3$np in HRTEM; (g) HRTEM sizes of nanoparticles; (h) hydrodynamic sizes of nanoparticles; (i) zeta potential of nanoparticles. FESEM, field emission scanning electron microscopy; HRTEM, high-resolution transmission electron microscopy.

Due to the porosity of $CaCO_3$np, the compound molecules were incorporated within the pores of $CaCO_3$np during the high-speed mixing of compounds and $CaCO_3$np when using the high-speed homogenizer for compound loading. After loading compounds, the mean diameters of compound-loaded $CaCO_3$np were slightly increased compared to the mean diameter of empty $CaCO_3$np, which may be attributed to the successful loading of compounds. Besides, the sizes of $CaCO_3$np and compound-loaded $CaCO_3$np are suitable for compound delivery since nanoparticles with sizes between 20 and 150 nm can reduce liver clearance and kidney filtration and prolong the circulation time *in vivo* (Di et al. 2021).

3.3.3 Elemental composition and crystalline nature

The elemental compositions of synthesized $CaCO_3$np, 5FU-$CaCO_3$np, and TQ-$CaCO_3$np were determined using EDX analysis. As shown in Table 3.2, $CaCO_3$np contained 16.06% of carbon, 62.42% of oxygen, 21.27% of calcium, and 0.25% of sodium. This analysis indicates that calcium carbonate derived from the cockle shell is almost 100% pure. Based on the conventional stoichiometrically derived ratio of $CaCO_3$, the Ca/C/O was in a molar ratio of almost 1:1:3. Moreover, according to the EDX data of 5FU-$CaCO_3$np and TQ-$CaCO_3$np, the elemental percentages of Ca/C/O change may be due to the successful loading of compounds.

Table 3.2: Elemental compositions of $CaCO_3$np, 5FU-$CaCO_3$np, and TQ-$CaCO_3$np.

Nanoparticles	C (%)	O (%)	Ca (%)	Na (%)	N (%)	F (%)
$CaCO_3$np	16.06	62.42	21.27	0.25	0	0
5FU-$CaCO_3$np	15.46	61.77	22.77	0	0	0
TQ-$CaCO_3$np	17.42	62.00	20.58	0	0	0

XRD was used to analyze the crystalline phase of $CaCO_3$np before and after compound loading. The $CaCO_3$np diffraction peaks (crystal planes) observed, including 26.22° (111), 27.23° (021), 33.15° (012), 36.12° (102), 37.90° (112), 38.42° (130), 42.92° (122), 45.87° (221), 48.33° (041), 50.25° (132), 52.48° (113), and 53.05° (023), confirmed the aragonite structure of $CaCO_3$np by comparing with the reference diffraction peaks of aragonite calcium carbonate nanoparticles, where the reference diffraction peaks PDF#75-2230 were from the Inorganic Crystal Structure Database (Figure 3.6(a)). The similarity in the diffraction peaks of $CaCO_3$np and compound-loaded $CaCO_3$np indicated that the crystallinity of $CaCO_3$np remained unchanged even

after loading with compounds 5-FU and TQ. In addition, it can be observed in Figures 3.6(b) and (c) that there were similar diffraction peaks between compounds and compound-loaded $CaCO_3$np, suggesting that the compounds have been successfully loaded. Moreover, the lattice parameters of $CaCO_3$np and compound-loaded $CaCO_3$np are displayed in Table 3.3. The crystallite size of $CaCO_3$np, 5FU-$CaCO_3$np, and TQ-$CaCO_3$np is 827, 965, and 848 Å, respectively, consistent with the size by HRTEM and Zetasizer, and the crystallinity of all nanoparticles is more than 95%. The changes in lattice parameters (a, b, c, crystallite size, and crystallinity) between $CaCO_3$np and compound-loaded $CaCO_3$np further demonstrated that the compounds have been successfully loaded. Based on the obtained lattice parameters (a, b, and c), the orthorhombic (Pmcn space group) crystalline morphology of aragonite $CaCO_3$np was created and exhibited in Figure 3.6(d).

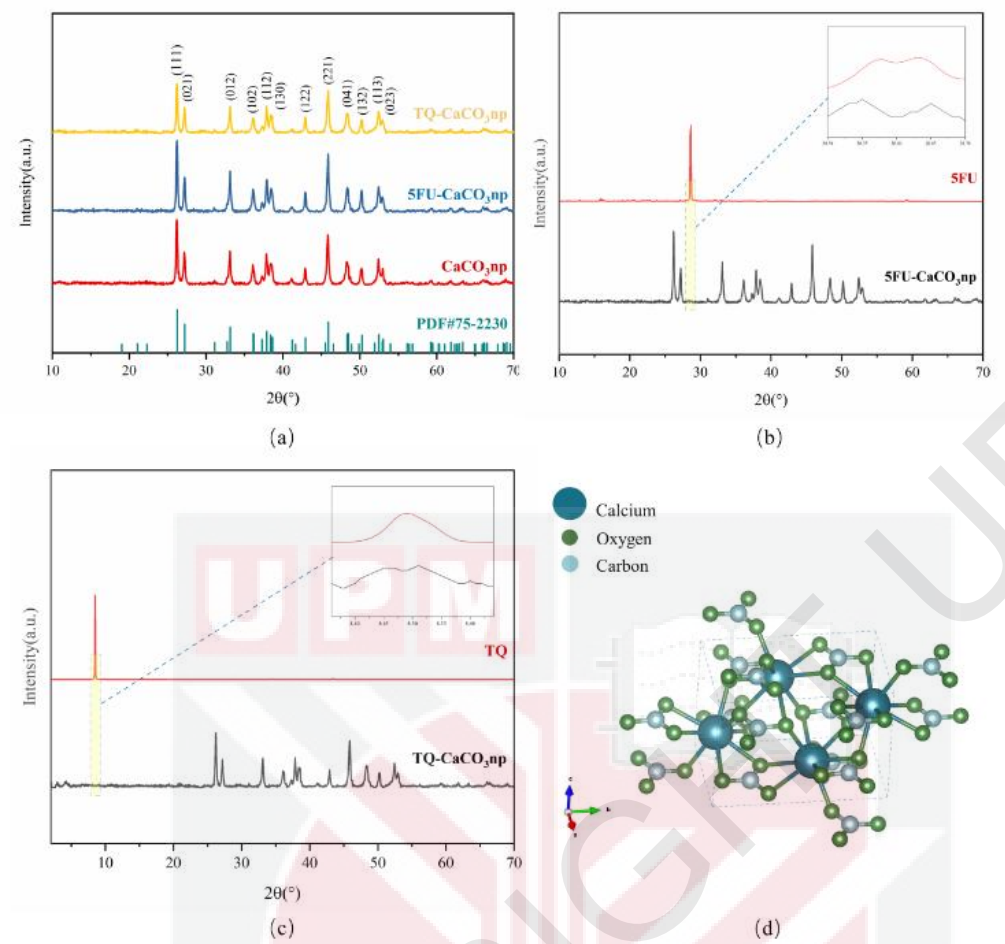

Figure 3.6: (a) XRD patterns of $CaCO_3$np, 5FU-$CaCO_3$np, and TQ-$CaCO_3$np and the reference diffraction peak (PDF#75-2230) of aragonite $CaCO_3$np from Inorganic Crystal Structure Database. Labeled are the Miller indices planes (characteristic peaks of aragonite phase); (b) XRD pattern comparison between 5-FU and 5FU-$CaCO_3$np; (c) XRD pattern comparison between TQ and TQ-$CaCO_3$np; (d) Orthorhombic crystalline morphology of aragonite $CaCO_3$np. XRD, X-ray diffraction.

Table 3.3: Lattice parameters of $CaCO_3$np, 5FU-$CaCO_3$np, and TQ-$CaCO_3$np.

Nanoparticles	a (Å)	b (Å)	c (Å)	Crystallite size (Å)	Crystallinity (%)
$CaCO_3$np	4.96662	7.96480	5.74860	827	96.35
5FU-$CaCO_3$np	4.96379	7.96368	5.74450	965	97.74
TQ-$CaCO_3$np	4.96283	7.96530	5.74325	848	98.18

As reported, other elements except for Ca, C, and O are found inside calcium carbonate nanoparticles synthesized by other methods, such as Si, Cu, P, and Mg (Kiranda et al. 2018; Minkowicz et al. 2021). By contrast, the synthesis method of nanocarrier and compound-loading method in this study produce purer $CaCO_3$np and compound-loaded $CaCO_3$np. Additionally, other calcium carbonate phases have own characteristic peaks (crystal planes), such as calcite phase at 29.32° (104), 35.90° (110), 39.36° (113), 47.47° (018), 48.43° (116), and 57.37° (122) as well as vaterite phase at 20.89° (002), 24.82° (100), 26.99° (101), 32.72° (102), 43.71° (110), 49.07° (112), 50.06° (104), and 55.74° (202), but these peaks do not appear in Figure 3.6(a), indicating the synthesized $CaCO_3$np is pure aragonite (Febrida et al. 2021). From the perspective of crystal structure, calcite and vaterite have a trigonal and hexagonal crystal system, respectively, whereas aragonite is stable with orthorhombic polymorphic crystal, illustrated in Figure 3.6(d).

3.3.4 Chemical properties

FTIR is applied to detect the functional groups of compounds and nanoparticles and analyze their chemical properties. The FTIR spectra of 5-FU, 5FU-$CaCO_3$np, TQ, TQ-$CaCO_3$np, and $CaCO_3$np are shown in Figure 3.7, and the peak vibration assignments of nanoparticles are presented in Table 3.4. $CaCO_3$np exhibited characteristic peaks at 707.41 (peak a), 854.8 (peak b), and 1082.21 (peak c) cm^{-1} corresponding to in-plane C-O bending vibration, out-of-plane C-O bending vibration, and symmetric C-O stretching of CO_3^{2-} in aragonite polymorph, respectively. It suggests that $CaCO_3$np is the crystal form of aragonite, in agreement with the result in XRD patterns. The prominent peak for the asymmetric C-O stretching of CO_3^{2-} appeared at 1450.53 cm^{-1} (peak d), and the weak peak at 1783.63 cm^{-1} (peak e) was attributed to symmetric

C-O stretching and in-plane C-O bending vibration of CO_3^{2-}. Moreover, it is interesting to know that 5-FU showed characteristic peaks at 544.13, 806.76, 1242.35, 1424.91, 1649.11, and 3119.2 cm^{-1} due to the vibration of imide stretch (amide II and amide III) and aromatic ring and TQ exhibited its major characteristic peaks for CH (sp_3), CH (sp_2), C=C, and trans C=C groups at 2962.28, 3256.94, 1639.50, and 931.67 cm^{-1}, respectively. The FTIR absorption peaks of 5FU-$CaCO_3$np and TQ-$CaCO_3$np remained the same with the peaks of aragonite $CaCO_3$np after compound loading, without new peaks generated and the same characteristic peaks of 5-FU or TQ. This implied that the aragonite polymorphism did not change and there was no chemical reaction between compounds and $CaCO_3$np.

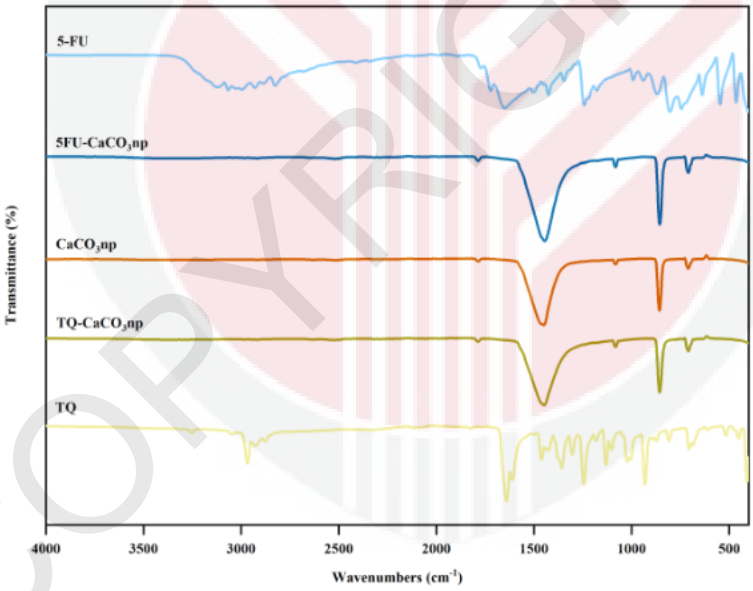

Figure 3.7: FTIR spectra of 5-FU, 5FU-$CaCO_3$np, $CaCO_3$np, TQ-$CaCO_3$np, and TQ. FTIR, Fourier transform infrared spectroscopy. The labeled peaks that represent certain peak assignments are stated in Table 3.4.

Table 3.4: FTIR peak assignments of $CaCO_3$np, 5FU-$CaCO_3$np, and TQ-$CaCO_3$np. FTIR, Fourier transform infrared spectroscopy.

Peak	Peak assignment	Wavenumber (cm^{-1})		
		$CaCO_3$np	**5FU-$CaCO_3$np**	**TQ-$CaCO_3$np**
a	In-plane C-O bending	707.47	710.68	707.47
b	Out of plane C-O bending	854.80	851.60	851.60
c	Symmetric C-O stretching	1082.21	1082.21	1082.21
d	Asymmetric C-O stretching	1450.53	1440.93	1447.33
e	Symmetric C-O stretching; in-plane C-O bending	1783.63	1783.63	1783.63

Besides XRD, FTIR is another tool for comparing different calcium carbonate phases, where the calcite, vaterite, and aragonite phases exhibit their characteristic absorption bands. The vibrational spectra of CO_3^{2-} include lattice mode (0-400 cm^{-1}) and four normal internal modes: in-plane C-O bending (650-720 cm^{-1}), out-of-plane C-O bending (840-910 cm^{-1}), symmetric C-O stretching (1000-1100 cm^{-1}), and asymmetric C-O stretching (1350-1600 cm^{-1}) (Stephanos & Addison 2017; Wang et al. 2019; Wehrmeister et al. 2010). The in-plane C-O bending vibration of CO_3^{2-} in aragonite phase is observed around 700 and 713 cm^{-1}, while calcite around 713 cm^{-1} and vaterite around 745 cm^{-1} (Ševčík et al. 2015). In addition, in comparison to the strong out-of-plane bending around 857 cm^{-1} and weak symmetric C-O stretching around 1082 cm^{-1} of aragonite, vaterite shows around 874 $cm^{-1}$and 1088 cm^{-1}, respectively, while calcite only presents out-of-plane bending around 872 cm^{-1} (Ferreira et al. 2023; Islam et al. 2011). Moreover, asymmetric C-O stretching vibration is strong and broad in calcite around 1396 cm^{-1} and aragonite around 1450 cm^{-1}, whereas vaterite exhibits a split

asymmetric C-O stretching band around 1397-1459 cm^{-1} (Ferreira et al. 2023; Kim et al. 2021; Zhuravlev & Atuchin 2020). Furthermore, shifting of peaks in 5FU-$CaCO_3$np and TQ-$CaCO_3$np may be attributed to the addition of compounds to $CaCO_3$np, such as peak from 707.47 cm^{-1} in $CaCO_3$np to 710.68 cm^{-1} in 5FU-$CaCO_3$np and peak from 1450.53 cm^{-1} in $CaCO_3$np to 1440.93 cm^{-1} in 5FU-$CaCO_3$np and 1447.33 cm^{-1} in TQ-$CaCO_3$np, respectively. Overall, the pure phase of nanoparticles and successful loading of compounds are further demonstrated by FTIR analysis.

3.3.5 Compound release kinetics

The compound release study was investigated at pH 7.4, 6.5, and 5.0, which modeled the blood and healthy tissue environment, the weakly acidic extracellular environment in malignant tumors, and the more acidic intracellular environment in malignant tumors, respectively (Mo & Gu 2016). As evident in Figure 3.8, the release of 5-FU and TQ from compound-loaded $CaCO_3$np was pH-dependent. The accumulative 5-FU release amounts of 5FU-$CaCO_3$np and accumulative TQ release amounts of TQ-$CaCO_3$np at pH 7.4 were 13.51% and 5.27% within 24 h as well as 23.57% and 13.30% within 120 h, respectively. The compound release rates of 5FU-$CaCO_3$np and TQ-$CaCO_3$np at pH 6.5 were higher than those at pH 7.4, with the accumulative release amounts 20.19% and 12.50% within 24 h as well as 34.58% and 27.01% within 120 h, respectively. At pH 5.0, the compound release rates were accelerated more obviously. The accumulative release amounts of 5FU-$CaCO_3$np at pH 5.0 were 32.58% within 24 h and 52.12% within 120 h, while TQ-$CaCO_3$np released 17.94% of TQ within 24 h and 33.77% within 120 h at pH 5.0. These results proved the pH-sensitive property of $CaCO_3$np and its benefit in increasing the intracellular accumulation of compounds in tumors, which may strengthen the anticancer effects of 5-FU and TQ.

The release profile of compounds from nanoparticles is divided into a sudden release and a sustained release. Sudden release of compounds can quickly reach effective therapeutic concentrations in the body, whereas sustained release can keep compounds within the effective therapeutic concentration range (Sun et al. 2017). As shown in Figure 3.8(a), there was a sudden release in 5FU-$CaCO_3$np at pH 5.0 (15.64% within 2 h), which could be attributed to the physical adsorption of a small amount of 5-FU on the surface of $CaCO_3$np, followed by a sustained release due to the slow diffusion of 5-FU from $CaCO_3$np. In contrast, pure 5-FU showed a rapid release with more than 95% within 4 h at the three pH values. Additionally, it is observed in Figure 3.8(b) that TQ-$CaCO_3$np suddenly released less than 6% within 2 h, while pure TQ rapidly released more than 95% within 8 h. Compared to the rapid release of pure compounds, the sustained release of 5FU-$CaCO_3$np and TQ-$CaCO_3$np can maintain the effective concentrations of 5-FU and TQ, thus reducing the dose, frequency of dosage, and adverse effects of compounds (Adepu & Ramakrishna 2021). It is noted that 5-FU was released faster from 5FU-$CaCO_3$np compared with TQ from TQ-$CaCO_3$np. This could be related to the hydrophobic nature of TQ, encapsulated deeper inside the $CaCO_3$np, which had to follow a lengthier diffusion path to reach the surface in comparison to water-soluble 5-FU encapsulated near the surface (Farzan et al. 2023). Interestingly, pure 5-FU exhibited a similar rapid release profile at pH 7.4, 6.5, and 5.0, while pure TQ released faster at the lower pH value, which may be due to the hydrophilic nature of 5-FU and the increased solubility of TQ at the decreased pH value (Salmani et al. 2014).

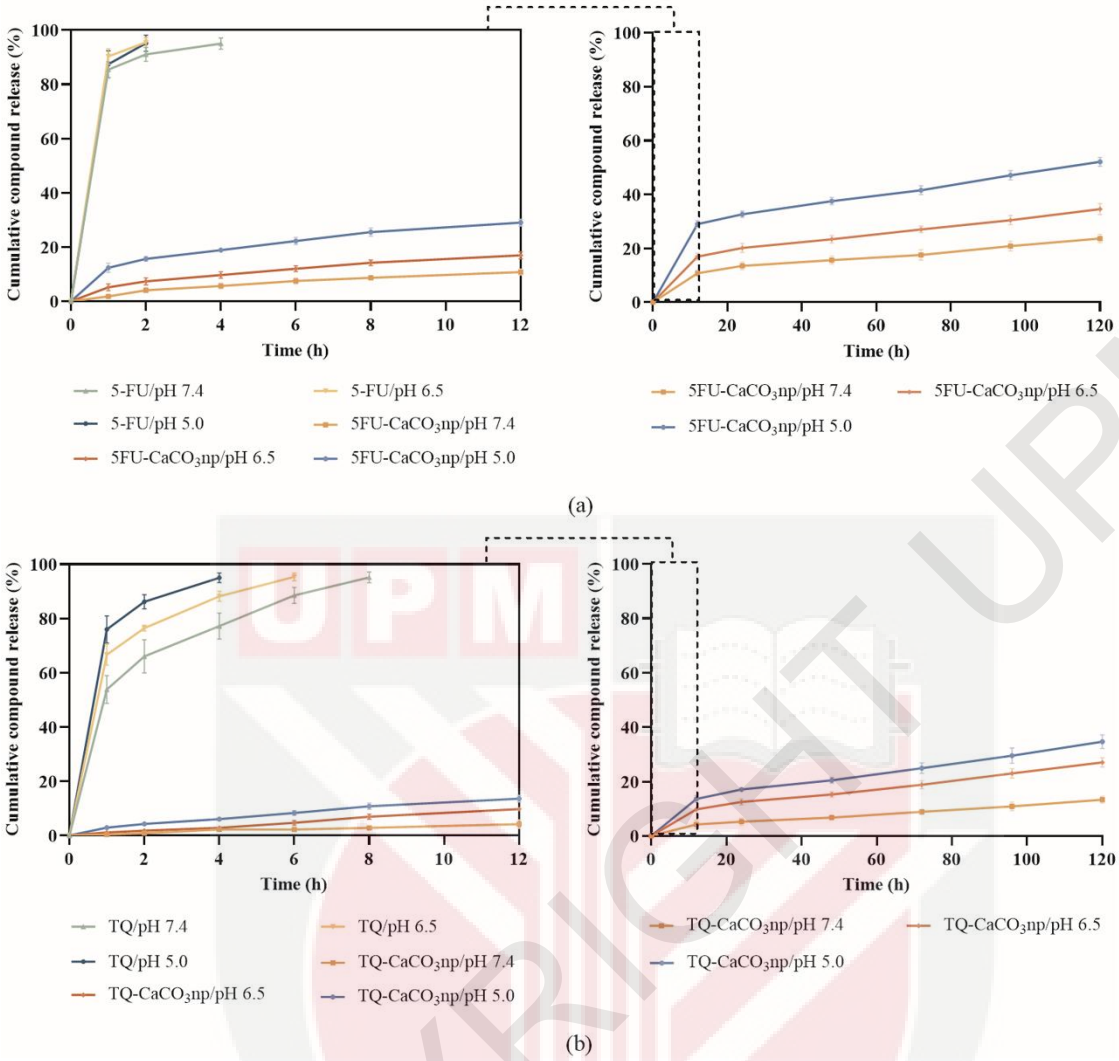

Figure 3.8: *In vitro* compound release profiles of (a) 5FU-$CaCO_3$np compared with 5-FU and (b) TQ-$CaCO_3$np compared with TQ in PBS with 1% (v/v) Tween 80 at 37°C and pH 7.4, 6.5, and 5.0. PBS, phosphate buffered saline.

The compound release patterns of 5FU-$CaCO_3$np and TQ-$CaCO_3$np were analyzed using zero-order, first-order, Higuchi, Hixon-Crowell, and Korsmeyer-Peppas models. From Table 3.5, it can be found that the Korsmeyer-Peppas model shows the best goodness of fit for 5FU-$CaCO_3$np (R^2 = 0.98258 at pH 7.4, R^2 = 0.98988 at pH 6.5, and R^2 = 0.99084 at pH 5.0), corresponding to the diffusion-controlled principal. TQ-$CaCO_3$np release curves at pH 7.4 and 5.0 exhibit the best fit with the Korsmeyer-Peppas model (R^2 = 0.98578 at pH 7.4 and R^2 = 0.98765 at pH 5.0). Higuchi is the best-fit model for TQ-$CaCO_3$np release at pH 6.5 (R^2 = 0.98363), indicating the

concentration of TQ released from TQ-$CaCO_3$np increases with the square root of time (Farzan et al. 2023). However, the high R^2 (0.98266) suggests the compound release pattern of TQ-$CaCO_3$np at pH 6.5 similarly follows the Korsmeyer-Peppas model. Moreover, the release exponents of 5FU-$CaCO_3$np reveal the Fickian diffusion mechanism of 5-FU released from 5FU-$CaCO_3$np, whereas TQ-$CaCO_3$np releases TQ following the non-Fickian transport mechanism (both diffusion and erosion-controlled principal) (Adepu & Ramakrishna 2021). Therefore, the solubility of compounds is crucial in the compound release kinetics and mechanism of compounds released from compound-loaded $CaCO_3$np, where the hydrophilic compound 5-FU releases faster with diffusion-controlled principal and the hydrophobic compound TQ releases slower with both diffusion and erosion-controlled principal.

Table 3.5: Kinetic analysis of compound release from 5FU-$CaCO_3$np and TQ-$CaCO_3$np at pH 7.4, 6.5, and 5.0 using various kinetic models. R^2, regression coefficient; n, release exponent.

Formulation	pH	Zero-order model R^2	First-order model R^2	Higuchi model R^2	Hixon-Crowell model R^2	Korsmeyer-Peppas model	
						R^2	n
5FU-$CaCO_3$np	7.4	0.84579	0.92832	0.96651	0.86380	0.98258	0.38839
	6.5	0.83112	0.90811	0.96204	0.86074	0.98988	0.34495
	5.0	0.76977	0.86509	0.92401	0.83058	0.99084	0.27514
TQ-$CaCO_3$np	7.4	0.95013	0.94527	0.98353	0.95486	0.98578	0.57060
	6.5	0.92144	0.95302	0.98363	0.93512	0.98266	0.53670
	5.0	0.90526	0.92793	0.98557	0.92571	0.98765	0.45530

3.3.6 Cytotoxicity of nanoparticles

Although calcium carbonate nanoparticles are well-known for excellent

biocompatibility and calcium carbonate has been approved by the FDA for clinical application, it is still necessary to evaluate the biocompatibility (such as toxicity and blood compatibility) of nanoparticles due to the potential problems in the process of nanoparticle preparation.

To investigate the cytotoxicity of nanoparticles, normal mouse embryonic fibroblast cell line NIH3T3 was employed as the cell model, and an extended incubation time of 96 h was chosen. According to the standard ISO 10993-5, non-toxicity is considered the reduction of cell viability by no more than 30% (ISO 2009). As demonstrated in Figure 3.9(a), blank $CaCO_3$np exhibited cell viability of more than 75% within the concentration range 0-1000 μg/mL after 96 h incubation, suggesting non-toxic to the NIH3T3 cell line. Figure 3.9(b) reveals that the presence of 5-FU in $CaCO_3$np led to a gradual increase in the cytotoxicity in a concentration-dependent manner, with obvious cytotoxic effects at the high concentrations of 120 and 480 μM. Additionally, the half-maximal inhibitory concentration (IC_{50}) value of 5FU-$CaCO_3$np was 65.33 ± 11.89 μM. In contrast, 5-FU showed much stronger cytotoxicity ($p<0.0001$), with an IC_{50} value of 2.12 ± 0.22 μM. Moreover, TQ was proved to be toxic to the NIH3T3 cell line in Figure 3.9(c), with an IC_{50} value of 21.08±2.49 μM, but TQ-$CaCO_3$np was non-toxic to the NIH3T3 cell line even at the high TQ concentration of 60 μM. This may be attributed to the prolonged release of 5-FU and TQ from $CaCO_3$np under the healthy cell environment of pH 7.4. Therefore, $CaCO_3$np is non-toxic to normal cells and can reduce the toxicity of loaded compounds, especially 5-FU, which has strong toxic effects on normal cells.

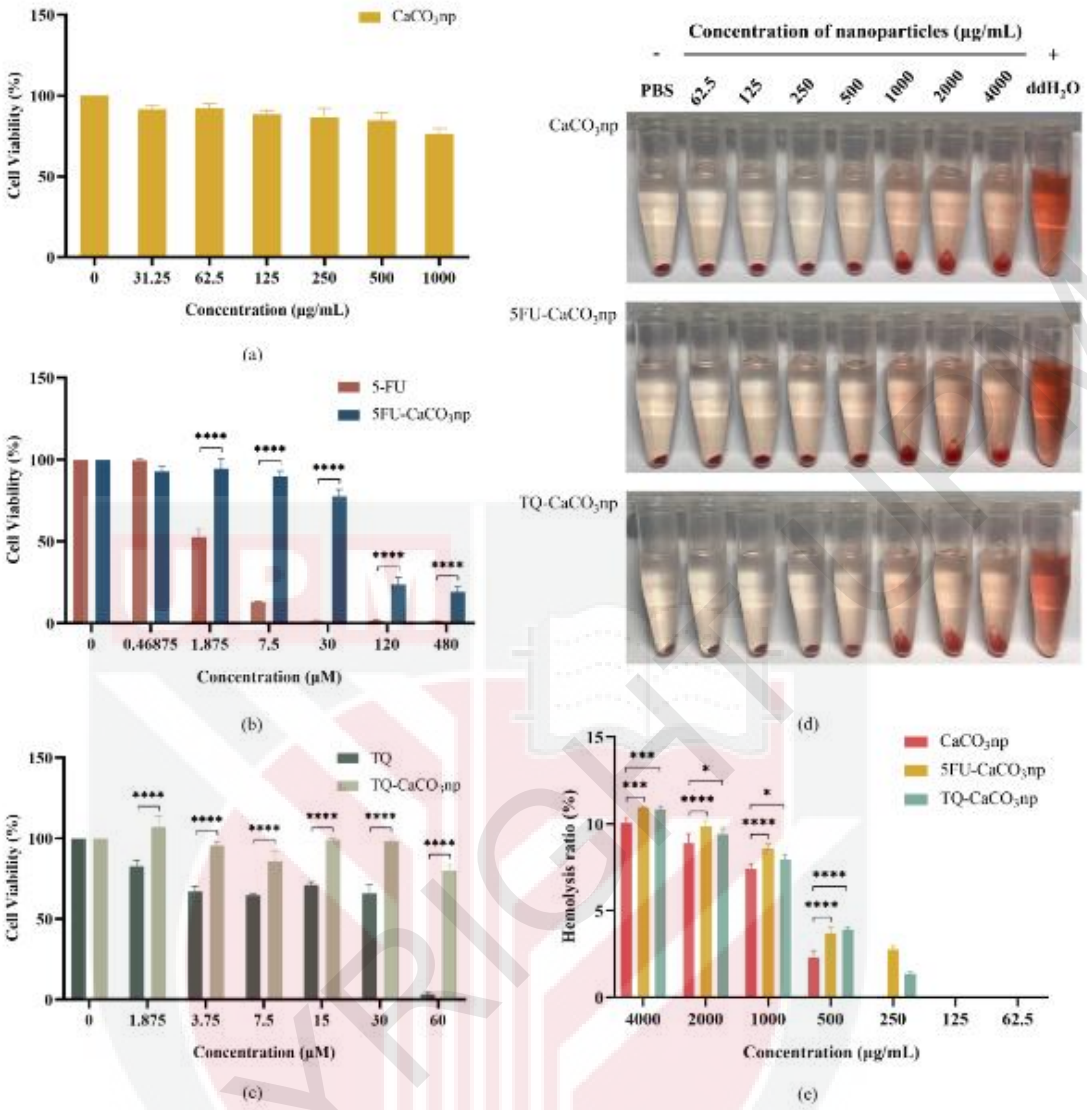

Figure 3.9: (a-c) Cytotoxicity of $CaCO_3$np (0-1000 µg/mL), 5-FU and 5FU-$CaCO_3$np (5FU concentrations: 0-480 µM), as well as TQ and TQ-$CaCO_3$np (TQ concentrations: 0-60 µM) in NIH3T3 mouse embryonic fibroblast cell line at 96 h incubation period; (d) Hemolysis phenomenon of $CaCO_3$np, 5FU-$CaCO_3$np, and TQ-$CaCO_3$np and (e) hemolysis ratio of the three samples. PBS solution and ddH_2O are used as the negative (0% hemolysis) and positive control (100% hemolysis), respectively. The solution with red color means the release of hemoglobin from the damaged erythrocytes and the red pellet at the bottom of the tube is intact erythrocytes by centrifugation. PBS, phosphate buffered saline; ddH_2O, deionized water. *p<0.05, ***p<0.001, ****p<0.0001.

3.3.7 Blood compatibility of nanoparticles

The blood compatibility of $CaCO_3$np, 5FU-$CaCO_3$np, and TQ-$CaCO_3$np was evaluated

by the *in vitro* erythrocyte-induced hemolysis test. This test assesses the release percentage of hemoglobin when nanoparticles are directly in contact with erythrocyte surfaces and cause cell lysis, regarded as the preliminary investigation for the *in vivo* toxicity evaluation of nanoparticles (Mukhopadhyay et al. 2019). During this test, isotonic PBS solution was used as the negative control, and the positive control was deionized water that can induce osmotic shock, leading to hemolysis (Sæbø et al. 2023). Figure 3.9(d) displays the results of the hemolysis test, revealing that the hemolysis of $CaCO_3$np and compound-loaded $CaCO_3$np was concentration-dependent. At the same time, complete lysis (the absence of precipitation) was observed in deionized water-treated erythrocytes. Generally, more than 25% of the hemolysis ratio is considered hemolytic and less than 10% is non-hemolytic (Amin & Dannenfelser 2006). It is seen from Figure 3.9(e) that $CaCO_3$np, 5FU-$CaCO_3$np, and TQ-$CaCO_3$np exhibited low hemolysis rates (below 12%) even at a high concentration (4000 µg/mL). Remarkably, the hemolysis ratio of $CaCO_3$np was significantly better than that of 5FU-$CaCO_3$np and TQ-$CaCO_3$np at every concentration ($p<0.05$), which may be related to the effects of 5-FU and TQ on erythrocytes. Moreover, the three samples with a concentration range from 62.5 to 500 µg/mL showed less than 5% hemolysis activity. Therefore, it can be obtained that the synthesized $CaCO_3$np, 5FU-$CaCO_3$np, and TQ-$CaCO_3$np possess great blood biocompatibility.

3.3.8 Toxicity of nanoparticles on brine shrimp

Brine shrimp (*Artemia salina*), an invertebrate species belonging to the zooplankton, was used to explore the toxicity of nanoparticles, owing to its advantages of a fast life cycle, adaptability to laboratory conditions, and low maintenance costs (Pinheiro et al. 2023; Rajabi et al. 2015). Moreover, Ntungwe N et al. (2020) reported a significant

correlation ($r = 0.85$; $p<0.05$) between lethal concentration 50 (LC_{50}) values from the brine shrimp assay and lethal dose 50 values from acute oral toxicity tests in mice. Based on the brine shrimp survival results after treatment of positive control $KMnO_4$, $KMnO_4$ exhibited toxicity to brine shrimp, with a LC_{50} value of 433.07 ± 77.00, 306.73 ± 18.91, and 110.23 ± 4.35 µg/mL within 24, 36, and 48 h of exposure, respectively. According to Clarkson's toxicity index, KMnO4 is non-toxic (LC_{50} value more than 1000 µg/mL) within 12 h of exposure but moderately toxic (LC_{50} value between 500 and 100 µg/mL) after further extended exposure to 24, 36, and 48 h (Clarkson et al. 2004). By contrast, the brine shrimp toxicity tests of $CaCO_3$np, 5FU-$CaCO_3$np, and TQ-$CaCO_3$np did not show any sign of toxicity since no dead brine shrimp was recorded in different concentrations of nanoparticles even for 48 h of incubation, indicating $CaCO_3$np, 5FU-$CaCO_3$np, and TQ-$CaCO_3$np are non-toxic. Moreover, the morphology of brine shrimp was observed using light microscopy. Figures 3.10(a) and (b) display the live brine shrimp with an eye, swimming legs, swimming setae, gut, and anus, whereas dead brine shrimp with damaged body exhibits in Figures 3.10(c) and (d). Based on these findings, and considering the results from blood compatibility evaluation and cytotoxicity analysis, the synthesized $CaCO_3$np is safe for drug delivery in the body, and the prepared 5FU-$CaCO_3$np and TQ-$CaCO_3$np have excellent blood biocompatibility.

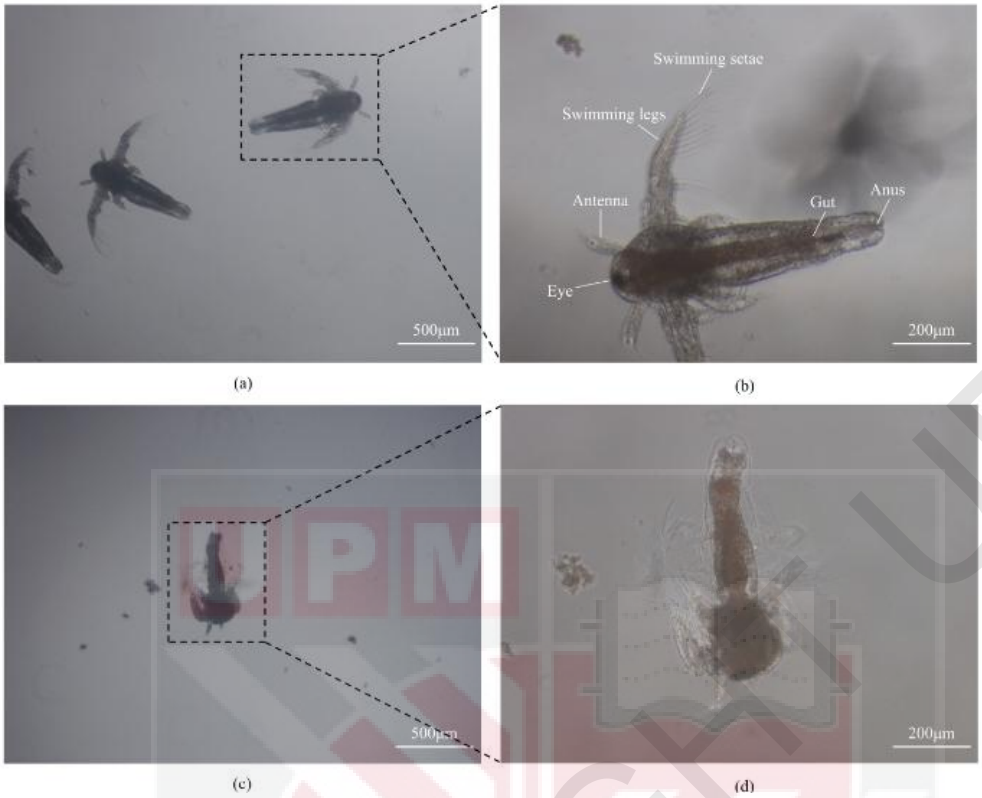

Figure 3.10: Live brine shrimp (a) at ×4 magnification and (b) at ×10 magnification; dead brine shrimp (c) at ×4 magnification and (d) at ×10 magnification.

3.4 Conclusion

In summary, porous cockle shell-derived calcium carbonate nanoparticles with a particle size of around 80 nm were developed using a facile mechanical ball milling method to deliver compounds 5-FU and TQ. This is the first attempt wherein different loading techniques, including using a shaking incubator and a high-speed homogenizer, have been explored for improving the loading capacity and encapsulation efficiency for the hydrophilic compound 5-FU and the hydrophobic compound TQ loaded into nanoparticles. As demonstrated, the high-speed homogenizer exhibited better compound loading results than the shaking incubator. Meanwhile, based on the loading results, a 1:20 weight ratio of 5-FU to $CaCO_3$np at 6000 rpm for 3 min and a 1:2 weight

ratio of TQ to $CaCO_3$np at 24000 rpm for 3 min were chosen as the best formulation for 5-FU and TQ loading, respectively. In addition, the high-speed homogenizer can result in a more efficient and homogenous compound loading, making it suitable for large-scale manufacturing of compound-loaded $CaCO_3$np. Therefore, the high-speed homogenizer was used as the compound loading method, and the best formulations were employed for the following studies.

HRTEM and Zetasizer determined the size of compound-loaded $CaCO_3$np is 100-140 nm and negative zeta potential, with the potential of prolonged circulating half-lives in the body. EDX, XRD, and FTIR results revealed that the synthesized $CaCO_3$np is pure aragonite calcium carbonate nanoparticles, and 5-FU and TQ were successfully loaded into $CaCO_3$np without chemical reaction or change in the aragonite phase. Besides, 5FU-$CaCO_3$np and TQ-$CaCO_3$np showed pH sensitivity that compound-loaded $CaCO_3$np release compounds faster at pH 6.5 and 5.0 of the cellular environment in malignant tumors than at pH 7.4 of the blood and healthy tissue environment. Furthermore, excellent blood compatibility of $CaCO_3$np and compound-loaded $CaCO_3$np, non-cytotoxicity toward normal NIH3T3 cell line (except for much less cytotoxicity of 5FU-$CaCO_3$np than 5-FU), and non-toxicity to brine shrimp were demonstrated. All these results indicated that the proposed $CaCO_3$np could be a promising compound delivery carrier, and 5FU-$CaCO_3$np and TQ-$CaCO_3$np synthesized by high-speed homogenizer could be promising cancer therapies with potential clinical applications.

CHAPTER 4

THYMOQUINONE-LOADED CALCIUM CARBONATE NANOPARTICLES IN COMBINATION WITH 5-FLUOROURACIL AGAINST COLON CANCER *IN VITRO*

4.1 Introduction

Combination therapy has emerged as an effective strategy in cancer treatment, aiming to enhance therapeutic efficacy by using multiple agents that target different pathways or mechanisms within cancer cells (Rejhová et al. 2018). The rationale behind combination therapy lies in the potential for synergistic interactions between drugs, which can lead to enhanced cancer cell death, reduced drug resistance, and minimized side effects compared to monotherapies (Boța et al. 2024; Mokhtari et al. 2017). In colon cancer, where drug resistance and recurrence are significant challenges, combining chemotherapeutic agents with natural compounds has shown promise. TQ, a bioactive compound derived from *Nigella sativa*, has demonstrated anticancer properties, including pro-apoptotic and anti-inflammatory effects, making it a compelling candidate for combination with conventional chemotherapy drugs like 5-FU (Lei et al. 2012; Zheng et al. 2021).

Based on the previous findings of the optimal formulations of 5FU-$CaCO_3$np and TQ-$CaCO_3$np, this chapter aimed to explore the combinatorial uses of 5FU-$CaCO_3$np or TQ-$CaCO_3$np for colon cancer treatment. In the pre-experiments, 5FU-$CaCO_3$np was combined with TQ-$CaCO_3$np against colon cancer CT26 cells. However, the combination of 5FU-$CaCO_3$np and TQ-$CaCO_3$np showed no synergistic therapeutic

effects at any concentration combination in CT26 cells. Therefore, the therapeutic potential of other combinatorial uses of 5FU-$CaCO_3$np or TQ-$CaCO_3$np, including 5FU-$CaCO_3$np combined with TQ and TQ-$CaCO_3$np combined with 5-FU, against colon cancer was investigated. The synergistic effects of these two combinations on colon cancer CT26 cells were compared to obtain the superior combination therapy for colon cancer treatment. Subsequently, a series of *in vitro* experiments were designed to investigate the efficacy of the superior combination therapy on colon cancer cell proliferation, apoptosis, migration, and spheroid growth, in comparison to the individual treatments.

4.2 Materials and methods

4.2.1 Cell culture

Colon cancer CT26 cells were cultured in RPMI-1640 medium supplemented with 10% (v:v) fetal bovine serum and 1% (v:v) antibiotic solution (100 U/mL penicillin and 100 mg/mL streptomycin) at 37°C in a 5% CO_2 humidified atmosphere.

4.2.2 MTT assay of TQ-$CaCO_3$np in combination with 5-FU and 5FU-$CaCO_3$np in combination with TQ

Colon cancer CT26 cells were seeded in 96-well plates for 24 h and treated with different concentrations of TQ-$CaCO_3$np, 5-FU, or in combination and 5FU-$CaCO_3$np, TQ, or in combination for 96 h. After treatment, the cells were incubated with MTT reagent for 4 h. The purple formazan crystals formed were solubilized with DMSO, and the absorbance at 570 nm (630 nm as the reference wavelength) was measured using the multimode microplate reader (Synergy H1, BioTek, USA). The cell viability

was determined with respect to the untreated control. IC_{50} value was calculated by nonlinear regression analysis in GraphPad Prism 8 software

4.2.3 Synergism analysis and comparison of the two combinations

The combination index (CI) was calculated using CompuSyn software as established by Chou and Talalay, where CI > 1 indicates antagonism, CI = 1 indicates additive, and CI < 1 indicates synergism (Chou 2008). The CI values of the two combinations were compared and the combination with the best CI value was chosen for further study.

4.2.4 Colony formation assay

After being cultured in 6-well plates for 48 h, CT26 cells were treated with TQ-$CaCO_3$np, 5-FU, and their combination. After treatment, the cells were allowed to form colonies for 7 days until the colonies were visible. They were then fixed with 100% methanol and stained with 0.5% crystal violet. The cells were photographed using a light microscope attached to a digital camera. The number of colonies was calculated using ImageJ software.

4.2.5 AO/PI staining

Following 96 h of treatment with TQ-$CaCO_3$np and 5-FU either alone or in combination, CT26 cells were washed with PBS and stained with 5 µg/mL acridine orange/propidium iodide (AO/PI) dual stain for 10 min at room temperature. The cells were photographed using an inverted fluorescence microscope (Carl Zeiss Microscopy GmbH, Germany). AO-viable cell density was calculated using ImageJ software

according to the presence or absence of non-viable cell staining (PI).

4.2.6 Cell cycle and apoptosis analysis

CT26 cells were cultured in 6-well plates with TQ-$CaCO_3$np and 5-FU either alone or in combination for 96 h. For cell cycle analysis, after being fixed in ethanol overnight at 4°C, cells were resuspended in PBS and exposed to RNase A solution (10 mg/mL) and PI solution (50 µg/mL) in the dark for 30 min. For apoptosis analysis, cells were resuspended in 1× binding buffer and stained with 5 µL of Annexin V-FITC and 5 µL of PI in the dark for 20 min. Thereafter, cell cycle and apoptosis were measured by the BD FACSCanto II flow cytometer (BD Biosciences, USA) and analyzed by BD FACSDiva software.

4.2.7 Wound healing assay

CT26 cells were seeded in 6-well plates and scraped with a sterile pipette tip when the cells achieved 90% confluence. The scratched cells were then cultured with TQ-$CaCO_3$np and 5-FU either alone or in combination for 48 h. Images were captured using an inverted fluorescence microscope after 0, 24, and 48 h. The wound healing area was measured and analyzed using ImageJ software.

4.2.8 3D spheroid culture

CT26 cells were seeded in agarose (50 µL, 0.6%, Sigma-Aldrich)-coated 96-well plates at 2000, 4000, 6000, 8000, 10000, 15000, and 20000 cells/well and incubated for 13 days at 37°C. Spheroids were observed and imaged using a light microscope on days 4, 7, 10, and 13. Image J software was used to measure the diameter of spheroids

and determine the volume of spheroids.

Spheroid volume (mm^3) = length of spheroid × (width of spheroid)^2 /2.

4.2.9 3D spheroid inhibition assay

CT26 cell seeding density was chosen for obtaining the spheroids with a diameter of 400-500 μM after 4-day incubation. Spheroids were then cultured with TQ-$CaCO_3$np and 5-FU either alone or in combination for 96 h and imaged for a period of 14 days using a light microscope. The diameter and volume of spheroids were determined using Image J software.

4.2.10 Statistical analysis

Data analysis was performed with at least triplicates using the GraphPad Prism 8 and Origin 2022 software. Statistical analysis involved one-way ANOVA followed by Turkey's post-test for multiple comparisons or Student's t-test for a single comparison and two-way ANOVA followed by Dunnett's post-test. P value < 0.05 ($p<0.05$) was considered statistically significant. Unless otherwise stated, the results were expressed as mean ± standard deviation.

4.3 Results and discussion

4.3.1 Superior combination against colon cancer

In the MTT pre-experiments, the inhibitory effects of 5FU-$CaCO_3$np and TQ-$CaCO_3$np on CT26 cells were compared over culture periods of 24, 48, 72, and 96 h. The results showed that the inhibitory effect was optimal at 96 h, which may be attributed to the sustained-release properties of 5FU-$CaCO_3$np and TQ-$CaCO_3$np.

Therefore, a 96-hour culture period was selected for the *in vitro* experiments. As shown in Figures 4.1A and C, 5FU-$CaCO_3$np, TQ-$CaCO_3$np, 5-FU, and TQ all exhibited concentration-dependent inhibitive effects on the cell viability of CT26 cells, with the IC_{50} values of 5.06, 23.35, 17.23, and 13.66 μM, respectively. In detail, Figure 4.1C displays a decreasing trend of cell viability while pure 5-FU concentration increased. Remarkably, 5FU-$CaCO_3$np showed a more pronounced reduction within the 0-7.5 μM in Figure 4.1A, indicating that the delivery system made 5-FU more effective against the cancer cells, with a lower IC_{50} value. However, at concentrations exceeding 7.5 μM, the decrease in cell viability following treatment with 5FU-$CaCO_3$np was gradual, with 5-FU exhibiting a more potent inhibitory effect on cell viability than 5FU-$CaCO_3$np. This outcome suggested a sustained and prolonged 5-FU release from 5FU-$CaCO_3$np (Bai et al. 2022). Therefore, $CaCO_3$np was proven to improve the targeted delivery of 5-FU to the colon cancer site. On the other hand, CT26 cell viability showed a slight reduction before the TQ concentration of 30 μM and a sharp decrease at 30 μM in Figure 4.1A. Although the IC_{50} value of TQ was better than that of TQ-$CaCO_3$np, the cell viability exhibited a gradually continuous downward trend after TQ-$CaCO_3$np treatment in Figure 4.1C, indicating that $CaCO_3$np improved the bioavailability of TQ, thereby resulting in a sustained and prolonged TQ release from TQ-$CaCO_3$np (Elumalai, Srinivasan & Shanmugam 2024; Huang et al. 2024). Overall, 5FU-$CaCO_3$np and TQ-$CaCO_3$np enhanced the accumulation of 5-FU and TQ in colon cancer CT26 cells due to the pH sensitivity of $CaCO_3$np, respectively, while decreasing. Therefore, $CaCO_3$np loaded with 5-FU and TQ improved therapeutic efficacy in colon cancer CT26 cells and minimized the toxicity of 5-FU and TQ to normal NIH3T3 cells. Importantly, 5FU-$CaCO_3$np and TQ-$CaCO_3$np allowed for the controlled release of 5-FU and TQ, respectively, ensuring a sustained therapeutic effect.

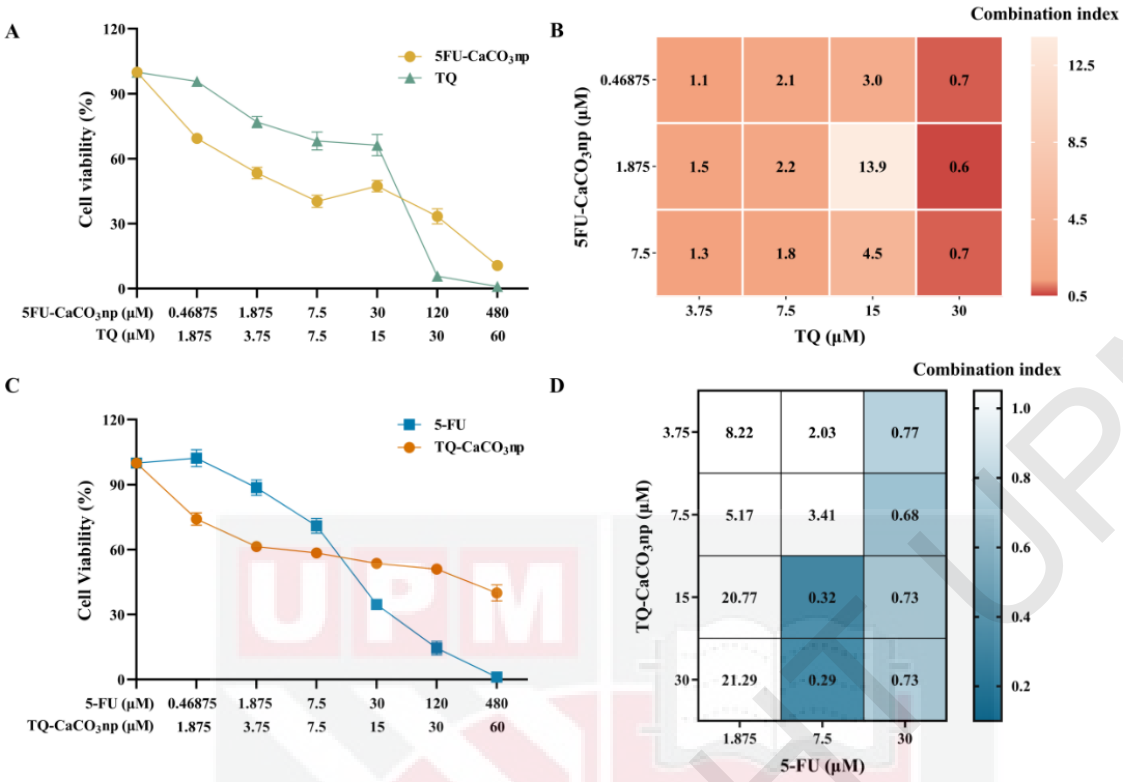

Figure 4.1: (A) Cytotoxicity of 5FU-$CaCO_3$np (5-FU: 0-480 µM) and TQ (0-60 µM) individually on CT26 cells for 96 h; (B) combination index heat map of 5FU-$CaCO_3$np and TQ in combination against CT26 cells; (C) cytotoxicity of TQ-$CaCO_3$np (TQ: 0-60 µM) and 5-FU (0-480 µM) individually on CT26 cells for 96 h; (D) combination index heat map of TQ-$CaCO_3$np and 5-FU in combination against CT26 cells.

On the basis of IC_{50} values, the combined concentrations of 0.46875, 1.875, and 7.5 µM for 5FU-$CaCO_3$np and 3.75, 7.5, 15, and 30 µM for TQ were selected, whereas the inhibitory effect of TQ-$CaCO_3$np (3.75, 7.5, 15, 30 µM) combined with 5-FU (1.875, 7.5, 30 µM) on CT26 cells was evaluated. The CI value of every combination was calculated to elucidate the synergistic effects of the two treatments (Duarte & Vale 2022a). In Figures 4.1B and D, the results showed that the CI values of 7.5 µM 5-FU combined with TQ-$CaCO_3$np (15 and 30 µM) and 30 µM 5-FU combined with TQ-$CaCO_3$np (3.75-30 µM) were all less than 1, indicating there was a synergistic effect between TQ-$CaCO_3$np and 5-FU. In contrast, only when the concentration of TQ was 30 µM, the combination of 5FU-$CaCO_3$np and TQ showed synergism, with CI values

0.6-0.7. Among all synergistic groups, 30 μM TQ-$CaCO_3$np combined with 7.5 μM 5-FU had the lowest CI value, suggesting the strongest synergistic effect, followed by 15 μM TQ-$CaCO_3$np combined with 7.5 μM 5-FU. However, considering that a smaller dose can achieve similar effects, 15 μM TQ-$CaCO_3$np combined with 7.5 μM 5-FU was selected to further analyze its inhibitive effects on colon cancer.

The synergism of two treatments can be inferred when the combination of the treatments at specific doses produces an effect greater than the sum of the effects achieved by the individual treatments at the same doses (Chou 2010). The CI values were calculated to measure the extent of drug interactions and revealed the optimal synergistic combination (CI = 0.32) of TQ-$CaCO_3$np and 5-FU against CT26 cells. The combinatorial effects of 5FU-$CaCO_3$np and TQ also showed synergism. Notably, the optimal CI value of TQ-$CaCO_3$np and 5-FU was superior to that (0.60) of 5FU-$CaCO_3$np and TQ, indicating that TQ-$CaCO_3$np and 5-FU exhibited better synergistically inhibitory effects on CT26 cells.

4.3.2 Cell proliferation inhibition

The colony-formation assay results clearly demonstrated the inhibitory effects of both TQ-$CaCO_3$np (15 μM) and 5-FU (7.5 μM) on CT26 cell proliferation. The significant reduction in colony numbers, with averages of 286 and 262 for TQ-$CaCO_3$np and 5-FU treatments, respectively, compared with the average of 555 in the control group, indicated that both treatments effectively limit the clonogenic capacity of colon cancer cells (Figure 4.2). In addition, as shown in Figure 4.2, the AO/PI staining results confirmed the reduction in viable cells after treatment, highlighting the cytotoxic effects of both agents. In this study, the AO/PI assay was used to examine the inhibitory

effects of TQ-$CaCO_3$np and 5-FU individually or in combination on cell proliferation, focusing on the quantification of viable cells after treatments. Therefore, after multiple washes of the cells, the remaining dead cells stained with PI were excluded from the number of viable cells. Notably, the combination of TQ-$CaCO_3$np and 5-FU exhibited a more pronounced suppression of colony formation and CT26 cell growth, aligning with the synergistic effect observed in the MTT assay. Overall, these findings imply the synergistic inhibitive effects between TQ-$CaCO_3$np and 5-FU on cell proliferation in colon cancer.

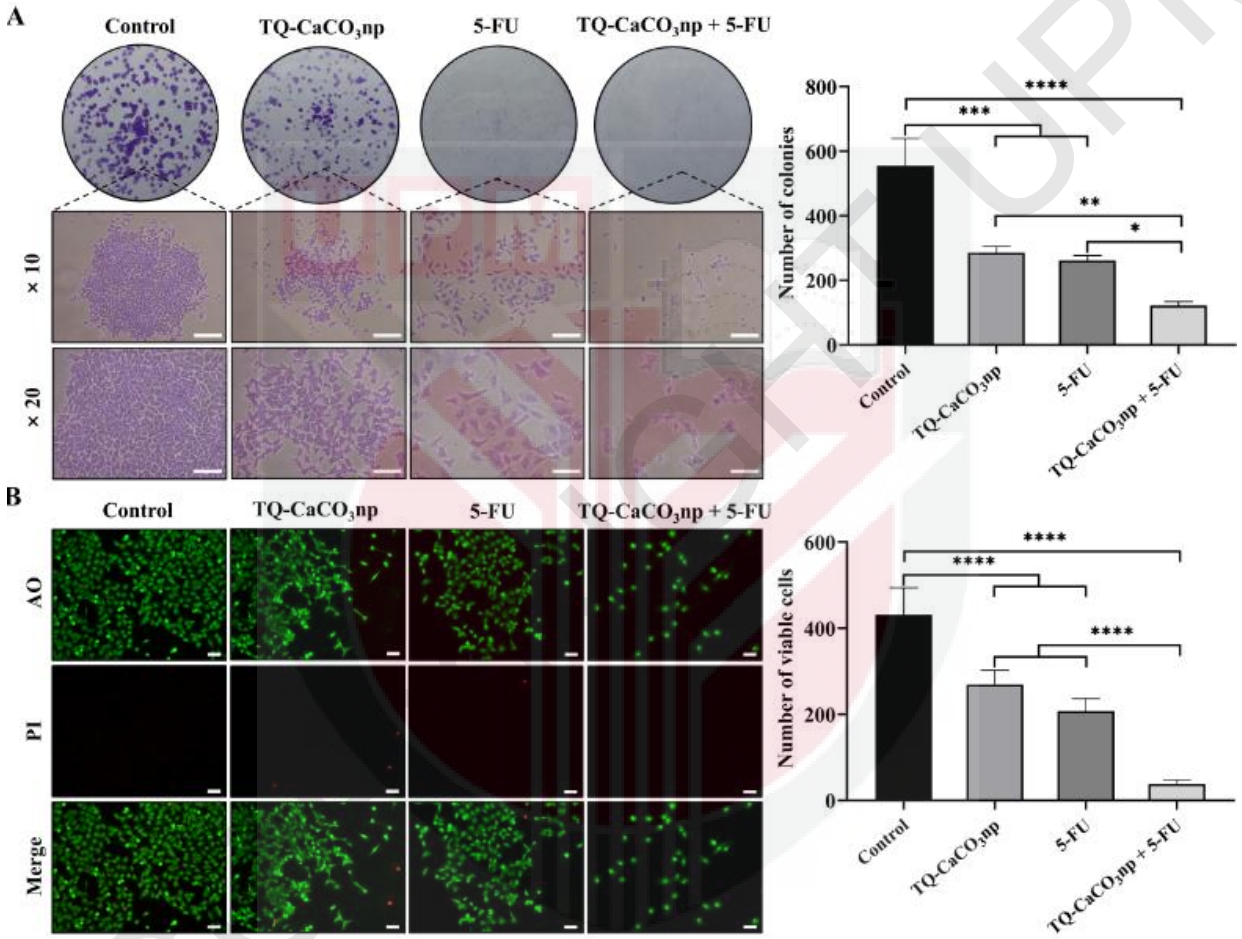

Figure 4.2: (A) colony formation assay of CT26 cells treated with TQ-CaCO3np (15 µM) and 5-FU (7.5 µM) alone or in combination, with the represented images under ×10 magnification (scale bar: 200 µm) and ×20 magnification (scale bar: 100 µm); (B) AO/PI staining assay of CT26 cells treated with TQ-CaCO3np (15 µM) and 5-FU (7.5 µM) alone or in combination, with the represented images (scale bar: 100 µm) where viable cells in green by AO staining and non-viable cells in red by PI staining. *p<0.05, **p<0.01, ***p<0.001, ****p<0.0001.

Colony formation assays are particularly valuable in assessing the long-term effects of drug treatments on cancer cells, as they reflect the ability of single cells to survive, proliferate, and form colonies (Franken et al. 2006). The significant reduction in colony numbers following treatment with TQ-$CaCO_3$np and 5-FU indicated that both agents impaired the ability of CT26 cells to undergo proliferation over time. This suggests that the combination therapy not only induced acute cytotoxicity but also had a lasting impact on the reproductive viability of the cells (Forgie et al. 2024). The AO/PI staining assay complements these findings by confirming that the reduction in colony formation is indeed due to a loss of cell viability rather than a temporary arrest in cell growth. This dual approach provides a robust assessment of the anticancer effects of the treatments (Gordon, Brown & Reynolds 2018; Zhong et al. 2015).

4.3.3 Cell cycle arrest and cell apoptosis induction

The effects of TQ-$CaCO_3$np in combination with 5-FU on cell cycle and apoptosis in CT26 cells were evaluated to investigate the underlying mechanism of TQ-$CaCO_3$np combined with 5-FU against colon cancer. As illustrated in the flow cytometry results in Figure 4.3A, cells treated with 5-FU or TQ-$CaCO_3$np combined with 5-FU prominently increased G_0/G_1 phase arrest and reduced cell number in the S and G_2/M phases. However, after TQ-$CaCO_3$np treatment, the proportion of cells in the S phase increased slightly, while that in the G_0/G_1 phase decreased slightly, and that in the G_2/M phase had no obvious change, indicating that TQ-$CaCO_3$np may arrest the cell cycle in the S phase. Additionally, treatment with TQ-$CaCO_3$np or 5-FU alone resulted in significant apoptosis of CT26 cells ($p<0.05$) (Figure 4.3B). The co-treatment of TQ-$CaCO_3$np and 5-FU showed a significant increase in the apoptotic cells (69.40%), including 54.17% of early apoptosis and 15.23% of late apoptosis, compared with the

individual treatments ($p<0.05$). In conclusion, the combination of TQ-$CaCO_3$np (15 µM) and 5-FU (7.5 µM) exerted synergistic antiproliferative effects on CT26 cells by inducing cell cycle arrest and apoptosis, ultimately causing cell death.

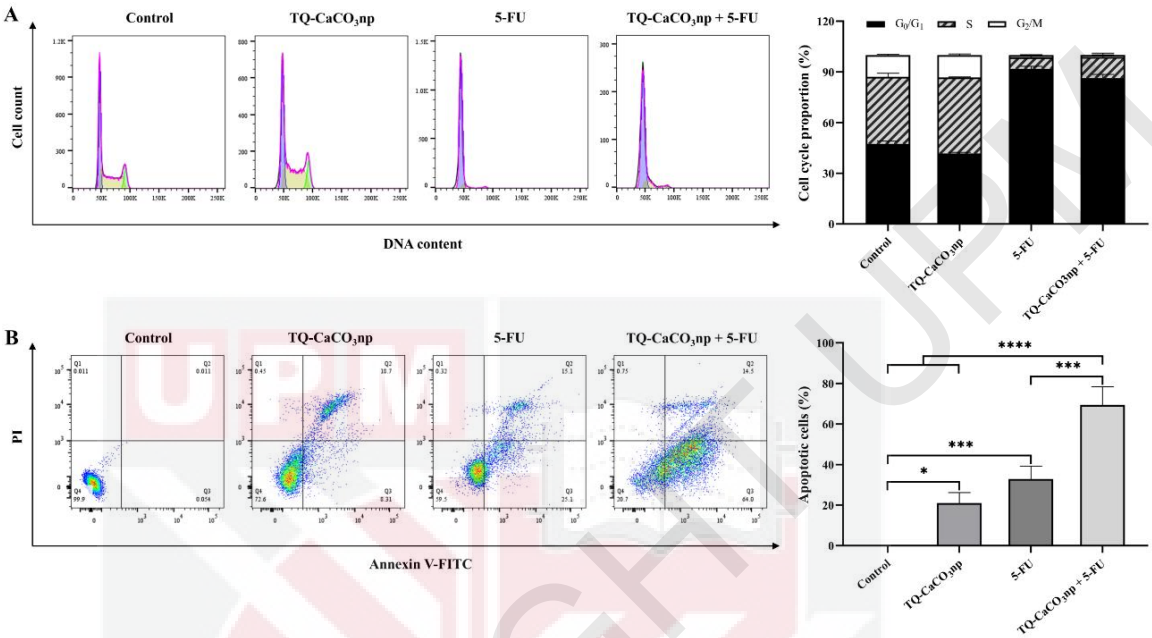

Figure 4.3: (A) Cell cycle assay of CT26 cells treated with TQ-$CaCO_3$np (15 µM) and 5-FU (7.5 µM) alone or in combination, with the represented images displaying cell cycle distributions; (B) Annexin V-FITC assay of CT26 cells treated with TQ-$CaCO_3$np (15 µM) and 5-FU (7.5 µM) alone or in combination, with the represented images depicting cells in different quadrants: necrosis (Q1), late apoptosis (Q2), early apoptosis (Q3), and live (Q4), where Q2 and Q3 are collectively called apoptotic cells. *$p<0.05$, ***$p<0.001$, ****$p<0.0001$.

5-FU increased the G_0/G_1 phase arrest of CT26 cells and reduced the cell number in the S and G_2/M phases, consistent with the mechanism of 5-FU, which inhibits thymidylate synthase, leading to the inhibition of DNA synthesis, induction of DNA damage, and a halt in cell cycle progression in the G1 or S phase (Vodenkova et al. 2020). In contrast, TQ-$CaCO_3$np slightly increased the cell number in the S phase and decreased in the G_0/G_1 phase. However, TQ-$CaCO_3$np and 5-FU combination prominently induced G_0/G_1 and S phases' cell cycle arrest in CT26 cells, suggesting that TQ-$CaCO_3$np may enhance the efficacy of 5-FU by further reinforcing the cell

cycle arrest in G_0/G_1 and S phases, resulting in a stronger inhibitory effect on cell proliferation. The enhancement of 5-FU inhibition of cell proliferation by TQ-$CaCO_3$np was further confirmed in the cell apoptosis assay. The increase in both early and late apoptosis indicates that the combination treatment not only halts the cell cycle but also promotes programmed cell death, further enhancing its anticancer efficacy. While the mechanism of 5-FU is predominantly linked to DNA damage and cell cycle arrest, TQ has been reported to activate multiple apoptotic pathways, including the mitochondrial pathway, which may explain the increase in cell death when used in combination (Farooqi, Attar & Xu 2022; Ma et al. 2020). As demonstrated, the ability of TQ to modulate apoptosis pathways can enhance the efficacy of conventional chemotherapeutic agents including 5-FU (Ballout et al. 2020; Idris et al. 2022; Khan et al. 2017; Zhang, Bai & Yang 2016b). Therefore, the combination of TQ-$CaCO_3$np and 5-FU exerted its antiproliferative effects through a dual mechanism involving both enhanced cell cycle arrest and increased apoptosis.

4.3.4 Cell migration inhibition

A wound healing assay was performed to investigate the potential effects of TQ-$CaCO_3$np in combination with 5-FU on CT26 cell migration rate. As displayed in Figure 4.4, both TQ-$CaCO_3$np and 5-FU exhibited a potent migration-inhibiting efficiency on CT26 cells. Nonetheless, the inhibitory effects of TQ-$CaCO_3$np combined with 5-FU were more noticeable than TQ-$CaCO_3$np or 5-FU alone, as the wound closure was distinctly disrupted. These results suggested that TQ-$CaCO_3$np (15 μM) and 5-FU (7.5 μM) synergistically inhibited the migration of CT26 cells.

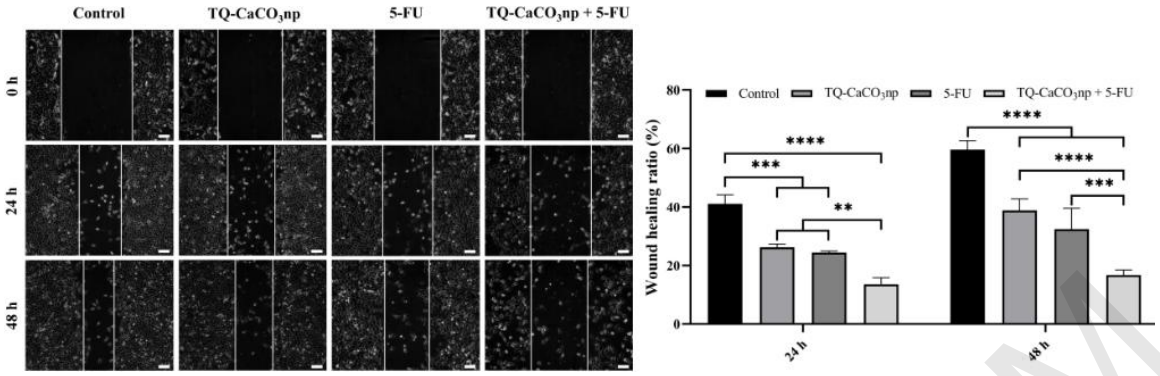

Figure 4.4: Wound healing assay of CT26 cells treated with TQ-$CaCO_3$np (15 µM) and 5-FU (7.5 µM) alone or in combination, with the represented images (scale bar: 100 µm) showing cell migration after 24 and 48 h. ** $p<0.01$, *** $p<0.001$, **** $p<0.0001$.

Cancer cell migration is an essential step for successful cancer metastasis associated with substantial mortality after surgical resection of primary cancer; thereby, inhibiting cell migration is a practical approach for anticancer therapy (Jiang et al. 2015; Xie et al. 2022). The wound-healing assay results revealed that TQ-$CaCO_3$np and 5-FU inhibited CT26 cell migration, while TQ-$CaCO_3$np combined with 5-FU exerted a more significant migration-inhibitory effect. Previous studies have also highlighted the anti-migratory properties of 5-FU and TQ in various cancer models, showing their abilities to suppress key proteins involved in cell migration, such as matrix metalloproteinases, membrane-associated RING-CH-1, and eukaryotic elongation factor 2 kinase, further supporting the potential of TQ-$CaCO_3$np in enhancing the efficacy of 5-FU against cell migration (Kabil et al. 2018; Park et al. 2021; Wang et al. 2021a).

4.3.5 3D spheroid growth suppression

Compared with conventional 2D cells, 3D spheroids provide a similar tissue structure with intact human tumors, consisting of concentric layers including proliferating zone,

quiescent zone, and necrotic core (Nath & Devi 2016). Different cell seeding densities were applied to monitor the size of CT26 spheroids. Figure 4.5 revealed that the size of spheroids was strongly dependent on the initial cell seeding density. CT26 spheroids formed at the initial cell seeding density of 15000 cells/well and cultured for 4 days had a diameter of 400-500 µm, conforming to the concentrically layered structure, thus serving as the model for spheroid inhibition analysis (Mehta et al. 2012).

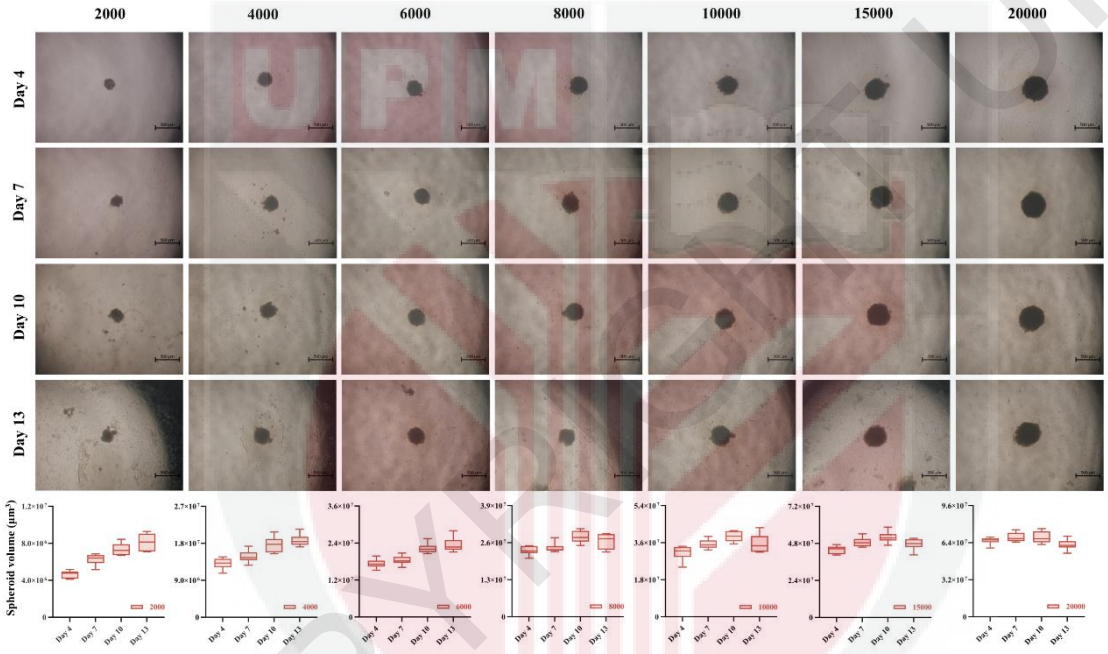

Figure 4.5: CT26 spheroid growth analysis for culturing 13 days, with the represented images (scale bar: 500 µm) showing that spheroid size and growth trend depend on the initial cell seeding density (2000 to 20000 cells/well).

After spheroid formation on day 4, CT26 spheroids were treated with TQ-$CaCO_3$np (15 µM) and 5-FU (7.5 µM) alone or in combination for 96 h. While untreated spheroids increased in size, both TQ-$CaCO_3$np and 5-FU exhibited inhibitory effects on spheroid growth (Figure 4.6). Besides, cell proliferation was significantly inhibited after incubation with the combination of TQ-$CaCO_3$np and 5-FU ($p<0.05$), and the outer layer of spheroids was severely destroyed on day 14, compared to the control spheroids. These data indicated that TQ-$CaCO_3$np combined with 5-FU could

significantly suppress CT26 spheroid growth.

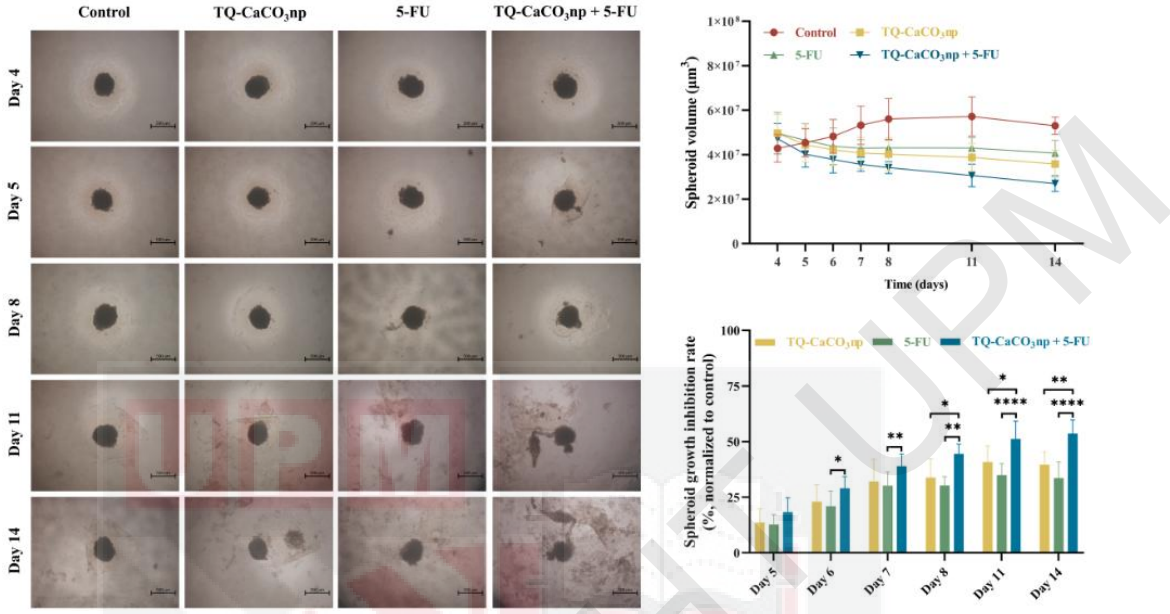

Figure 4.6: Growth inhibition analysis of CT26 spheroids treated with TQ-$CaCO_3$np (15 µM) and 5-FU (7.5 µM) alone or in combination, with the represented images (scale bar: 500 µm) displaying the spheroid volume and growth inhibition. *p<0.05, **p<0.01, ****p<0.0001.

Before clinical trials, drugs must undergo a series of tests to ensure their effectiveness and safety, the first step of which is usually *in vitro* experiments based on 2D cells. However, compared with traditional 2D cells, 3D cell spheroids *in vitro* models with similar characteristics to solid tumors *in vivo* can better predict drug effects, bridging the gap between in vitro 2D cells and *in vivo* animal models (Nath & Devi 2016). In this study, agarose-based liquid overlay technology was applied to produce 3D spheroids, which has the advantage of allowing rapid aggregation of cells into spheroids with reproducible morphology (Jubelin et al. 2022). Typically, when 3D spheroids are 400–500 µm in size, cell layers similar to those in solid tumors can be formed, including an outer layer composed of proliferating cells, a middle layer of quiescent cells, and a hypoxic inner layer of necrotic cells (Mehta et al. 2012).

However, limited literature has explored the optimal initial cell seeding density for CT26 cells to form the expected spheroid size. To achieve a 3D spheroid size typical of solid tumors, we used increased cell seeding densities (2000, 4000, 6000, 8000, 10,000, 15,000, and 20,000 cells/well) to culture spheroids. It was observed that when the cell density was 15,000 cells/well, the spheroids cultured for 4 days were stable and uniform and reached the expected size, thereby being used for a spheroid-inhibition assay. As observed in Figure 4.6, 5-FU had a less inhibitive effect on CT26 spheroids, possibly due to the spheroids exhibiting resistance to 5-FU. Nonetheless, the addition of TQ-$CaCO_3$np to 5-FU showed a high inhibitory effect on the spheroids, indicating that TQ-$CaCO_3$np enhanced the chemosensitivity of 5-FU to CT26 spheroids, thereby improving the therapeutic effect on colon cancer. Especially after 3 days of treatment, the inhibitory effect of 5-FU and TQ-$CaCO_3$np co-treatment was significantly better than that of the individual treatment ($p<0.05$).

4.4 Conclusion

Taken together, TQ-$CaCO_3$np combined with 5-FU exhibited superior synergistic anti-colon cancer effects than 5FU-$CaCO_3$np combined with TQ in CT26 cells. Moreover, TQ-$CaCO_3$np combined with 5-FU showed synergism by inhibiting CT26 cell proliferation and migration, inducing cell apoptosis and cell cycle arrest in G0/G1 phase, and suppressing CT26 spheroid growth. In other words, TQ-$CaCO_3$np effectively enhanced the anti-colon cancer efficacy of 5-FU, indicating possibly reducing 5-FU dose while improving its effects, thereby decreasing the toxic effects of 5-FU. These findings may open new possibilities for colon cancer treatment. Therefore, it is imperative to further verify TQ-$CaCO_3$np combined with 5-FU *in vivo* therapeutic efficacy and comprehensive therapeutic mechanisms against colon cancer.

CHAPTER 5

THYMOQUINONE-LOADED CALCIUM CARBONATE NANOPARTICLES IN COMBINATION WITH 5-FLUOROURACIL AGAINST COLON CANCER *IN VIVO*

5.1 Introduction

To advance the understanding of the therapeutic potential of TQ-$CaCO_3$np combined with 5-FU, it is necessary to move beyond *in vitro* experiments and assess its effects in a more dynamic and biologically relevant *in vivo* setting. *In vitro* studies, while informative, are limited in their ability to replicate the complexity of living organisms, where factors such as the tumor microenvironment, immune response, and systemic drug interactions play critical roles (Kciuk et al. 2023; Saeidnia, Manayi & Abdollahi 2016; Xu et al. 2023c). Utilizing an *in vivo* model, such as CT26 tumor-bearing mice, allows for a more comprehensive evaluation of the treatment efficacy and safety (Demeckova et al. 2022; Makaremi et al. 2021). This model not only facilitates the investigation of tumor growth inhibition but also provides insight into potential immune modulation and toxicological effects that are crucial for translating laboratory findings into clinical practice (Zhu et al. 2016a). Furthermore, the interaction between the nanoparticles and the immune system in a living organism is a key area of interest, as nanoparticles have been shown to influence immune responses, potentially enhancing or suppressing tumor activity (Lôbo et al. 2021; Perez-Potti et al. 2023).

Therefore, this chapter focuses on evaluating the *in vivo* anticancer efficacy of the combination of TQ-$CaCO_3$np and 5-FU using the CT26 tumor-bearing mouse model.

While previous *in vitro* studies demonstrated that TQ-$CaCO_3$np significantly enhanced the anti-colon cancer effects of 5-FU in CT26 cells, it is crucial to validate these findings in a more complex and physiologically relevant *in vivo* system and explore the therapeutic potential of this combination in mice, assessing its impact on tumor growth, immune function, and overall toxicity. By investigating these parameters, the research seeks to determine whether the promising *in vitro* results can translate into effective and safe *in vivo* outcomes, ultimately contributing to the development of improved treatment strategies for colon cancer.

5.2 Materials and methods

5.2.1 Cells and animals

Colon cancer CT26 cells were cultured in RPMI-1640 medium supplemented with 10% (v:v) fetal bovine serum and 1% (v:v) antibiotic solution (100 U/mL penicillin and 100 mg/mL streptomycin) at 37°C in a 5% CO_2 humidified atmosphere.

Female Balb/c mice at the age of 6 to 8 weeks weighing 20-26 g were procured from Laboratory Animal Facility and Management, Faculty of Pharmacy, Universiti Teknologi MARA. The mice were maintained in the animal research house of the Comparative Medicine and Technology Unit, Institute of Bioscience, Universiti Putra Malaysia, under standard laboratory conditions with a 12-h light/dark cycle at 24 ± 2 °C with 45 ± 5% relative humidity and fed standard pellet-diet *ad libitum* with free access to water during the whole period of study. The animals were acclimatized for 1 week before the experiments. All animal use protocols for the experimental mice were reviewed and approved by the Institute Animal Care and Use Committee of Universiti Putra Malaysia (approval No. UPM/IACUC/AUP-R065/2023-Appendix A).

5.2.2 Development of allograft mouse model and treatment

After acclimatization, the hairs of the right flank area of BALB/c mice were shaved, and CT26 cells (1×10^6 cells in 100 µl) were injected subcutaneously on the right flank. When the tumors became palpable and the volume of tumors was measurable (approximately 100 mm^3), the mice were randomly divided into 4 groups of 6 mice each: TQ-$CaCO_3$np (TQ: 20 mg/kg) treatment group; 5-FU (20 mg/kg) treatment group; TQ-$CaCO_3$np (TQ: 20 mg/kg) + 5-FU (20 mg/kg) treatment group; tumor control group. The dosages for these treatment groups were based on previous studies on 5-FU and TQ (Demeckova et al. 2022; Lei et al. 2012; Opattova et al. 2019; Zhu et al. 2016b). Treatments were given via intraperitoneal injection trice every week. Mice in the tumor control group received the same volume of the physiological saline injection with the same schedule as the treated mice.

5.2.3 Gross observation and body weight measurement

All mice were monitored daily for clinical signs, and body weights were measured using an electronic balance and recorded every day. The mice were euthanized when one of the following endpoints was reached: changes in behavior, clinical signs of distress, 20% weight loss, presence of an ulcerated necrotic tumor, or a tumor volume greater than 2000 mm^3.

5.2.4 Tumor progression analysis

Growth of the tumors was observed daily using vernier caliper measurement of the length and width of the tumor. Tumor volume was calculated as the following formula:

$$\text{Tumor volume } (mm^3) = \text{length of tumor} \times (\text{width of tumor})^2 / 2.$$

After the sacrifice, the tumors were excised and weighed. Tumor inhibition ratio was then calculated using the following formula:

$$\text{Tumor inhibition ratio (\%)} = (U - T) / U \times 100\%,$$

where U is the average tumor weight of the tumor control group, and T is the average tumor weight of the treated group.

5.2.5 Organ weight and colon length measurement

Major organs (heart, liver, lung, kidney, spleen, and colon) were rapidly excised and flushed with 0.9% saline after the sacrifice. The weights of heart, liver, lung, kidney, and spleen were measured using a precision electronic balance within 5 min. Organ index was calculated using the following formula:

$$\text{Organ index} = \text{organ weight (mg)} / \text{body weight (g)}.$$

Moreover, colon length was measured using a vernier caliper. Colon index was calculated using the following formula:

$$\text{Colon index} = \text{colon length (mm)} / \text{body weight (g)}.$$

5.2.6 Serum biochemical analysis

Blood was collected in anticoagulant-free serum blood collection tubes for serum biochemical analysis from overnight-fasting mice by cardiac puncture following light anesthesia with ketamine and xylazine cocktail. After complete coagulation, the serum was centrifuged at 4000 rpm for 15 min using a centrifuge. The serum was then transferred to 1.5 mL Eppendorf tubes and stored at -80°C until analysis. Aspartate aminotransferase (AST), alanine aminotransferase (ALT), alanine phosphatase (ALP), creatinine, and urea levels were evaluated using an automatic biochemistry analyzer.

5.2.7 Histopathological examinations

Collected tumors tissues masses were fixed in 10% neutral formalin for at least 48 h. The tumors were trimmed to a 0.5 ± 0.1 cm thickness and placed in a plastic box, and then dehydrated using an automatic tissue processor. Subsequently, the tumors were embedded in paraffin wax and cut into 5 µm thickness. The tumor sections were mounted on glass slides with a hot plate and stained with hematoxylin and eosin (H&E). The histological changes were then observed and captured using a light microscope.

5.2.8 Statistical analysis

Data analysis was performed with at least triplicates using the GraphPad Prism 8 software. Statistical analysis involved one-way ANOVA followed by Turkey's post-test for multiple comparisons or Student's t-test for single comparison and two-way ANOVA followed by Dunnett's post-test. P value < 0.05 ($p<0.05$) was considered statistically significant. Unless otherwise stated, the results were expressed as mean ± standard deviation.

5.3 Results and discussion

5.3.1 Tumor growth inhibition

CT26 tumor-bearing mouse model was employed to explore the *in vivo* anti-colon cancer efficacy of TQ-$CaCO_3$np (TQ: 20 mg/kg) in combination with 5-FU (20 mg/kg), with the experimental design schematically represented in Figure 5.1A. All mice successfully developed tumors and showed normal behavior and activities, without mouse death and significant body weight loss throughout the study (Figure 5.1B). As

displayed in Figure 5.1C, the tumor volume rapidly increased from day 8 in the tumor control group, while tumor growth was suppressed following the treatment with TQ-$CaCO_3$np and 5-FU. The combination of TQ-$CaCO_3$np and 5-FU significantly reduced the tumor volume compared with 5-FU alone at the end of treatment ($p<0.0001$), also observed in Figure 5.1D, indicating an obvious synergism. Based on the tumor weight, the tumor inhibition ratios of TQ-$CaCO_3$np, 5-FU, and TQ-$CaCO_3$np combined with 5-FU treatment groups were 78.4%, 59.9%, and 94.0%, respectively (Figure 5.1E).

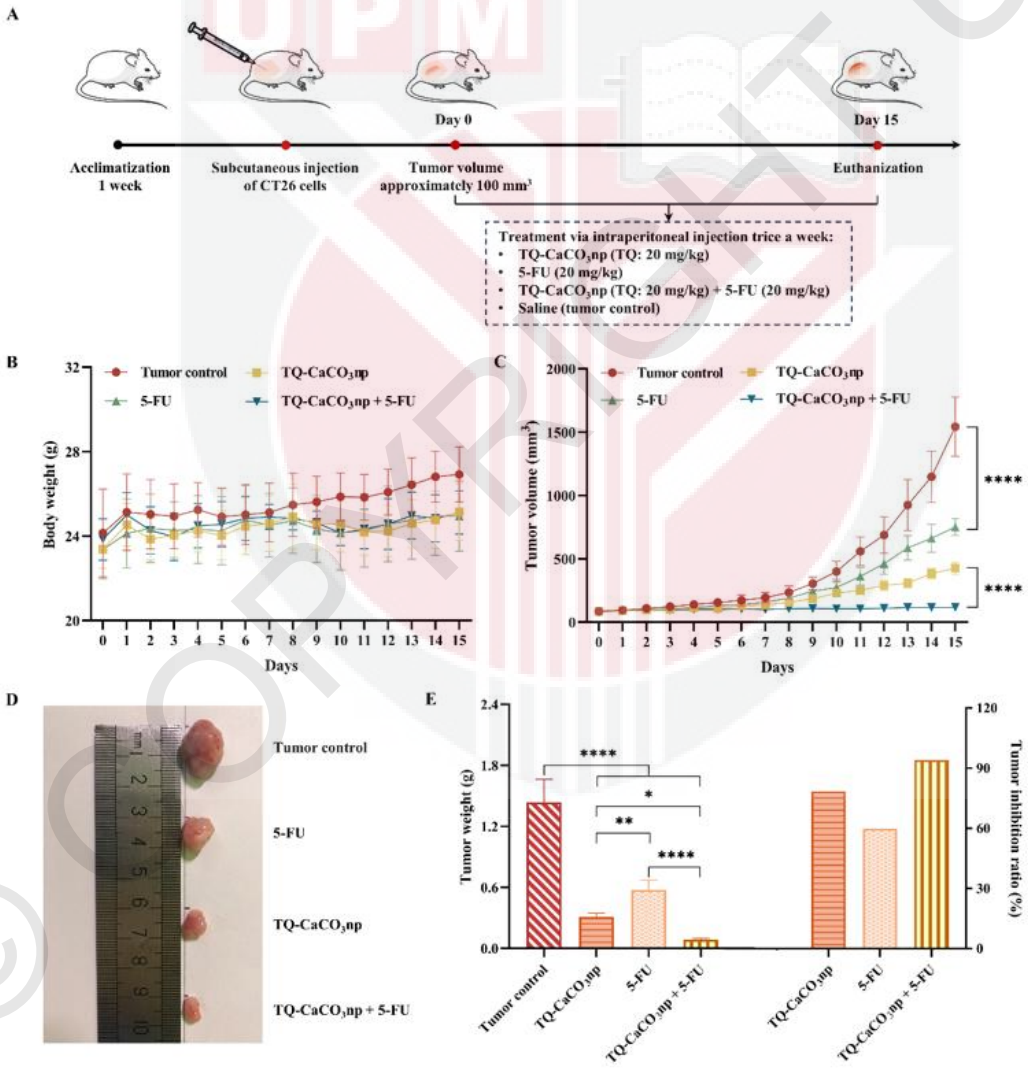

Figure 5.1: (A) Schematic diagram of *in vivo* experimental design; (B) body weights recorded daily during treatment; (C) tumor volumes recorded daily during treatment; (D) image of represented solid tumor of each group; (E) tumor weight of each group and tumor inhibition ratios of treatment groups relative to the tumor control group. *p<0.05, **p<0.01, ****p<0.0001.

The combination of TQ-$CaCO_3$np and 5-FU exhibited significant anti-tumor activity in the CT26 tumor-bearing mouse model, demonstrating superior efficacy compared to 5-FU monotherapy. The marked reduction in tumor volume and the high tumor inhibition ratio in the combination group highlight the potential synergistic effect between TQ-$CaCO_3$np and 5-FU. This enhanced anti-tumor response is likely attributed to the dual action of TQ-$CaCO_3$np and 5-FU. The improved delivery and retention of TQ at the tumor site facilitated by the $CaCO_3$np may allow for a sustained release and higher local concentration of TQ. Such finding is consistent with previous studies that have shown the benefits of nanoparticle-based compound delivery systems in enhancing the bioavailability and efficacy of natural compounds (Baksi et al. 2018; Chung et al. 2020; Sulaiman et al. 2020). On the other hand, TQ may sensitize tumor cells to 5-FU, thereby improving overall treatment efficacy. Previous studies have shown that TQ, a bioactive compound with anti-cancer properties, can enhance the efficacy of 5-FU in the treatment of triple-negative breast cancer and gastric cancer (Lei et al. 2012; Zheng et al. 2021). The significant tumor suppression observed in this study is consistent with findings from these previous studies. Moreover, the absence of significant body weight loss or mortality in the treated groups suggests that this combination therapy may offer a more effective and safer alternative to chemotherapy regimens, particularly for colon cancer treatment.

5.3.2 Histopathological analysis

H&E staining of tumor tissue masses sections in Figure 5.2 revealed that compared to the tumor control group where the tumor cells were dense with evenly distributed nucleus and cytoplasm, the tumor cells in the 5-FU group and TQ-$CaCO_3$np group were sparse with shrunken and dissolved nuclei, resulting in increased necrosis.

Remarkably, the tumor tissue structure destruction in the combination treatment group was more severe than that in the single treatment groups, with more nuclear fragments and obvious cavities. All these results are consistent with the results in tumor growth inhibition, indicating that TQ-$CaCO_3$np enhanced the antitumor efficacy of 5-FU, suggesting the superior therapeutic value of TQ-$CaCO_3$np combined with 5-FU.

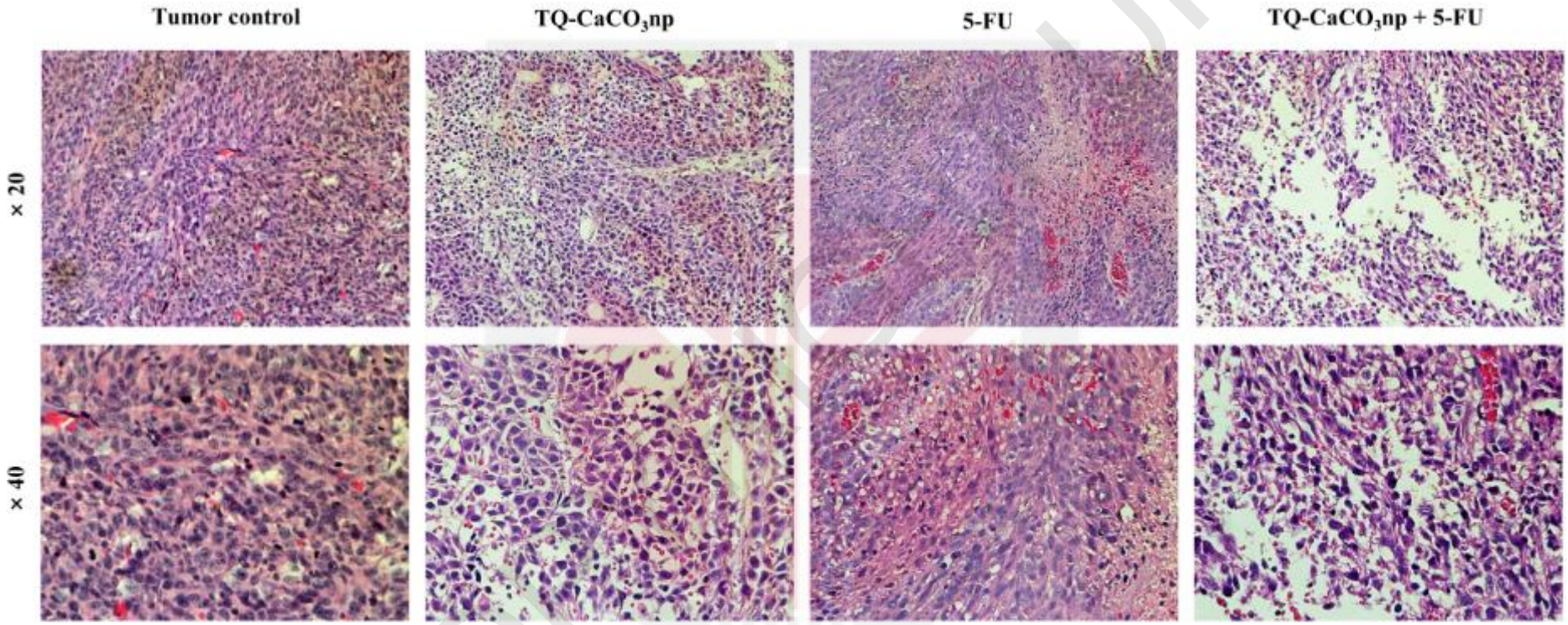

Figure 5.2: Histopathological images (×20 and ×40 magnifications) of tumor tissue sections stained with hematoxylin-eosin staining for each group. Tumor control group: dense tumor cells with evenly distributed nucleus and cytoplasm; TQ-$CaCO_3$np/5-FU group: sparse tumor cells with shrunken and dissolved nuclei; TQ-$CaCO_3$np + 5-FU group: more nuclear fragments and obvious cavities.

5.3.3 Organ index analysis

Toxicity evaluation is an essential step in developing a new cancer therapy for clinical application. No obvious tumor metastasis or organ injury was observed with the naked eye. As shown in Figure 5.3, the spleen index in the 5-FU treatment group was significantly lower than the tumor control group and TQ-$CaCO_3$np treatment group ($p<0.0001$), while the addition of TQ-$CaCO_3$np remarkably increased the spleen index of 5-FU treatment group ($p<0.01$). Although there was no significant change in the thymus index, the trend of changes across all groups was consistent with that of the spleen index. The spleen and thymus indexes directly reflected the immune function of the body, indicating that TQ-$CaCO_3$np improved the mild immunosuppressive effect caused by 5-FU. In addition, the heart, lung, liver, kidney, and colon indexes in the 5-FU treatment group were lower than those in the tumor control group. In contrast, all these organ indexes in the combination treatment group were slightly higher than those in the 5-FU treatment group, supporting the alexipharmic effect of TQ-$CaCO_3$np in 5-FU treatment.

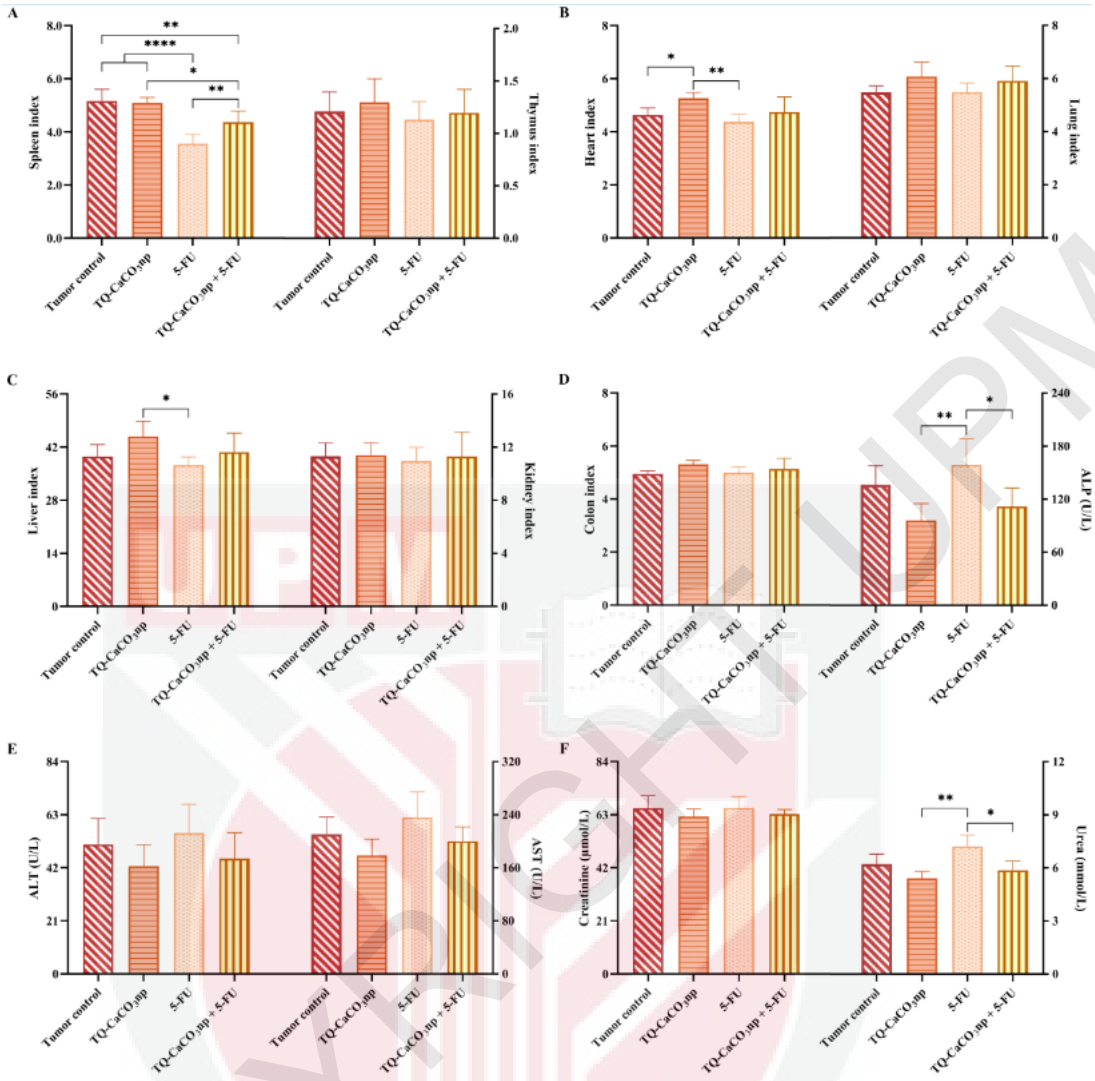

Figure 5.3: (A) Spleen and thymus indexes after treatment; (B) heart and lung indexes after treatment; (C) liver and kidney indexes after treatment; (D) colon index and ALP level in serum after treatment; (E) ALT and AST levels in serum after treatment; (F) creatinine and urea levels in serum after treatment. ALP, alkaline phosphatase; ALT, alanine aminotransferase; AST, aspartate aminotransferase. * $p<0.05$, ** $p<0.01$, ** $p<0.001$, **** $p<0.0001$.

5.3.4 Serum biochemistry analysis

Biochemical analysis of ALP, ALT, AST, creatinine, and urea levels in serum showed no significant difference between the tumor control group and treatment groups (Figures 5.3D-F). However, compared with the 5-FU treatment group, the significantly reduced ALP and urea levels in the combination treatment group revealed that

supplementation of TQ-$CaCO_3$np decreased the toxicity of 5-FU ($p<0.05$). Overall, organ index analysis and serum biochemistry analysis indicated that TQ-$CaCO_3$np and 5-FU in combination which enhanced the antitumor efficacy of 5-FU exhibited reduced toxicity.

While 5-FU treatment alone led to a significant reduction in the spleen index, indicative of an immunosuppressive effect, the addition of TQ-$CaCO_3$np markedly improved the spleen index, suggesting an enhancement of immune function. This improvement was also reflected in the thymus index, further supporting the immunoprotected role of TQ-$CaCO_3$np. Additionally, the organ indexes for the heart, lung, liver, kidney, and colon in the 5-FU treatment group were lower than those in the tumor control group, indicative of 5-FU-induced toxicity. One of the most common side effects associated with 5-FU use is liver and kidney dysfunction, which leads to a reduction in therapeutic activity and patient survival time (He et al. 2003). However, the slight increase in these organ indexes in the combination treatment group compared to the 5-FU group suggests that TQ-$CaCO_3$np may mitigate some of the organ-specific toxicities associated with 5-FU. This is further corroborated by the biochemical analysis, where a significant reduction in ALP and urea levels in the combination group compared to the 5-FU group indicates reduced hepatotoxicity and nephrotoxicity. These findings are consistent with the conclusions of other studies that TQ showed hepatoprotective and renal protective properties against chemotherapy drug toxicity, affecting key enzymes involved in detoxification, such as aspartate transaminase and alanine transaminase (Khan & Younus 2018). Moreover, TQ could mitigate common side effects such as mucositis and gastrointestinal toxicity associated with 5-FU treatment (Madani et al. 2023). These findings suggest that the combination of TQ-$CaCO_3$np with 5-FU not only enhances the anti-tumor efficacy but also reduces the

systemic toxicity of 5-FU, highlighting the potential of TQ-$CaCO_3$np as a valuable adjunct in chemotherapy regimens aimed at minimizing adverse effects while maximizing therapeutic outcomes.

5.4 Conclusion

In conclusion, the findings from this animal study underscore the potential of TQ-$CaCO_3$np in enhancing the therapeutic efficacy of 5-FU for the treatment of colon cancer. The combination of TQ-$CaCO_3$np with 5-FU not only demonstrated significant tumor growth inhibition but also improved the overall safety profile of 5-FU by mitigating its immunosuppressive effects and reducing organ-specific toxicities. Histopathological analysis revealed more extensive tumor tissue destruction in the combination treatment group, further supporting the synergistic anti-tumor effects of TQ-$CaCO_3$np and 5-FU. Additionally, the biochemical analysis indicated that TQ-$CaCO_3$np could reduce the hepatotoxicity and nephrotoxicity typically associated with 5-FU treatment. Overall, these results suggest that the combination of TQ-$CaCO_3$np and 5-FU may offer a promising strategy to enhance the efficacy and reduce the toxicity of conventional chemotherapeutic agent 5-FU, paving the way for more effective and safer cancer therapies.

CHAPTER 6

THYMOQUINONE-LOADED CALCIUM CARBONATE NANOPARTICLES IN COMBINATION WITH 5-FLUOROURACIL AGAINST COLON CANCER: UNDERLYING MOLECULAR MECHANISM

6.1 Introduction

The therapeutic potential of TQ-$CaCO_3$np in combination with 5-FU against colon cancer *in vitro* and *in vivo* has been explored in the previous chapters. However, the underlying molecular mechanisms remain to be fully elucidated. Understanding these mechanisms is critical for identifying potential biomarkers for treatment response. Proteomics and metabolomics are powerful tools for uncovering the global changes in protein expression and metabolic pathways that occur in response to therapeutic interventions (Al-Daffaie et al. 2024; Hasin, Seldin & Lusis 2017). Proteomics allows for the identification of differentially expressed proteins that may play key roles in drug response, while metabolomics provides insights into the alterations in metabolic pathways that are essential for cancer cell survival and proliferation (Chen et al. 2020; Kwon et al. 2021; Schmidt et al. 2021).

In this chapter, an integrated proteomic and metabolomic approach was employed to investigate the molecular mechanisms underlying the therapeutic effects of TQ-$CaCO_3$np in combination with 5-FU in colon cancer cells. By analyzing the differentially expressed proteins and metabolites, this study aims to identify the key pathways and hub molecules involved in the anti-colon cancer effects of this combination therapy. The current findings provide a comprehensive understanding of

the metabolic and proteomic alterations induced by TQ-$CaCO_3$np and 5-FU, offering potential targets for enhancing therapeutic efficacy and overcoming drug resistance in colon cancer. This integrated analysis not only sheds light on the molecular basis of the observed therapeutic effects but also paves the way for the development of more effective and targeted treatment strategies for colon cancer.

6.2 Materials and methods

6.2.1 Proteomic analysis

6.2.1.1 Protein extraction and trypsin digestion

CT26 cells were treated with TQ-$CaCO_3$np (TQ: 15 μM) and 5-FU (7.5 μM) alone or in combination for 96 h. After treatment, the cells were washed with PBS twice and harvested using a cell scraper. Proteins were extracted from the cell pellets with lysis buffer (8 M urea, 75 mM NaCl, 50 mM HEPES, protease inhibitor cocktail, pH 7.4) followed by centrifugation at 14000 rpm for 15 min at 4 ℃. The protein concentration was determined using the BCA protein assay. Subsequently, proteins were reduced with 10 mM DTT for 1 h at 37 ℃ and alkylated with 20 mM IAA for 1 h at 25 ℃. The protein samples were diluted with 50 mM NH_4HCO_3 to ensure urea concentration below 1 M before adding trypsin at a ratio of 1:20 (w/w) to digest the protein samples overnight at 37 ℃, followed by quenching with 1% formic acid. Digested peptides were further purified with C18 tips to remove the salt for nano LC-MS/MS analysis.

6.2.1.2 Nano LC-MS/MS analysis

Desalted peptides were analyzed using the Dionex Ultimate 3000 RSLCnano coupled

to an Orbitrap Fusion mass spectrometer (Thermo Fisher Scientific). The peptides were separated by EASY-Spray PepMap column (C18, 100 Å, 2 μm, 50 μm × 15 cm) using mobile phases of A (0.1% formic acid in water) and B (0.1% formic acid in acetonitrile) at a flow rate of 250 nL/min, with a gradient as follows: 5-40% B for 91 min; 40-85% B for 2 min; 85% B for 3 min; 85-5% B for 1 min; 5% B for 4 min. The mass spectrometer was operated in positive ion mode and data-dependent mode. The full scan was performed at the range of 310-1800 m/z at a resolution of 120000 with a maximum injection time of 50 ms. Only precursors with a charge state of 2-7 were further analyzed for MS/MS and filtered using a 20 s dynamic exclusion window and an intensity threshold of 5000. Precursors were fragmented by high-energy collision dissociation and collision-induced dissociation at a normalized collision energy of 28% and 30%, respectively.

6.2.1.3 Data analysis

Each group consists of three biological samples and each biological sample was injected three times into nano LC-MS/MS as three technical replicates. The raw MS files were processed using the Proteome Discoverer 2.5 software and searched against the UniProt *Mus musculus* database using the SEQUEST HT search algorithm. False discovery rate tolerance in the Percolator node was set to 0.01 and at least one identified unique peptide was required to filter proteins. Student's t-test was used to identify differentially expressed proteins between two groups, where proteins with |fold change|>1.5 and $p<0.05$ were considered significant. The volcano plot and heatmap were generated using R software, and Gene Ontology (GO) and Kyoto Encyclopedia of Genes and Genomes (KEGG) enrichment analyses were performed using R software.

6.2.2 Metabolomic analysis

6.2.2.1 Sample preparation for ^{1}H-NMR analysis

CT26 cells were treated with TQ-$CaCO_3$np (TQ: 15 μM) and 5-FU (7.5 μM) alone or in combination for 96 h. After treatment, cells were washed with PBS twice, and methanol was added to quench the cells while scraping with cell scrapers. Approximately 1×10^7 cells were employed as one sample for NMR analysis, and the cell suspension was transferred into a fresh 15 mL centrifuge tube. Chloroform and ultrapure water were added to the cell suspension, with a mixture of methanol, chloroform, and water in the volume ratio 1:1:0.95. Afterward, the mixture was vortexed and centrifuged at 14000 rpm for 10 min at 4°C. The upper phase was transferred and lyophilized. The lyophilized sample was reconstituted in 600 μL of 99.9% D_2O (containing 100 mM KH_2PO_4, 0.01% TSP, pH 7.4) and centrifuged at 14000 rpm for 10 min at 4°C. The supernatant was then transferred to a 5mm NMR tube for ^{1}H-NMR analysis.

6.2.2.2 ^{1}H-NMR analysis

The ^{1}H-NMR spectra of the samples were acquired on a 500 MHz Varian Unity INOVA NMR spectrometer (Varian Inc., Palo Alto, USA). All spectra were subjected to a 64-scan presaturation pulse sequence to suppress water signals. The Carr-Purcell-Meiboom-Gill pulse sequence was then employed to suppress macromolecule signals, with a spectral width of -2 to 14 ppm, 128 scans, a relaxation delay of 4 s, and an acquisition time of 8.12 min.

6.2.2.3 Data processing and analysis

The acquired spectra were phased and baseline-adjusted manually, and the chemical shift of TSP was referenced at δ 0.0. The spectra were then processed using the Chenomx NMR Suite 5.1 Professional. Region (δ 4.7-4.9) distorted due to residual water was excluded. The spectral regions of δ 0.3 to 10.0 ppm were segmented at 0.04 ppm intervals and all data points were normalized for further analysis. Assignments of metabolites were conducted using a combination of the Human Metabolome Data Base, Biological Magnetic Resonance Data Bank, and relevant published references. The normalized data were uploaded into the SIMCA 14.1 software for multivariate data analysis. The identified metabolites were screened as differentially expressed metabolites with variable importance in the projection exceeding 1 (VIP>1) and $p<0.05$. Volcano plot was carried out to visualize the differences of metabolite expressions, and the pathway enrichment analysis of differentially expressed metabolites was performed by R software based on the KEGG database.

6.2.3 Integrated analysis of proteomics and metabolomics

KEGG pathway analysis was used to integrate proteomics and metabolomics data. The enriched co-regulated pathways were screened to elucidate the mechanism of TQ-$CaCO_3$np in combination with 5-FU against colon cancer.

6.2.4 Enzyme-linked immunosorbent assay

Aconitate hydratase, mitochondrial (Aco2), glyceraldehyde-3-phosphate dehydrogenase (Gapdh), phosphoserine phosphatase (Psph), and pyruvate dehydrogenase E1 component subunit beta, mitochondrial (Pdhb) enzyme-linked immunosorbent assay (Elisa) kits were used to analyze the protein levels in mice tumor (obtained from Chapter 5). Briefly, the tumors were thawed at room temperature and

homogenized by bead beating in PBS with a protease inhibitor cocktail at 4℃. After centrifuging at 12000 rpm for 10 min, the supernatant was collected for the Elisa test. The procedures followed the manufacturer's instructions of Aco2 (Yubo Biotechnology, Shanghai, China), Gapdh (Baiyi Biotechnology, Shanghai, China), Psph (Baiyi Biotechnology, Shanghai, China), and Pdhb (Baiyi Biotechnology Shanghai, China) Elisa kits.

6.2.5 Statistical analysis

Data analysis was performed with at least triplicates using the GraphPad Prism 8 software. Statistical analysis involved one-way ANOVA followed by Turkey's post-test for multiple comparisons or Student's t-test for single comparison and two-way ANOVA followed by Dunnett's post-test. P value < 0.05 ($p<0.05$) was considered statistically significant. Unless otherwise stated, the results were expressed as mean ± standard deviation.

6.3 Results and discussion

6.3.1 Differentially expressed protein screening

To explore the underlying molecular mechanisms of TQ-$CaCO_3$np combined with 5-FU against colon cancer, a label-free quantification proteomic strategy was used to identify the differentially expressed proteins in colon cancer CT26 cells after treatment with TQ-$CaCO_3$np and 5-FU alone and in combination. Figure 6.1A illustrates the differentially expressed proteins among the groups. Compared with the control group, 218 differentially expressed proteins were obtained in the combination group, including 165 significantly upregulated proteins and 53 significantly downregulated

proteins. Meanwhile, compared with the control group, 133 differentially expressed proteins (67 upregulated and 66 downregulated) and 181 differentially expressed proteins (141 upregulated and 40 downregulated) were identified in the 5-FU and TQ-$CaCO_3$np groups, respectively. Interestingly, 78 and 31 significantly up- and downregulated proteins were found in the combination group compared to the 5-FU group, respectively, while 102 and 95 significantly up- and downregulated proteins were identified in the combination group compared to the TQ-$CaCO_3$np group, respectively. The variations in abundance of the top 50 differentially expressed proteins between the combination and control groups were visually represented in the heatmap, revealing that the two groups were separated from each other, and three samples in each group exhibited favorable reproducibility (Figure 6.1B).

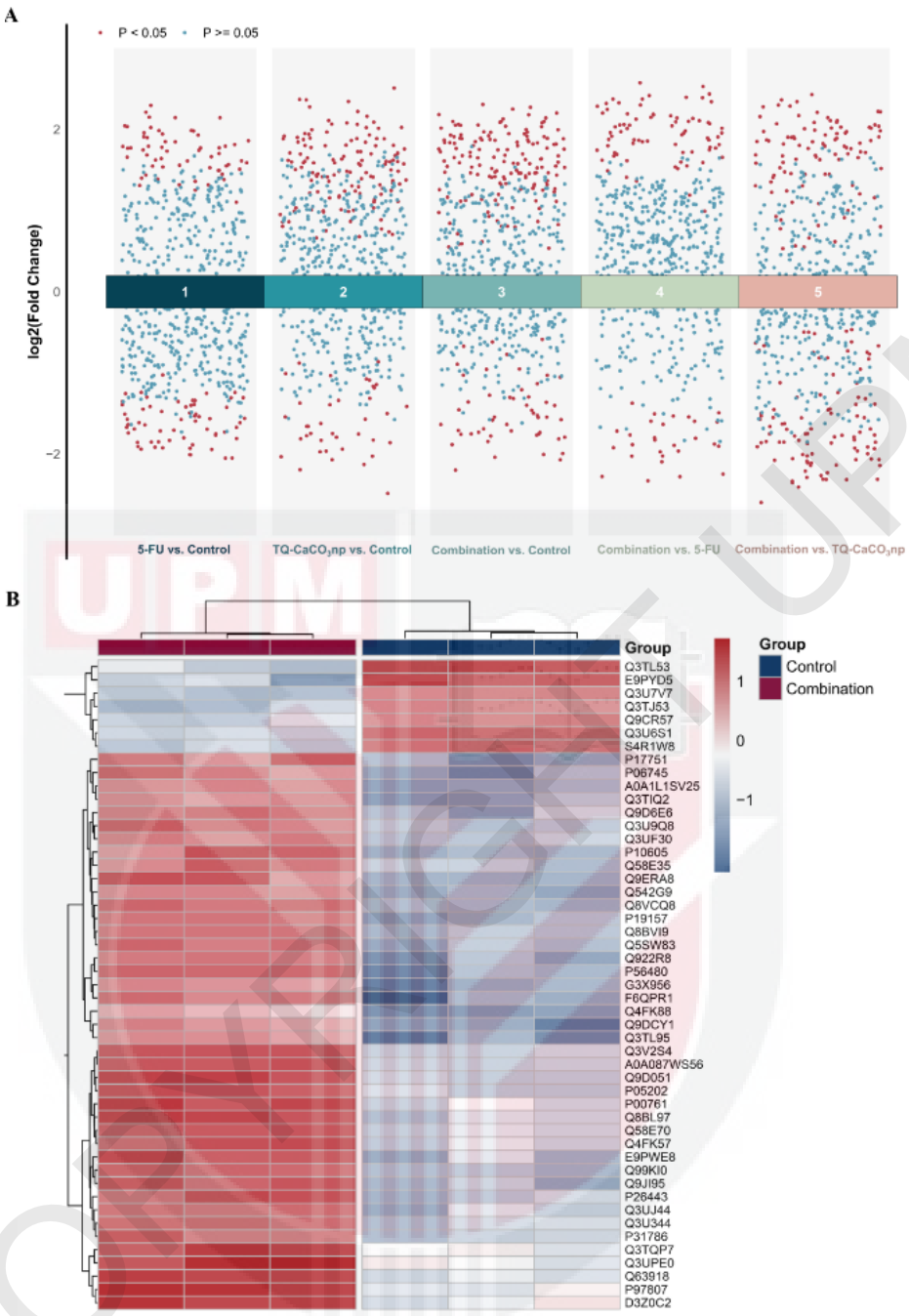

Figure 6.1: (A) A volcano plot visualizing the differentially expressed proteins among different groups; (B) heatmap of top 50 differentially expressed proteins between TQ-$CaCO_3$np combined with 5-FU and control groups.

Based on the above findings, both 5-FU and TQ-$CaCO_3$np individually influenced the proteins in colon cancer CT26 cells, demonstrating their therapeutic potential. However, the combination of 5-FU and TQ-$CaCO_3$np led to a more significant

modulation of the differentially expressed proteins, as evidenced by the greater number and distinct profile of regulated proteins. This suggests that the combination therapy not only enhanced the individual effects of 5-FU and TQ-$CaCO_3$np but also exerted a synergistic effect, resulting in improved anti-colon cancer efficacy, consistent with the findings in cell and animal studies. Figure 6.1A encapsulates the dysregulated proteins after the treatment of 5-FU combined with TQ-$CaCO_3$np, including upregulated Q9D051 and Q99KI0 and downregulated Q3U6S1 and Q3U7V7. Q9D051, known as pyruvate dehydrogenase E1 component subunit beta (Pdhb), is located in mitochondria and functions as catalyzing the conversion of glucose-derived pyruvate to acetyl coenzyme A, thereby regulating oxidative phosphorylation (Solmonson & DeBerardinis 2018). It has been reported that the overexpression of Pdhb was associated with the inhibition of cell proliferation and invasion in colon cancer (Zhu et al. 2017). Q99KI0, identified as aconitate hydratase (Aco2), catalyzing the interconversion of citrate to isocitrate in the second step of the TCA cycle, is an essential enzyme that bridges the TCA cycle and lipid metabolism (Ciccarone et al. 2020). Knockdown of Aco2 in CRC cells promotes cell proliferation and tumor formation, while ectopic expression of Aco2 restrains tumor growth (You et al. 2021). Q3U6S1, vimentin (Vim), is positively correlated with the degree of malignancy of cancer cells, highly expressed in colorectal cancer cells (Wang et al. 2021b). Q3U7V7, profilin (Pfn1), is an indispensable and ubiquitously expressed actin-binding protein, and its expression was significantly upregulated in colorectal cancer tissues and cells (Huang et al. 2020b).

6.3.2 Enrichment analysis of differentially expressed proteins

The differentially expressed proteins between the combination and control groups

were annotated based on GO categories (biological process, cellular component, molecular function) and KEGG pathways to better understand the functions and characteristics of these proteins. According to the annotation of cellular components, the differentially expressed proteins were mainly localized in the myelin sheath, catalytic step 2 spliceosome, spliceosomal complex, mitochondrial matrix, and nuclear periphery (Figure 6.2A). mRNA binding, translation regulator activity, unfolded protein binding, single-stranded DNA binding, and actin binding were the most significant terms of enrichment from molecular function. Biological process enrichment analysis showed that the treatment of TQ-$CaCO_3$np in combination with 5-FU was primarily involved in RNA splicing, mRNA splicing, ribonucleoprotein complex biogenesis, mRNA processing, and cytoplasmic translation. Moreover, these proteins were annotated in 42 significantly enriched pathways in the KEGG database (Figure 6.2B). The top 10 pathways include carbon metabolism, citrate cycle (TCA cycle), biosynthesis of amino acids, spliceosome, glycolysis / gluconeogenesis, pyruvate metabolism, proteasome, 2-oxocarboxylic acid metabolism, Parkinson disease, and protein processing in endoplasmic reticulum.

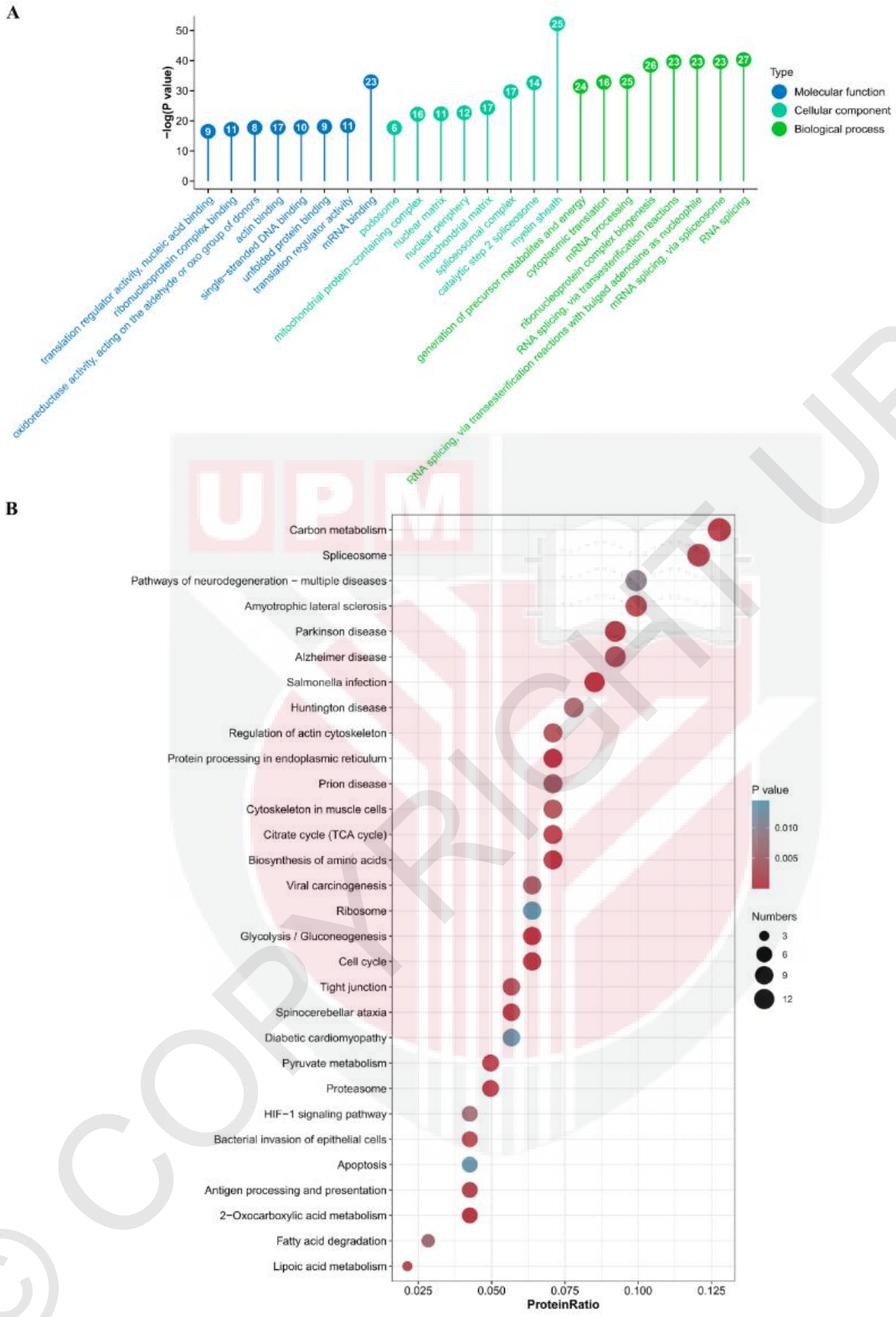

Figure 6.2: (A) GO functional enrichment analysis of differentially expressed proteins, including biological process, cellular component, and molecular function, with the labeled number indicating protein number in each GO term; (B) KEGG pathway enrichment analysis of differentially expressed proteins, with the top 30 enriched pathways.

The functional annotation of differentially expressed proteins between the combination (TQ-$CaCO_3$np and 5-FU) and control groups provides insights into the molecular mechanisms driving the enhanced anticancer effects observed in colon cancer cells. The localization of these proteins to critical cellular components such as the myelin sheath, catalytic step 2 spliceosome, spliceosomal complex, mitochondrial matrix, and nuclear periphery suggests that the combination therapy impacts essential cellular structures involved in maintaining cellular homeostasis and function (Bravo et al. 2013; Guerbette, Boudry & Lan 2022; Ivanova et al. 2023; Manabile et al. 2023; Sette & Paronetto 2022; Williamson & Lyons 2018). In terms of molecular function, the enrichment of terms such as mRNA binding, translation regulator activity, unfolded protein binding, and single-stranded DNA binding indicates a strong emphasis on managing gene expression and protein quality control. The involvement of unfolded protein binding highlights a possible unfolded protein response, which cancer cells often exploit to survive under stressful conditions such as chemotherapy (Zhang et al. 2024). The biological process enrichment further strengthens the hypothesis that the combination treatment significantly impacts gene regulation. The involvement in RNA splicing, mRNA splicing, and ribonucleoprotein complex biogenesis suggests that the treatment may affect the post-transcriptional regulation of gene expression (Blijlevens, Li & van Beusechem 2021; O'Brien et al. 2018). Spliceosomal complexes, the key to RNA splicing, are often dysregulated in cancer, leading to alternative splicing patterns that promote tumorigenesis (Zhang et al. 2021). The effect on cytoplasmic translation indicates alterations in protein synthesis machinery, likely affecting cell growth and proliferation (Browning & Bailey-Serres 2015). Overall, the results suggest that the combined treatment exerts its anticancer effects by disrupting critical processes involved in RNA metabolism and protein synthesis, thereby impeding cancer cell

survival.

Moreover, the KEGG pathway analysis identified significant enrichment in pathways related to carbon metabolism, glycolysis/gluconeogenesis, and the citrate cycle (TCA cycle), which are central to energy production and biosynthesis in cells (Icard et al. 2021; Newman & Maddocks 2017). The involvement of pathways such as spliceosome, proteasome, and protein processing in the endoplasmic reticulum indicates that the TQ-$CaCO_3$np and 5-FU co-treatment may also affect gene expression, protein degradation, and protein folding, contributing to its therapeutic efficacy (Schwarz & Blower 2016; Xie et al. 2020). The enrichment of pathways related to neurodegeneration and Parkinson's disease suggests potential off-target effects or broader impacts on cellular processes shared between colon cancer and neurodegenerative diseases (Wang et al. 2024). Remarkably, the treatment of TQ-$CaCO_3$np combined with 5-FU modulated the cell cycle and apoptosis pathways, in consistent with the previous finding that TQ-$CaCO_3$np in combination with 5-FU induced cell cycle arrest and apoptosis in colon cancer CT26 cells. Collectively, these findings highlight the multifaceted nature of the effects of TQ-$CaCO_3$np in combination with 5-FU on colon cancer cells, underscoring its potential to disrupt multiple pathways simultaneously, thereby enhancing its anti-colon cancer efficacy.

6.3.3 Metabolite identification and multivariate analysis

Typical ^{1}H NMR spectra obtained from four groups, including the control, TQ-$CaCO_3$np, 5-FU, and combination (TQ-$CaCO_3$np + 5-FU) groups, are displayed in Figure 6.3. A total of 26 metabolites were assigned, where all groups shared high similarity regarding identified metabolites while differing in peak intensity.

Subsequently, orthogonal partial least squares discriminant analysis (OPLS-DA) was performed to explore the metabolic changes induced by different treatments. In the OPLS-DA score plot (Figure 6.4, left panels), all pair-wise comparisons exhibited good group separation with a high coefficient of determination (R^2) and good prediction accuracy (Q^2). Model parameters of permutation analysis for pair-wise comparison indicated the good fit obtained by the model (Figure 6.4, right panels).

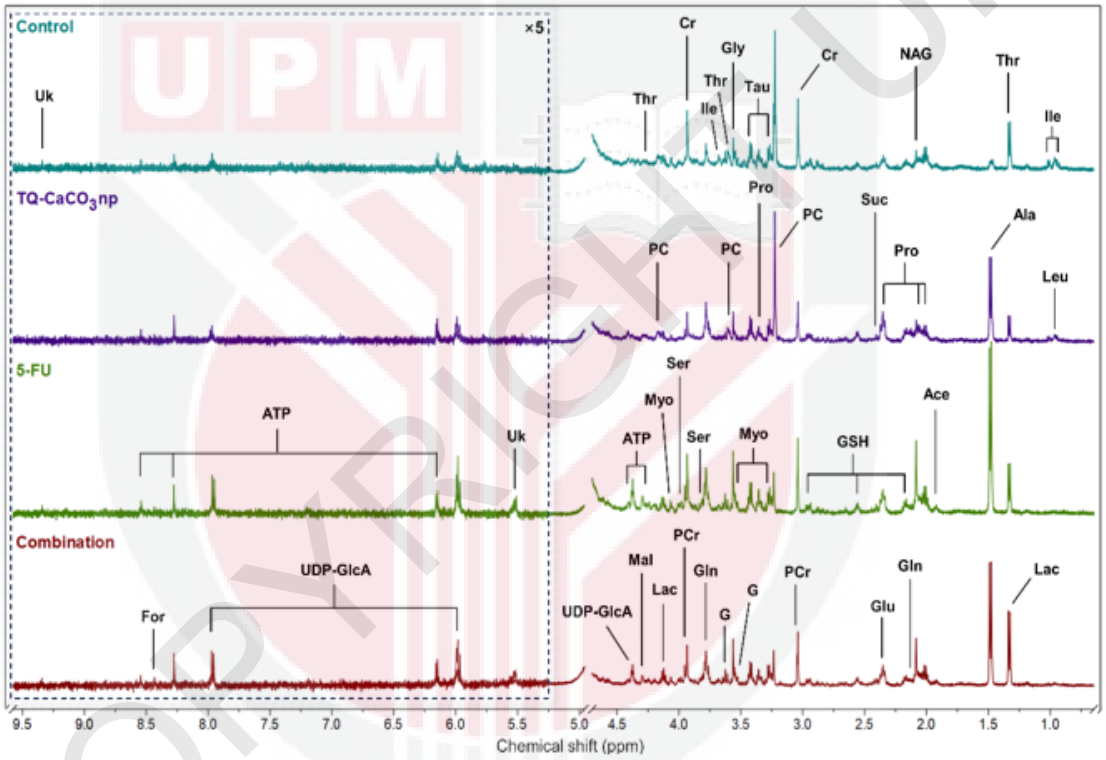

Figure 6.3: Typical metabolic profiles revealed by ^{1}H-NMR spectra. Assignments were made as labeled for each group. Spectral regions from 5.25 to 9.58 ppm were displayed with a different scale for visual convenience. Abbreviations were defined as follows: Ile, isoleucine; Leu, leucine; Lac, lactate; Thr, threonine; Ala, alanine; Ace, acetate; Pro, proline; NAG, N-acetyl glycoprotein; Gln, glutamine; GSH, glutathione; Glu, glutamate; Suc, succinate; Cr, creatine; PCr, phosphocreatine; PC, phosphocholine; Tau, taurine; Myo, myo-inositol; G, glycerol; Gly, glycine; Ser, serine; ATP, Adenosine 5'-triphosphate; Mal, malate; UDP-GlcA, UDP-glucuronate; Uk, unknown; For, formate.

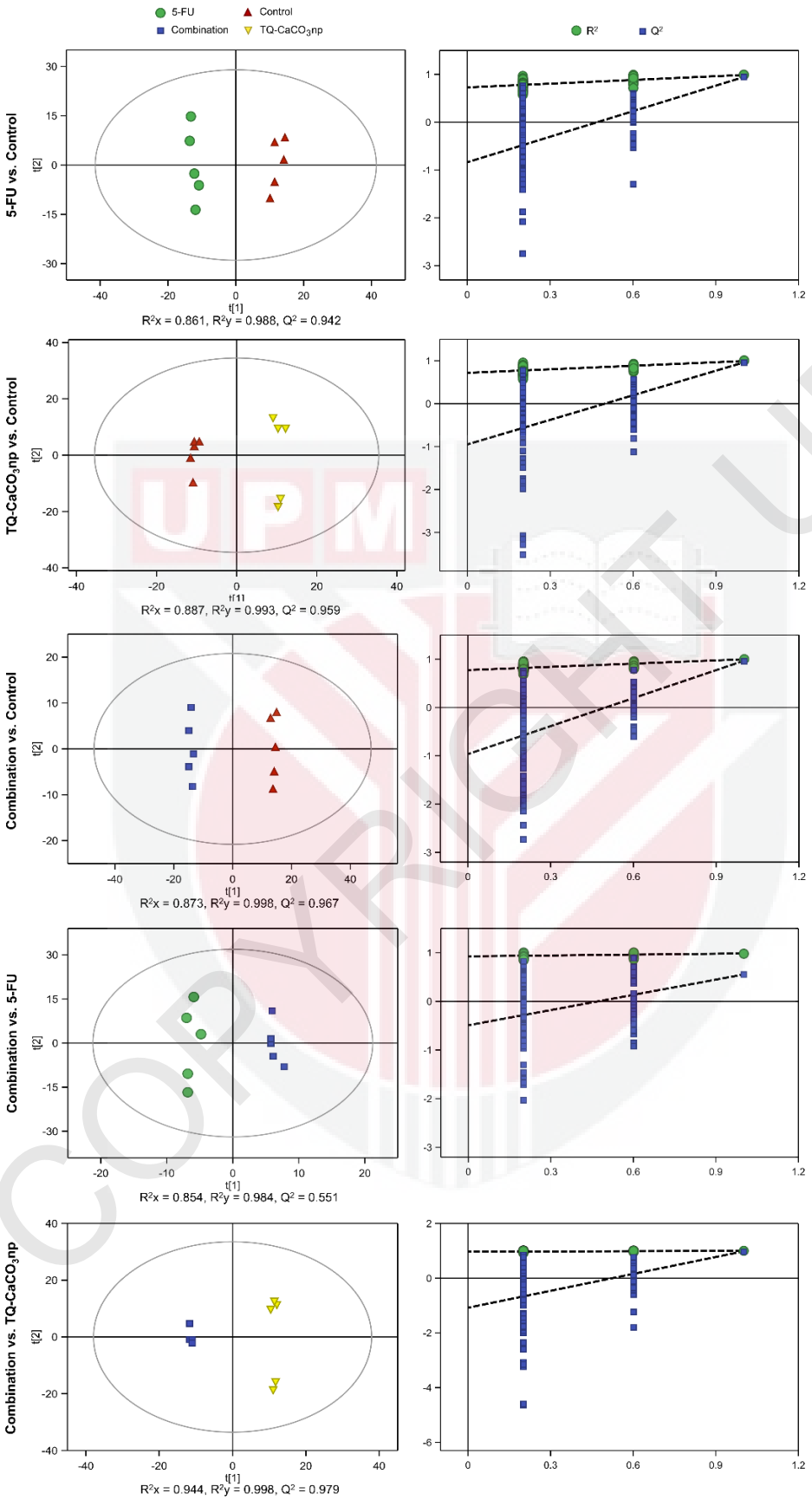

Figure 6.4: OPLS-DA score plots (left panel) and corresponding permutation plots (right panel) derived from different comparison models based on ^{1}H-NMR spectra.

The OPLS-DA score plots demonstrated clear group separation across all pair-wise comparisons, underscoring the distinct metabolic profiles induced by the control, individual treatments, and combination therapy. The high R^2 and Q^2 values indicated that the models generated from these comparisons were robust and reliable, reflecting true biological differences rather than random variation. In addition, the permutation analysis confirmed the validity of the OPLS-DA models, supporting the conclusion that the observed metabolic alterations are statistically significant and treatment-specific. These findings suggest that the combination of TQ-$CaCO_3$np and 5-FU induced unique metabolic shifts that could underlie its enhanced therapeutic efficacy.

6.3.4 Differentially expressed metabolite screening and KEGG pathway enrichment

The differentially expressed metabolites between the pair-wise groups were screened based on the VIP values from multivariate analyses and p values from univariate analyses. As illustrated in the volcano plot (Figure 6.5A), compared with the control group, 12 of the metabolites showed significant changes in the 5-FU group, whereas 10 differentially expressed metabolites were screened in the TQ-$CaCO_3$np group. Notably, 15 metabolites were significantly changed after treatment with TQ-$CaCO_3$np combined with 5-FU, including higher levels of alanine, glutamate, N-acetyl glycoprotein, proline, adenosine 5'-triphosphate, UDP-glucuronate, glutathione, lactate, glutamine, threonine, and myo-inositol and lower levels of phosphocholine, glycerol, leucine, and isoleucine. Additionally, there were 4 differentially expressed metabolites between the combination group and 5-FU group and 12 metabolites changed significantly between the combination group and TQ-$CaCO_3$np group. Further querying of the KEGG database revealed the differentially expressed

metabolites after the treatment of TQ-$CaCO_3$np and 5-FU to be significantly associated with metabolic pathways such as ABC transporters, central carbon metabolism in cancer, protein digestion and absorption, aminoacyl-tRNA biosynthesis, mineral absorption, biosynthesis of amino acids, biosynthesis of plant secondary metabolites, alanine, aspartate and glutamate metabolism, glutamatergic synapse, and GABAergic synapse (Figure 6.5B).

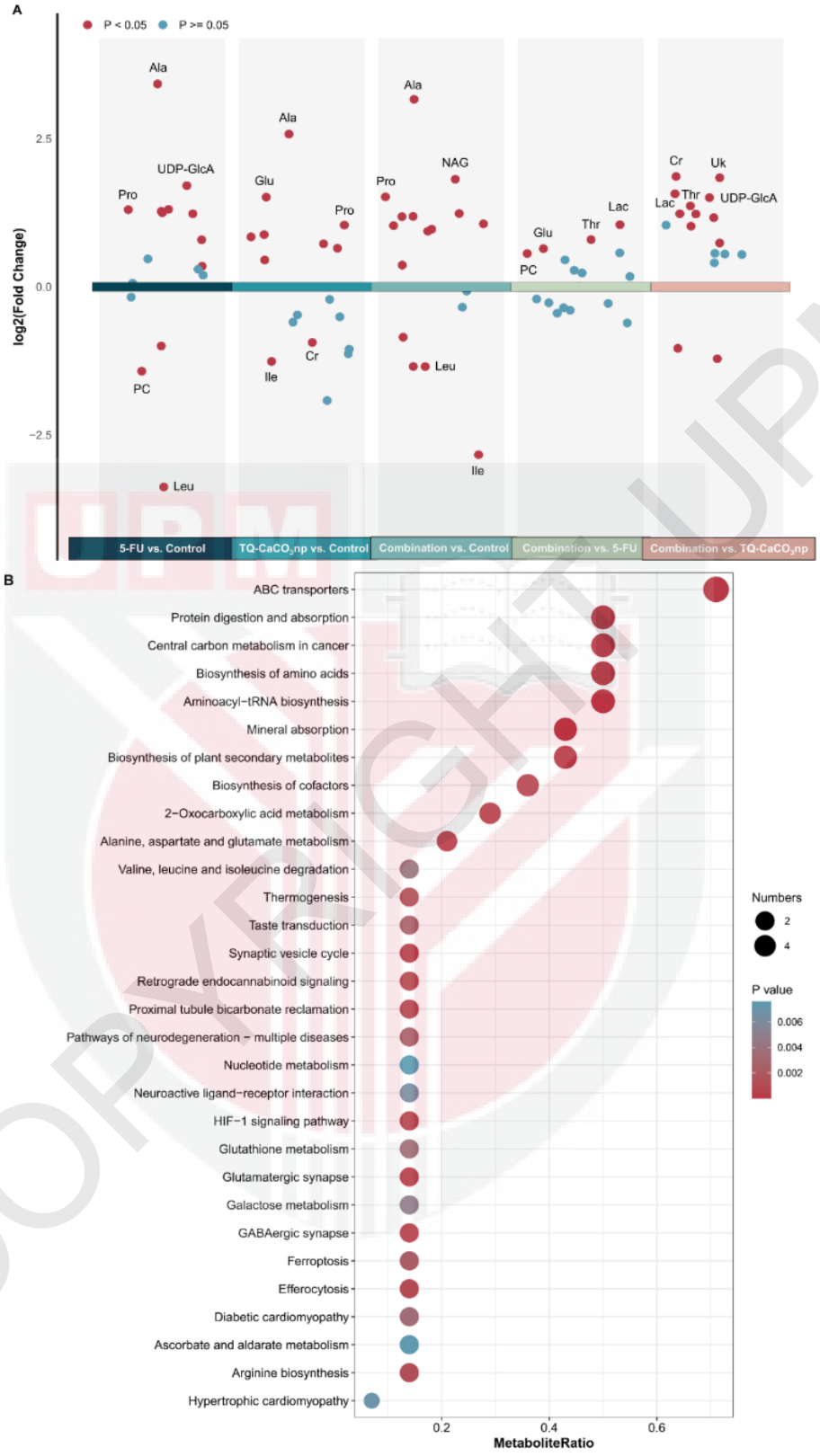

Figure 6.5: (A) A volcano plot visualizing the differentially expressed metabolites among different groups, with labeled top 5 significantly expressed metabolites; (B) KEGG pathway enrichment analysis of differentially expressed metabolite, with the top 30 enriched pathways.

The increased levels of amino acids such as alanine, proline, glutamate, and glutamine, along with key energy-related metabolites such as adenosine 5'-triphosphate and lactate, indicate a heightened metabolic activity that could be linked to increased cellular stress or enhanced cancer cell death mechanisms (Jin et al. 2023; Patriarca et al. 2021). The reduction in branched-chain amino acids (isoleucine and leucine), glycerol, and phosphocholine further supports the disruption of essential metabolic processes critical for cancer cell survival and proliferation (Saito et al. 2022; Sivanand & Vander Heiden 2020). The KEGG database revealed that these differentially expressed metabolites are significantly associated with multiple metabolic pathways. For instance, the modulation of the ABC transporters pathway may reduce drug resistance, improving the ability of therapeutic agents to remain active within the cells, thereby enhancing treatment efficacy (Li et al. 2016). Increased activity in pathways such as protein digestion and absorption and aminoacyl-tRNA biosynthesis suggests that the treatment impacts protein synthesis, potentially reducing the ability of cancer cells to sustain rapid growth (Sung et al. 2022). Moreover, the changes in central carbon metabolism in cancer pathway indicate that the treatment targets the metabolic reprogramming cancer cells rely on, thereby limiting their ability to harness glucose and other nutrients for uncontrolled proliferation (Asai et al. 2020; Wong, Che & Ma 2017). These findings reveal the potential of targeting multiple metabolic pathways simultaneously to disrupt the cell metabolism of colon cancer and improve therapeutic outcomes.

6.3.5 Integrated analysis of proteomics and metabolomics and Elisa validation

To identify the underlying regulatory mechanisms that the combination of TQ-$CaCO_3$np and 5-FU treated colon cancer, an integrated analysis of proteomics and

metabolomics was performed. Based on the KEGG database, there were total 60 co-regulated pathways of differentially expressed proteins and metabolites (Figure 6.6A). A pathway enrichment analysis was conducted to further screen the significant regulated pathways and hub proteins and metabolites. As a result, 13 co-regulated pathways were enriched, where the most relevant to colon cancer and most significantly enriched pathways ($p<0.01$) were biosynthesis of amino acids, 2-oxocarboxylic acid metabolism, and HIF-1 signaling pathway (Figure 6.6B). In the three key pathways, Aco2, pyruvate dehydrogenase E1 component subunit alpha, somatic form, mitochondrial (Pdha1), Pdhb, alanine, glutamate, proline, glutamine, threonine, ATP, and lactate were up-regulated following treatment with TQ-$CaCO_3$np in combination with 5-FU in CT26 cells. In contrast, glyceraldehyde-3-phosphate dehydrogenase (Gapdh), phosphoserine phosphatase (Psph), small ribosomal subunit protein eS6 (Rps6), leucine, and isoleucine were down-regulated. Among these, the changes in the expression level of the four proteins (Aco2, Pdhb, Gapdh, and Psph) were further analyzed in mice tumors treated with the combination of TQ-$CaCO_3$np and 5-FU to validate the results in proteomic analysis in CT26 cells. As a result, the expression levels of Aco2 and Pdhb were up-regulated and those of Gapdh and Psph were down-regulated (Figure 6.6C), consistent with the results in proteomic analysis of CT26 cells.

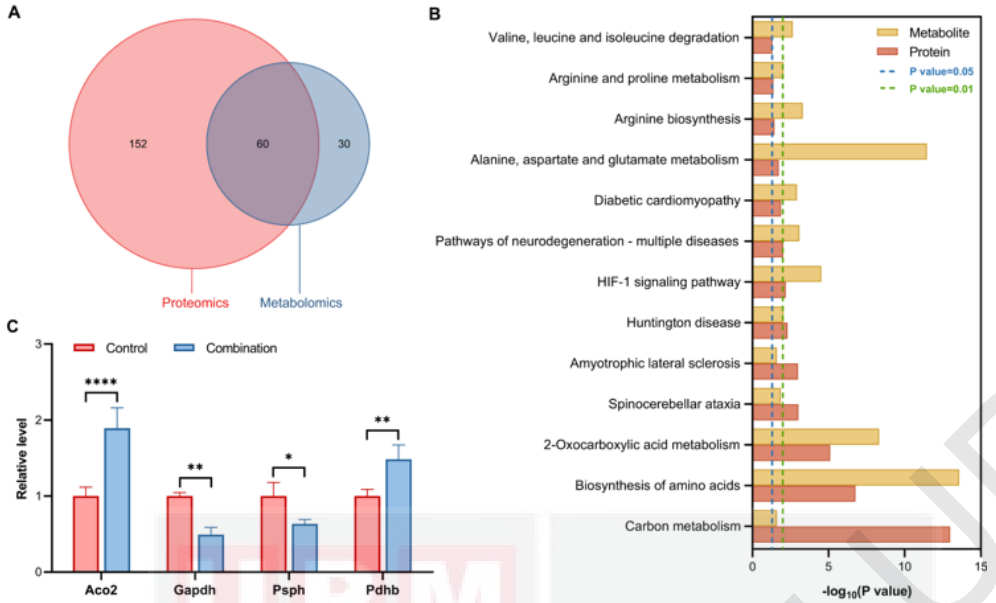

Figure 6.6: (A) The Venn diagram of the KEGG pathway involved in the differentially expressed proteins and metabolites, where the overlap indicates the co-regulated pathways; (B) the enriched co-regulated pathways of the differentially expressed proteins and metabolites; (C) the relative expression levels of Aco2, Gapdh, Psph, and Pdhb in tumors detected by Elisa. *p<0.05, **p<0.01, ****p<0.0001.

The findings of the integrated analysis underscore the positive impact of the treatment with TQ-$CaCO_3$np in combination with 5-FU on colon cancer cells, particularly through the modulation of key metabolic pathways, as illustrated in Figure 6.7. The most significantly enriched pathways—biosynthesis of amino acids, 2-oxocarboxylic acid metabolism, and HIF-1 signaling pathway—demonstrate the potential of the co-treatment for targeted metabolic intervention in colon cancer. In these pathways, the up-regulation of Aco2 and Pdhb can induce metabolic rearrangements and proliferation defects in cancer cells (Ciccarone et al. 2020; Zhu et al. 2017). Gapdh is a key enzyme that catalyzes the redox reaction in the glycolytic pathway by converting glyceraldehyde-3-phosphate to 1,3-bisphosphoglycerate, known as a housekeeping protein (Wang et al. 2023). Gapdh expression was reported to be significantly up-regulated in colorectal carcinoma tissues and cells, thus the down-regulation of Gadph

indicates the inhibitive effects of TQ-$CaCO_3$np combined with 5-FU on colon cancer development (Tang et al. 2012). Psph, an enzyme involved in the process of L-serine biosynthesis, plays a role in multiple aspects of cell behaviors such as proliferation and differentiation by producing precursors for the biosynthesis of diverse compounds including neurotransmitters, glycolipids, and thymidine (Huang et al. 2022). Psph is overexpressed in colon tumor tissues and positively correlated with depth of invasion and distant metastasis, suggesting that the down-regulation of Psph after the TQ-$CaCO_3$np and 5-FU co-treatment suppressed the progression and metastasis of colon cancer, supporting the findings in previous *in vitro* and *in vivo* studies (Sato et al. 2017).

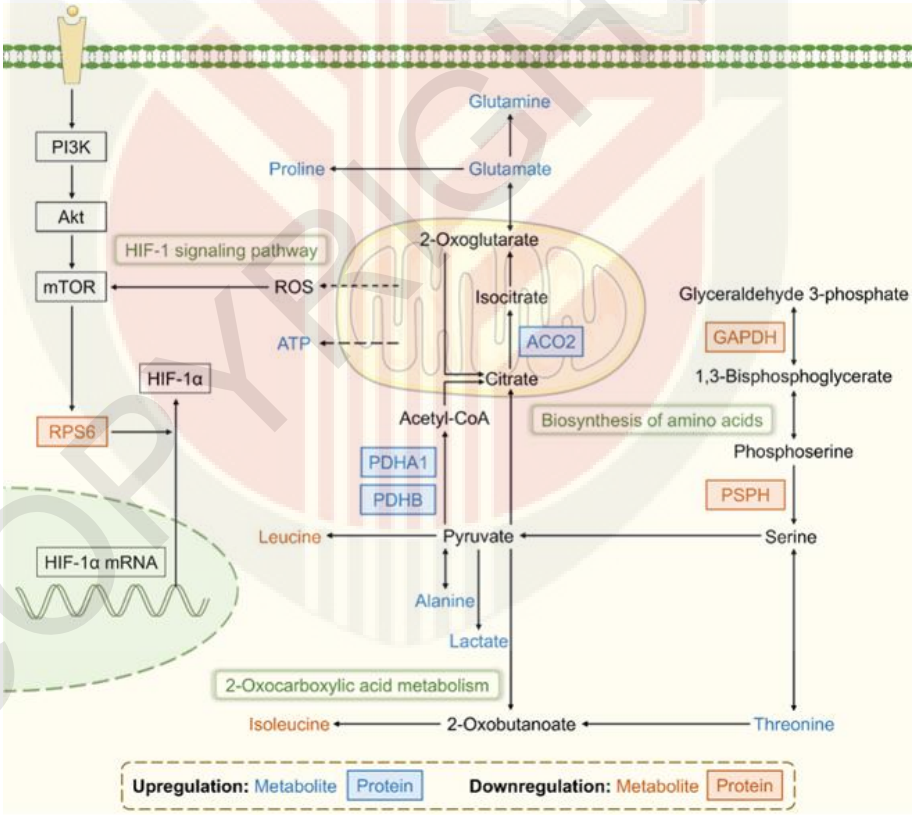

Figure 6.7: Illustration of the molecular therapeutic mechanism of the TQ-$CaCO_3$np and 5-FU combination for colon cancer.

The decrease in leucine and isoleucine levels observed in CT26 cells following treatment with TQ-$CaCO_3$np combined with 5-FU provides further insight into the

metabolic disruption induced by this co-treatment. Leucine and isoleucine, as branched-chain amino acids, are essential for various anabolic processes, including protein synthesis and cellular energy production (Holeček 2018). Their reduced levels may reflect a suppression of these anabolic pathways, which are crucial for cancer cell growth and proliferation (Xu et al. 2023b). By limiting the availability of these branched-chain amino acids, the co-treatment may hinder the ability of CT26 cells to sustain their rapid growth, contributing to the overall anti-proliferative effects.

6.4 Conclusion

The comprehensive analysis of proteomic and metabolic alterations induced by the combination treatment of TQ-$CaCO_3$np and 5-FU in colon cancer CT26 cells revealed a multifaceted disruption of critical metabolic pathways. The significant upregulation of hub proteins such as Aco2, Pdha1, and Pdhb underscores the importance of amino acid biosynthesis, 2-oxocarboxylic acid metabolism, and HIF-1 signaling in mediating the therapeutic effects. The increase in metabolites such as lactate and ATP in CT26 cells following co-treatment with TQ-$CaCO_3$np and 5-FU suggests that the combination therapy induced oxidative stress and metabolic strain, forcing colon cancer cells to upregulate compensatory pathways. The reduction in leucine and isoleucine levels, along with the downregulation of Gapdh, Psph, and Rps6, suggests that the combination therapy induces metabolic stress, impairing the ability of cancer cells to proliferate and survive. This metabolic vulnerability likely enhances the effectiveness of the treatment. The integration of proteomic and metabolomic data in this study elucidated the mechanisms underlying the combination therapy, demonstrating that TQ-$CaCO_3$np combined with 5-FU is a promising therapeutic strategy for colon cancer.

CHAPTER 7

CONCLUSION AND RECOMMENTDATION FOR FUTURE RESEARCH

7.1 Conclusion

In conclusion, this research has successfully developed and characterized porous $CaCO_3$np derived from cockle shells as an innovative delivery system for the anticancer compounds 5-FU and TQ. By optimizing the loading process using a high-speed homogenizer, the study achieved efficient encapsulation of both hydrophilic and hydrophobic compounds, demonstrating the potential for large-scale manufacturing. TQ-$CaCO_3$np in combination with 5-FU exhibited a superior combination index value than 5FU-$CaCO_3$np in combination with TQ, thus TQ-$CaCO_3$np in combination with 5-FU was further analyzed against colon cancer. The *in vitro* and *in vivo* studies consistently showed that TQ-$CaCO_3$np significantly enhances the therapeutic efficacy of 5-FU, offering a synergistic effect that effectively inhibits colon cancer cell proliferation, migration, and tumor growth. Furthermore, the combination therapy not only improved the antitumor efficacy but also mitigated the toxic side effects typically associated with 5-FU, including immunosuppression and organ-specific toxicities.

The mechanistic insights provided by the proteomic and metabolic analyses revealed that the combination of TQ-$CaCO_3$np and 5-FU disrupts critical metabolic pathways in colon cancer cells, leading to increased cellular stress and vulnerability. These findings underscore the potential of TQ-$CaCO_3$np as a novel and promising strategy for enhancing the efficacy and safety of conventional chemotherapy. Collectively, this research paves the way for the development of more effective and safer cancer therapies, with the TQ-$CaCO_3$np and 5-FU combination holding significant promise

for future clinical applications in the treatment of colon cancer.

7.2 Recommendation for future research

Based on the promising findings of this study, future research should focus on further optimizing the TQ-$CaCO_3$np and 5-FU combination therapy to maximize its therapeutic potential. One area of exploration could involve fine-tuning the nanoparticle formulation to enhance targeted delivery specifically to cancer cells, thereby reducing off-target effects and further minimizing toxicity. Investigating the therapeutic effects, pharmacokinetics, and biodistribution of TQ-$CaCO_3$np and its combination with 5-FU in more complex animal models or patient-derived xenograft models with control groups could provide valuable insights into the behaviour of these nanoparticles in a more clinically relevant setting.

Additionally, future studies should explore the underlying molecular mechanisms of the observed synergistic effects in greater detail. A deeper understanding of these mechanisms could facilitate the identification of biomarkers for patient stratification, helping to personalize treatment strategies for colon cancer. Expanding this research to include other types of cancer may also reveal broader applications for TQ-$CaCO_3$np, potentially establishing it as a versatile platform for enhancing the efficacy and safety of various chemotherapeutic agents.

REFERENCES

Abbas, M., Gururani, M. A., Ali, A., Bajwa, S., Hassan, R., Batool, S. W., Imam, M., & Wei, D. 2024. Antimicrobial Properties and Therapeutic Potential of Bioactive Compounds in Nigella sativa: A Review. *Molecules* 29(20): 4914.

Abuetabh, Y., Wu, H. H., Chai, C., Al Yousef, H., Persad, S., Sergi, C. M., & Leng, R. 2022. DNA damage response revisited: The p53 family and its regulators provide endless cancer therapy opportunities. *Experimental & Molecular Medicine* 54(10): 1658-1669.

Adepu, S. & Ramakrishna, S. 2021. Controlled Drug Delivery Systems: Current Status and Future Directions. *Molecules* 26(19): 5905.

Afrin, S., Giampieri, F., Gasparrini, M., Forbes-Hernández, T.Y., Cianciosi, D., Reboredo-Rodriguez, P., Zhang, J., Manna, P.P., Daglia, M., Atanasov, A.G. & Battino, M. 2020. Dietary phytochemicals in colorectal cancer prevention and treatment: A focus on the molecular mechanisms involved. *Biotechnology Advances* 38: 107322.

Aiello, P., Sharghi, M., Mansourkhani, S.M., Ardekan, A.P., Jouybari, L., Daraei, N., Peiro, K., Mohamadian, S., Rezaei, M., Heidari, M., Peluso, I., Ghorat, F., Bishayee, A. & Kooti, W. 2019. Medicinal plants in the prevention and treatment of colon cancer. *Oxidative Medicine and Cellular Longevity* 2019: 2075614.

Alam, M.N., Almoyad, M. & Huq, F. 2018. Polyphenols in Colorectal Cancer: Current State of Knowledge including Clinical Trials and Molecular Mechanism of Action. *BioMed Research International* 2018: 4154185.

Al-Ani, L.A., Kadir, F.A., Hashim, N.M., Julkapli, N.M., Seyfoddin, A., Lu, J., AlSaadi, M.A. & Yehye, W.A. 2020. The impact of curcumin-graphene based nanoformulation on cellular interaction and redox-activated apoptosis: An in vitro colon cancer study. *Heliyon* 6(11): e05360.

Al-Daffaie, F.M., Al-Mudhafar, S.F., Alhomsi, A., Tarazi, H., Almehdi, A.M., El-Huneidi, W., Abu-Gharbieh, E., Bustanji, Y., Alqudah, M.A.Y., Abuhelwa, A.Y., Guella, A., Alzoubi, K.H. & Semreen, M.H. 2024. Metabolomics and Proteomics in Prostate Cancer Research: Overview, Analytical Techniques, Data Analysis, and Recent Clinical Applications. *International Journal of Molecular Sciences* 25(10): 5071.

Alibolandi, M., Abnous, K., Mohammadi, M., Hadizadeh, F., Sadeghi, F., Taghavi, S., Jaafari, M.R. & Ramezani, M. 2017. Extensive preclinical investigation of polymersomal formulation of doxorubicin versus Doxil-mimic formulation. *Journal of Controlled Release* 264: 228-236.

Alkharfy, K.M., Ahmad, A., Khan, R.M.A. & Al-Shagha, W.M. 2015. Pharmacokinetic plasma behaviors of intravenous and oral bioavailability of thymoquinone in a rabbit model. *European Journal of Drug Metabolism and Pharmacokinetics* 40(3): 319-323.

Almajali, B., Al-Jamal, H.A.N., Taib, W.R.W., Ismail, I., Johan, M.F., Doolaanea, A.A. & Ibrahim, W.N. 2021. Thymoquinone, as a novel therapeutic candidate of cancers. *Pharmaceuticals* 14(4): 369.

Amin, K. & Dannenfelser, R.M. 2006. In vitro hemolysis: Guidance for the pharmaceutical scientist. *Journal of Pharmaceutical Sciences* 95(6): 1173-1176.

Araste, F., Aliabadi, A., Abnous, K., Taghdisi, S.M., Ramezani, M. & Alibolandi, M. 2021. Self-assembled polymeric vesicles: Focus on polymersomes in cancer treatment. *Journal of Controlled Release* 330: 502-528.

Arthur-Baidoo, E., Schöpfer, G., Ončák, M., Chomicz-Mańka, L., Rak, J., & Denifl, S. 2022. Electron Attachment to 5-Fluorouracil: The Role of Hydrogen Fluoride in Dissociation Chemistry. *International Journal of Molecular Sciences* 23(15): 8325.

Asai, A., Konno, M., Koseki, J., Taniguchi, M., Vecchione, A. & Ishii, H. 2020. One-carbon metabolism for cancer diagnostic and therapeutic approaches. *Cancer letters* 470: 141-148.

Babaei, M., Abnous, K., Taghdisi, S.M., Taghavi, S., Sh. Saljooghi, A., Ramezani, M. & Alibolandi, M. 2020. Targeted rod-shaped mesoporous silica nanoparticles for the co-delivery of camptothecin and survivin shRNA in to colon adenocarcinoma in vitro and in vivo. *European Journal of Pharmaceutics and Biopharmaceutics* 156: 84-96.

Bahrami, B., Hojjat-Farsangi, M., Mohammadi, H., Anvari, E., Ghalamfarsa, G., Yousefi, M. & Jadidi-Niaragh, F. 2017. Nanoparticles and targeted drug delivery in cancer therapy. *Immunology Letters* 190: 64-83.

Bai, X., Smith, Z.L., Wang, Y., Butterworth, S. & Tirella, A. 2022. Sustained Drug Release from Smart Nanoparticles in Cancer Therapy: A Comprehensive Review. *Micromachines* 13(10): 1623.

Baksi, R., Singh, D.P., Borse, S.P., Rana, R., Sharma, V. & Nivsarkar, M. 2018. In vitro and in vivo anticancer efficacy potential of Quercetin loaded polymeric nanoparticles. *Biomedicine and Pharmacotherapy* 106: 1513-1526.

Ballout, F., Monzer, A., Fatfat, M., El Ouweini, H., Jaffa, M.A., Abdel-Samad, R., Darwiche, N., Abou-Kheir, W. & Gali-Muhtasib, H. 2020. Thymoquinone induces apoptosis and DNA damage in 5-fluorouracil-resistant colorectal cancer stem/progenitor cells. *Oncotarget* 11(31): 2959-2972.

Banerjee, A., Pathak, S., Subramanium, V.D., Dharanivasan, G., Murugesan, R. & Verma, R.S. 2017. Strategies for targeted drug delivery in treatment of colon cancer: current trends and future perspectives. *Drug Discovery Today* 22(8): 1224-1232.

Bastos, F.R., Soares da Costa, D., Reis, R.L., Alves, N.M., Pashkuleva, I. & Costa, R.R. 2023. Layer-by-layer coated calcium carbonate nanoparticles for targeting breast cancer cells. *Biomaterials Advances* 153: 213563.

Bharatham, H., Zakaria, M.Z.A.B., Perimal, E.K., Yusof, L.M. & Hamid, M. 2014. Mineral and physiochemical evaluation of Cockle shell (Anadara granosa) and other selected Molluscan shell as potential biomaterials. *Sains Malaysiana* 43(7): 1023-1029.

Bhaskaran, N.A. & Kumar, L. 2021. Treating colon cancers with a non-conventional yet strategic approach: An overview of various nanoparticulate systems. *Journal of controlled release* 336: 16-39.

Bhattacharya, S., Ahir, M., Patra, P., Mukherjee, S., Ghosh, S., Mazumdar, M., Chattopadhyay, S., Das, T., Chattopadhyay, D. & Adhikary, A. 2015. PEGylated-thymoquinone-nanoparticle mediated retardation of breast cancer cell migration by deregulation of cytoskeletal actin polymerization through miR-34a. *Biomaterials* 51: 91-107.

Blijlevens, M., Li, J. & van Beusechem, V.W. 2021. Biology of the mrna splicing machinery and its dysregulation in cancer providing therapeutic opportunities. *International journal of molecular sciences* 22(10): 5110.

Bogaert, J. & Prenen, H. 2014. Molecular genetics of colorectal cancer. *Annals of Gastroenterology* 27(1): 9.

Borrego-Sánchez, A., Sánchez-Espejo, R., Albertini, B., Passerini, N., Cerezo, P., Viseras, C. & Sainz-Díaz, C.I. 2019. Ground calcium carbonate as a low cost and biosafety excipient for solubility and dissolution improvement of praziquantel. *Pharmaceutics* 11(10): 533.

Boța, M., Vlaia, L., Jîjie, A.-R., Marcovici, I., Crișan, F., Oancea, C., Dehelean, C.A., Mateescu, T. & Moacă, E.-A. 2024. Exploring Synergistic Interactions between Natural Compounds and Conventional Chemotherapeutic Drugs in Preclinical Models of Lung Cancer. *Pharmaceuticals* 17(5): 598.

Boulos, R.A., Zhang, F., Tjandra, E.S., Martin, A.D., Spagnoli, D. & Raston, C.L. 2014. Spinning up the polymorphs of calcium carbonate. *Scientific Reports* 4: 3616.

Brandi, G., De Lorenzo, S., Nannini, M., Curti, S., Ottone, M., Dall'Olio, F.G., Barbera, M.A., Pantaleo, M.A. & Biasco, G. 2016. Adjuvant chemotherapy for resected colorectal cancer metastases: Literature review and meta-analysis. *World Journal of Gastroenterology* 22(2): 519-533.

Bravo, R., Parra, V., Gatica, D., Rodriguez, A.E., Torrealba, N., Paredes, F., Wang, Z. V., Zorzano, A., Hill, J.A., Jaimovich, E., Quest, A.F.G. & Lavandero, S. 2013. Endoplasmic Reticulum and the Unfolded Protein Response. Dynamics and Metabolic Integration. *International Review of Cell and Molecular Biology* 301: 215-290.

Bray, F., Laversanne, M., Sung, H., Ferlay, J., Siegel, R.L., Soerjomataram, I. & Jemal, A. 2024. Global cancer statistics 2022: GLOBOCAN estimates of incidence and mortality worldwide for 36 cancers in 185 countries. *CA: A Cancer Journal for Clinicians* 74(3): 229-263.

Brouwer, N.P.M., Bos, A.C.R.K., Lemmens, V.E.P.P., Tanis, P.J., Hugen, N., Nagtegaal, I.D., de Wilt, J.H.W. & Verhoeven, R.H.A. 2018. An overview of 25 years of incidence, treatment and outcome of colorectal cancer patients. *International Journal of Cancer* 143(11): 2758-2766.

Browning, K.S. & Bailey-Serres, J. 2015. Mechanism of Cytoplasmic mRNA Translation. *The Arabidopsis Book* 13: e0176.

Butt, A.S., Nisar, N. & Mughal, T. 2018. A review: Therapeutics potentials of phytochemical drugs and their loading in pH specific degradable nano-drug carrier targeting colorectal cancer. *Journal of the Pakistan Medical Association* 68(4): 607-614.

Caicedo-Pineda, G.A., Prada-Fonseca, M.C., Casas-Botero, A.E. & Martínez-Tejada, H.V. 2018. Effect of the tryptone concentration on the calcium carbonate biomineralization mediated by Bacillus cereus. *DYNA (Colombia)* 85(205): 69-75.

Chemmalar, S., Intan-Shameha, A.R., Abdullah, C.A.C., Razak, N.A.A., Yusof, L.M., Ajat, M., Gowthaman, N.S.K. & Bakar, M.Z.A. 2021. Synthesis and Characterization of Gefitinib and Paclitaxel Mono and Dual Drug-Loaded Blood Cockle Shells (Anadara granosa)-Derived Aragonite CaCO3 Nanoparticles. *Nanomaterials* 11(8): 1988.

Chen, M.C., Lee, N.H., Hsu, H.H., Ho, T.J., Tu, C.C., Chen, R.J., Lin, Y.M., Viswanadha, V.P., Kuo, W.W. & Huang, C.Y. 2017. Inhibition of NF-κB and metastasis in irinotecan (CPT-11)-resistant LoVo colon cancer cells by thymoquinone via JNK and p38. *Environmental Toxicology* 32(2): 669-678.

Chen, Y., Ni, J., Gao, Y., Zhang, J., Liu, X., Chen, Y., Chen, Z. & Wu, Y. 2020. Integrated proteomics and metabolomics reveal the comprehensive characterization of antitumor mechanism underlying Shikonin on colon cancer patient-derived xenograft model. *Scientific Reports* 10(1): 14092.

Chiu, C.C., Lin, W.L., Shi, H.Y., Huang, C.C., Chen, J.J., Su, S. Bin, Lai, C.C., Chao, C.M., Tsao, C.J., Chen, S.H. & Wang, J.J. 2019. Comparison of oncologic outcomes in laparoscopic versus open surgery for non-metastatic colorectal cancer: Personal experience in a single institution. *Journal of Clinical Medicine* 8(6): 875.

Chis, A. A., Dobrea, C., Morgovan, C., Arseniu, A. M., Rus, L. L., Butuca, A., Juncan, A. M., Totan, M., Vonica-Tincu, A. L., Cormos, G., Muntean, A. C., Muresan, M. L., Gligor, F. G., & Frum, A. 2020. Applications and Limitations of Dendrimers in Biomedicine. *Molecules* 25(17): 3982.

Chou, T.-C. 2008. Preclinical *versus* clinical drug combination studies. *Leukemia & Lymphoma* 49(11): 2059-2080.

Chou, T.-C. 2010. Drug Combination Studies and Their Synergy Quantification Using the Chou-Talalay Method. *Cancer Research* 70(2): 440-446.

Christensen, S., Van der Roest, B., Besselink, N., Janssen, R., Boymans, S., Martens, J.W.M., Yaspo, M.L., Priestley, P., Kuijk, E., Cuppen, E. & Van Hoeck, A. 2019. 5-Fluorouracil treatment induces characteristic T>G mutations in human cancer. *Nature Communications* 10(1): 4571.

Chung, C.H., Jung, W., Keum, H., Kim, T.W. & Jon, S. 2020. Nanoparticles Derived from the Natural Antioxidant Rosmarinic Acid Ameliorate Acute Inflammatory Bowel Disease. *ACS Nano* 14(6): 6887-6896.

Chuzeville, L., Boury, F., Duday, D., Anand, R., Moretto, E. & Thomann, J.S. 2022. Eco-friendly processes for the synthesis of amorphous calcium carbonate nanoparticles in ethanol and their stabilisation in aqueous media. *Green Chemistry* 24(3): 1270-1284.

Ciccarone, F., Di Leo, L., Lazzarino, G., Maulucci, G., Di Giacinto, F., Tavazzi, B. & Ciriolo, M.R. 2020. Aconitase 2 inhibits the proliferation of MCF-7 cells promoting mitochondrial oxidative metabolism and ROS/FoxO1-mediated autophagic response. *British Journal of Cancer* 122(2): 182-193.

Clarkson, C., Maharaj, V.J., Crouch, N.R., Grace, O.M., Pillay, P., Matsabisa, M.G., Bhagwandin, N., Smith, P.J. & Folb, P.I. 2004. In vitro antiplasmodial activity of medicinal plants native to or naturalised in South Africa. *Journal of Ethnopharmacology* 92(2-3): 177-191.

Criado, A., Gómez, I. J., & Mosquera, J. 2022. Dendrimers: Exploring Their Wide Structural Variety and Applications. *Polymers* 15(22): 4369.

Demeckova, V., Mudronova, D., Gancarcikova, S., Kubatka, P., Kajo, K., Kassayova, M., Bojkova, B., Adamkov, M. & Solár, P. 2022. 5-Fluorouracil Treatment of CT26 Colon Cancer Is Compromised by Combined Therapy with IMMODIN. *International Journal of Molecular Sciences* 23(12): 6374.

Deng, X., Yang, Z., Han, M., Ismail, N., Esa, N. M., Razis, A. F. A., Bakar, M. Z. A., & Chan, K. W. 2024. Comprehensive Insights into the Combinatorial Uses of Selected Phytochemicals in Colorectal Cancer Prevention and Treatment: Isothiocyanates, Quinones, Carotenoids, and Alkaloids. *Phytotherapy Research*. Advance online publication.

Dey, D., Kumar, P. & Samantaray, S. 2017. A review of nanofluid preparation, stability, and thermo-physical properties. *Heat Transfer - Asian Research* 46(8): 1413-1442.

Di, J., Gao, X., Du, Y., Zhang, H., Gao, J. & Zheng, A. 2021. Size, shape, charge and "stealthy" surface: Carrier properties affect the drug circulation time in vivo. *Asian Journal of Pharmaceutical Sciences* 16(4): 444-458.

Dong, Z., Feng, L., Hao, Y., Li, Q., Chen, M., Yang, Z., Zhao, H. & Liu, Z. 2020. Synthesis of CaCO3-Based Nanomedicine for Enhanced Sonodynamic Therapy via Amplification of Tumor Oxidative Stress. *Chem* 6(6): 1391-1407.

Duarte, D. & Vale, N. 2022a. Evaluation of synergism in drug combinations and reference models for future orientations in oncology. *Current Research in Pharmacology and Drug Discovery* 3: 100110.

Duarte, D. & Vale, N. 2022b. Combining repurposed drugs to treat colorectal cancer. *Drug Discovery Today* 27(1): 165-184.

Eatemadi, A., Daraee, H., Karimkhanloo, H., Kouhi, M., Zarghami, N., Akbarzadeh, A., Abasi, M., Hanifehpour, Y. & Joo, S.W. 2014. Carbon nanotubes: Properties, synthesis, purification, and medical applications. *Nanoscale Research Letters* 9(1): 393.

Elumalai, K., Srinivasan, S. & Shanmugam, A. 2024. Review of the efficacy of nanoparticle-based drug delivery systems for cancer treatment. *Biomedical Technology* 5: 109-122.

Fang, H., Ni, K., Wu, J., Li, J., Huang, L. & Reible, D. 2019. The effects of hydrogen bonding on the shear viscosity of liquid water. *International Journal of Sediment Research* 34(1): 8-13.

Farooq, M.U., Novosad, V., Rozhkova, E.A., Wali, H., Ali, A., Fateh, A.A., Neogi, P.B., Neogi, A. & Wang, Z. 2018. Gold Nanoparticles-enabled Efficient Dual Delivery of Anticancer Therapeutics to HeLa Cells. *Scientific Reports* 8(1): 2907.

Farooqi, A.A., Attar, R. & Xu, B. 2022. Anticancer and Anti-Metastatic Role of Thymoquinone: Regulation of Oncogenic Signaling Cascades by Thymoquinone. *International journal of molecular sciences* 23(11): 6311.

Farooqi, A.A., de la Roche, M., Djamgoz, M.B.A. & Siddik, Z.H. 2019. Overview of the oncogenic signaling pathways in colorectal cancer: Mechanistic insights. *Seminars in Cancer Biology* 58: 65-79.

Farzan, M., Roth, R., Schoelkopf, J., Huwyler, J. & Puchkov, M. 2023. The processes behind drug loading and release in porous drug delivery systems. *European Journal of Pharmaceutics and Biopharmaceutics* 189: 133-151.

Fearon, E.R. & Vogelstein, B. 1990. A genetic model for colorectal tumorigenesis. *Cell* 61(5): 759-767.

Febrida, R., Cahyanto, A., Herda, E., Muthukanan, V., Djustiana, N., Faizal, F., Panatarani, C. & Joni, I.M. 2021. Synthesis and characterization of porous caco3 vaterite particles by simple solution method. *Materials* 14(16): 4425.

Ferreira, A.M., Vikulina, A., Cave, G.W.V., Loughlin, M., Puddu, V. & Volodkin, D. 2023. Vaterite vectors for the protection, storage and release of silver nanoparticles. *Journal of Colloid and Interface Science* 631: 165-180.

Forgie, B.N., Prakash, R., Goyeneche, A.A. & Telleria, C.M. 2024. Vitality, viability, long-term clonogenic survival, cytotoxicity, cytostasis and lethality: what do they mean when testing new investigational oncology drugs? *Discover oncology* 15(1): 5.

Franken, N.A.P., Rodermond, H.M., Stap, J., Haveman, J. & van Bree, C. 2006. Clonogenic assay of cells in vitro. *Nature Protocols* 1(5): 2315-2319.

Fu, W., Mohd Noor, M.H., Yusof, L.M., Ibrahim, T.A.T., Keong, Y.S., Jaji, A.Z. & Zakaria, M.Z.A.B. 2017. In vitro evaluation of a novel pH sensitive drug delivery system-based cockle shell-derived aragonite nanoparticles against osteosarcoma. *Journal of Experimental Nanoscience* 12(1): 166-187.

Fu, W., Rameli, M.A. bin P., Ibrahim, T.A.T., Noor, M.H.M., Yusof, L.M. & Zakaria, M.Z.A.B. 2019. In vivo evaluation of anticancer efficacy of drug loaded cockle shell-derived aragonite nanoparticles. *Journal of Biomedical Materials Research - Part B Applied Biomaterials* 107(6): 1898-1907.

Ghaji, M.S., Zakaria, Z.A.B., Intan Shameha, A.R., Noor, M.H.M. & Hazilawati, H. 2018. Novel synthesis of nanoparticles from cockle shells via mechanical method for cytarabine drug release. *Journal of Computational and Theoretical Nanoscience* 15(4): 1128-1136.

Gordon, J.L., Brown, M.A. & Reynolds, M.M. 2018. Cell-Based Methods for Determination of Efficacy for Candidate Therapeutics in the Clinical Management of Cancer. *Diseases* 6(4): 85.

Grivicich, I., Mans, D.R.A., Peters, G.J. & Schwartsmann, C. 2001. Irinotecan and oxaliplatin: An overview of the novel chemotherapeutic options for the treatment of advanced colorectal cancer. *Brazilian Journal of Medical and Biological Research* 34(9): 1087-1103.

Guerbette, T., Boudry, G. & Lan, A. 2022. Mitochondrial function in intestinal epithelium homeostasis and modulation in diet-induced obesity. *Molecular metabolism* 63: 101546.

Gulbake, A., Jain, A., Jain, A., Jain, A. & Jain, S.K. 2016. Insight to drug delivery aspects for colorectal cancer. *World Journal of Gastroenterology* 22(2): 582-599.

Guo, Q., Jin, Y., Chen, X., Ye, X., Shen, X., Lin, M., Zeng, C., Zhou, T., & Zhang, J. 2024. NF-κB in biology and targeted therapy: New insights and translational implications. *Signal Transduction and Targeted Therapy* 9(1): 1-37.

Guo, X., Wang, L., Wei, X. & Zhou, S. 2016. Polymer-based drug delivery systems for cancer treatment. *Journal of Polymer Science, Part A: Polymer Chemistry* 54(22): 843.

Hamidu, A., Mokrish, A., Mansor, R., Razak, I.S.A., Danmaigoro, A., Jaji, A.Z. & Bakar, Z.A. 2019. Modified methods of nanoparticles synthesis in ph-sensitive nano-carriers production for doxorubicin delivery on MCF-7 breast cancer cell line. *International Journal of Nanomedicine* 14: 3615-3627.

Hammadi, N.I., Abba, Y., Hezmee, M.N.M., Razak, I.S.A., Kura, A.U. & Zakaria, Z.A.B. 2017. Evaluation of in vitro efficacy of docetaxel-loaded calcium carbonate aragonite nanoparticles (DTX-CaCO3NP) on 4T1 mouse breast cancer cell line. *In Vitro Cellular and Developmental Biology - Animal* 53(10): 896-907.

Handali, S., Moghimipour, E., Rezaei, M., Ramezani, Z., Kouchak, M., Amini, M., Angali, K.A., Saremy, S. & Dorkoosh, F.A. 2018. A novel 5-Fluorouracil targeted delivery to colon cancer using folic acid conjugated liposomes. *Biomedicine and Pharmacotherapy* 108: 1259-1273.

Hani, U., Honnavalli, Y.K., Begum, M.Y., Yasmin, S., Osmani, R.A.M. & Ansari, M.Y. 2021. Colorectal cancer: A comprehensive review based on the novel drug delivery systems approach and its management. *Journal of Drug Delivery Science and Technology* 63: 102532.

Haq, A. & Michniak-Kohn, B. 2018. Effects of solvents and penetration enhancers on transdermal delivery of thymoquinone: Permeability and skin deposition study. *Drug Delivery* 25(1): 1943–1949.

Hasin, Y., Seldin, M. & Lusis, A. 2017. Multi-omics approaches to disease. *Genome biology* 18(1): 83.

He, W. ting, Zhu, Y. hua, Zhang, T., Abulimiti, P., Zeng, F. ye, Zhang, L. ping, Luo, L. juan, Xie, X. mei & Zhang, H. liang. 2019. Curcumin Reverses 5-Fluorouracil Resistance by Promoting Human Colon Cancer HCT-8/5-FU Cell Apoptosis and Down-regulating Heat Shock Protein 27 and P-Glycoprotein. *Chinese Journal of Integrative Medicine* 25(6): 416-424.

He, Y.C., Chen, J.W., Cao, J., Pan, D.Y. & Qiao, J.G. 2003. Toxicities and therapeutic effect of 5-fluorouracil controlled release implant on tumor-bearing rats. *World Journal of Gastroenterology* 9(8): 1795-1798.

Heinz, H., Pramanik, C., Heinz, O., Ding, Y., Mishra, R.K., Marchon, D., Flatt, R.J., Estrela-Lopis, I., Llop, J., Moya, S. & Ziolo, R.F. 2017. Nanoparticle decoration with surfactants: Molecular interactions, assembly, and applications. *Surface Science Reports* 72(1): 1-58.

Henamayee, S., Banik, K., Sailo, B.L., Shabnam, B., Harsha, C., Srilakshmi, S., Naidu, V.G.M., Baek, S.H., Ahn, K.S. & Kunnumakkara, A.B. 2020. Therapeutic emergence of rhein as a potential anticancer drug: A review of its molecular targets and anticancer properties. *Molecules* 25(10): 2278.

Hoar, T.P. & Schulman, J.H. 1943. Transparent water-in-oil dispersions: The oleopathic hydro-micelle. *Nature* 152(3847): 102-103.

Holeček, M. 2018. Branched-chain amino acids in health and disease: Metabolism, alterations in blood plasma, and as supplements. *Nutrition & metabolism* 15: 33.

Homayoonfal, M., Asemi, Z. & Yousefi, B. 2022. Potential anticancer properties and mechanisms of thymoquinone in osteosarcoma and bone metastasis. *Cellular & molecular biology letters* 27(1): 21.

Hoque, M.E. 2013. Processing and Characterization of Cockle Shell Calcium Carbonate (CaCO3) Bioceramic for Potential Application in Bone Tissue Engineering. *Journal of Material Science & Engineering* 2(4): 1-5.

Hsu, H.H., Chen, M.C., Day, C.H., Lin, Y.M., Li, S.Y., Tu, C.C., Padma, V.V., Shih, H.N., Kuo, W.W. & Huang, C.Y. 2017. Thymoquinone suppresses migration of LoVo human colon cancer cells by reducing prostaglandin E2 induced COX-2 activation. *World Journal of Gastroenterology* 23(7): 1171–1179.

Huang, H., Zhang, W., Liu, Z., Guo, H. & Zhang, P. 2020a. Smart responsive-calcium carbonate nanoparticles for dual-model cancer imaging and treatment. *Ultrasonics* 108: 106198.

Huang, L., Huang, X.H., Yang, X., Hu, J.Q., Zhu, Y.Z., Yan, P.Y. & Xie, Y. 2024. Novel nano-drug delivery system for natural products and their application. *Pharmacological research* 201: 107100.

Huang, M.Y., Liu, X.Y., Shao, Q., Zhang, X., Miao, L., Wu, X.Y., Xu, Y.X., Wang, F., Wang, H.Y., Zeng, L. & Deng, L. 2022. Phosphoserine phosphatase as a prognostic biomarker in patients with gastric cancer and its potential association with immune cells. *BMC Gastroenterology* 22(1): 1.

Huang, Y., Sun, H., Ma, X., Zeng, Y., Pan, Y., Yu, D., Liu, Z. & Xiang, Y. 2020b. HLA-F-AS1/miR-330-3p/PFN1 axis promotes colorectal cancer progression. *Life Sciences* 254: 117180.

Huber, M., Stark, W.J., Loher, S., Maciejewski, M., Krumeich, F. & Baiker, A. 2005. Flame synthesis of calcium carbonate nanoparticles. *Chemical Communications* (5): 648-650.

Ibiyeye, K.M., Idris, S.B. & Zuki, A.B.Z. 2020. Cockle shell-derived aragonite calcium carbonate nanoparticle for targeting cancer and breast cancer stem cells. *Cancer Nanotechnology* 11(1): 10.

Ibrahim, W.N., Rosli, L.M.B.M. & Doolaanea, A.A. 2020. Formulation, cellular uptake and cytotoxicity of thymoquinone-loaded plga nanoparticles in malignant melanoma cancer cells. *International Journal of Nanomedicine* 15: 8059–8074.

Icard, P., Coquerel, A., Wu, Z., Gligorov, J., Fuks, D., Fournel, L., Lincet, H. & Simula, L. 2021. Understanding the central role of citrate in the metabolism of cancer cells and tumors: An update. *International journal of molecular sciences* 22(12): 6587.

Idris, S., Refaat, B., Almaimani, R.A., Ahmed, H.G., Ahmad, J., Alhadrami, M., El-Readi, M.Z., Elzubier, M.E., Alaufi, H.A.A., Al-Amin, B., Alghamdi, A.A., Bahwerth, F., Minshawi, F., Kabrah, S.M. & Aslam, A. 2022. Enhanced in vitro tumoricidal effects of 5-Fluorouracil, thymoquinone, and active vitamin D3 triple therapy against colon cancer cells by attenuating the PI3K/AKT/mTOR pathway. *Life Sciences* 296: 120442.

Idris, S.B., Kadir, A.A., Jesse, F.F.A., Ramanoon, S.Z., Basit, M.A., Zakaria, Z.A. & Zakaria, M.Z.A.B. 2019. Synthesis, characterization, and in vitro release of oxytetracycline loaded in pH-responsive CaCO3 nanoparticles. *Journal of Applied Pharmaceutical Science* 9(11): 19-27.

Isa, T., Zakaria, Z.A.B., Rukayadi, Y., Hezmee, M.N.M., Jaji, A.Z., Imam, M.U., Hammadi, N.I. & Mahmood, S.K. 2016. Antibacterial activity of ciprofloxacin-encapsulated cockle shells calcium carbonate (Aragonite) nanoparticles and its biocompatability in macrophage J774A.1. *International Journal of Molecular Sciences* 17(5): 713.

Islam, K.N., Bakar, M.Z.B.A., Ali, M.E., Hussein, M.Z. Bin, Noordin, M.M., Loqman, M.Y., Miah, G., Wahid, H. & Hashim, U. 2013. A novel method for the synthesis of calcium carbonate (aragonite) nanoparticles from cockle shells. *Powder Technology* 235: 70-75.

Islam, K.N., Bakar, M.Z.B.A., Noordin, M.M., Hussein, M.Z. Bin, Rahman, N.S.B.A. & Ali, M.E. 2011. Characterisation of calcium carbonate and its polymorphs from cockle shells (Anadara granosa). *Powder Technology* 213(1): 188-191.

ISO 10993-5:2009. *Biological evaluation of medical devices – Part 5: Tests for in vitro cytotoxicity*.

Ivanova, O.M., Anufrieva, K.S., Kazakova, A.N., Malyants, I.K., Shnaider, P. V., Lukina, M.M. & Shender, V.O. 2023. Non-canonical functions of spliceosome components in cancer progression. *Cell death & disease* 14(2): 77.

Janjua, T. I., Cao, Y., Kleitz, F., Linden, M., Yu, C., & Popat, A. 2023. Silica nanoparticles: A review of their safety and current strategies to overcome biological barriers. *Advanced Drug Delivery Reviews* 203: 115115.

Jazayeri, M.H., Amani, H., Pourfatollah, A.A., Pazoki-Toroudi, H. & Sedighimoghaddam, B. 2016. Various methods of gold nanoparticles (GNPs) conjugation to antibodies. *Sensing and Bio-Sensing Research* 9: 17-22.

Jha, R. K., Kouzine, F., & Levens, D. 2023. MYC function and regulation in physiological perspective. *Frontiers in Cell and Developmental Biology* 11: 1268275.

Jiang, W.G., Sanders, A.J., Katoh, M., Ungefroren, H., Gieseler, F., Prince, M., Thompson, S.K., Zollo, M., Spano, D., Dhawan, P., Sliva, D., Subbarayan, P.R., Sarkar, M., Honoki, K., Fujii, H., Georgakilas, A.G., Amedei, A., Niccolai, E., Amin, A., Ashraf, S.S., Ye, L., Helferich, W.G., Yang, X., Boosani, C.S., Guha, G., Ciriolo, M.R., Aquilano, K., Chen, S., Azmi, A.S., Keith, W.N., Bilsland, A., Bhakta, D., Halicka, D., Nowsheen, S., Pantano, F. & Santini, D. 2015. Tissue invasion and metastasis: Molecular, biological and clinical perspectives. *Seminars in Cancer Biology* 35: S244-S275.

Jin, J., Byun, J.K., Choi, Y.K. & Park, K.G. 2023. Targeting glutamine metabolism as a therapeutic strategy for cancer. *Experimental & molecular medicine* 55(4): 706-715.

Jin, K.T., Lu, Z.B., Chen, J.Y., Liu, Y.Y., Lan, H.R., Dong, H.Y., Yang, F., Zhao, Y.Y. & Chen, X.Y. 2020. Recent Trends in Nanocarrier-Based Targeted Chemotherapy: Selective Delivery of Anticancer Drugs for Effective Lung, Colon, Cervical, and Breast Cancer Treatment. *Journal of Nanomaterials* 2020(1): 9184284.

Jrah-Harzallah, H., Ben-Hadj-Khalifa, S., Almawi, W.Y., Maaloul, A., Houas, Z. & Mahjoub, T. 2013. Effect of thymoquinone on 1,2-dimethyl-hydrazine-induced oxidative stress during initiation and promotion of colon carcinogenesis. *European Journal of Cancer* 49(5): 1127–1135.

Ju, Y.M., Zhao, Y., Guan, Q.F., Yang, S.Y., Wang, W., Yan, B.B., Meng, Y.F., Li, S.C., Tang, P.P., Mao, L.B. & Yu, S.H. 2022. Amorphous Calcium Carbonate Cluster Nanospheres in Water-Deficient Organic Solvents. *Angewandte Chemie - International Edition* 61(47): e202211254.

Jubelin, C., Muñoz-Garcia, J., Griscom, L., Cochonneau, D., Ollivier, E., Heymann, M.-F., Oliver, L. & Heymann, D. 2022. Three-dimensional in vitro culture models in oncology research. *Cell & Bioscience* 12(1): 155.

Jung, B., Staudacher, J.J. & Beauchamp, D. 2017. Transforming Growth Factor β Superfamily Signaling in Development of Colorectal Cancer. *Gastroenterology* 152(1): 36-52.

Kabil, N., Bayraktar, R., Kahraman, N., Mokhlis, H.A., Calin, G.A., Lopez-Berestein, G. & Ozpolat, B. 2018. Thymoquinone inhibits cell proliferation, migration, and invasion by regulating the elongation factor 2 kinase (eEF-2K) signaling axis in triple-negative breast cancer. *Breast Cancer Research and Treatment* 171(3): 593-605.

Kciuk, M., Yahya, E.B., Mohamed Ibrahim Mohamed, M., Rashid, S., Iqbal, M.O., Kontek, R., Abdulsamad, M.A. & Allaq, A.A. 2023. Recent Advances in Molecular Mechanisms of Cancer Immunotherapy. *Cancers* 15(10): 2721.

Kensara, O.A., El-Shemi, A.G., Mohamed, A.M., Refaat, B., Idris, S. & Ahmad, J. 2016a. Thymoquinone subdues tumor growth and potentiates the chemopreventive effect of 5-fluorouracil on the early stages of colorectal carcinogenesis in rats. *Drug Design, Development and Therapy* 10: 2239-2253.

Kensara, O.A., El-Shemi, A.G., Mohamed, A.M., Refaat, B., Idris, S. & Ahmad, J. 2016b. Thymoquinone subdues tumor growth and potentiates the chemopreventive effect of 5-fluorouracil on the early stages of colorectal carcinogenesis in rats. *Drug Design, Development and Therapy* 10: 2239.

Kezuka, Y., Kawai, K., Eguchi, K. & Tajika, M. 2017. Fabrication of single-crystalline calcite needle-like particles using the aragonite-calcite phase transition. *Minerals* 7(8): 133.

Khalid, K., Tan, X., Mohd Zaid, H.F., Tao, Y., Lye Chew, C., Chu, D.T., Lam, M.K., Ho, Y.C., Lim, J.W. & Chin Wei, L. 2020. Advanced in developmental organic and inorganic nanomaterial: a review. *Bioengineered* 11(1): 328-355.

Khan, M.A., Tania, M., Fu, S. & Fu, J. 2017. Thymoquinone, as an anticancer molecule: From basic research to clinical investigation. *Oncotarget* 8(31): 51907-51919.

Khan, M.A. & Younus, H. 2018. Thymoquinone Shows the Diverse Therapeutic Actions by Modulating Multiple Cell Signaling Pathways: Single Drug for Multiple Targets. *Current Pharmaceutical Biotechnology* 19(12): 934-945.

Khan, S., Imran, M., Butt, T.T., Ali Shah, S.W., Sohail, M., Malik, A., Das, S., Thu, H.E., Adam, A. & Hussain, Z. 2018. Curcumin based nanomedicines as efficient nanoplatform for treatment of cancer: New developments in reversing cancer drug resistance, rapid internalization, and improved anticancer efficacy. *Trends in Food Science and Technology* 80: 8-22.

Kim, Y., Caumon, M.C., Barres, O., Sall, A. & Cauzid, J. 2021. Identification and composition of carbonate minerals of the calcite structure by Raman and infrared spectroscopies using portable devices. *Spectrochimica Acta - Part A: Molecular and Biomolecular Spectroscopy* 261: 119980.

Kiranda, H.K., Mahmud, R., Abubakar, D. & Zakaria, Z.A. 2018. Fabrication, characterization and cytotoxicity of spherical-shaped conjugated gold-cockle shell derived calcium carbonate nanoparticles for biomedical applications. *Nanoscale Research Letters* 13(1): 1.

Kirchhoff, P., Clavien, P.A. & Hahnloser, D. 2010. Complications in colorectal surgery: Risk factors and preventive strategies. *Patient Safety in Surgery* 4(1): 5.

Kotelevets, L., Chastre, E., Desmaële, D. & Couvreur, P. 2016. Nanotechnologies for the treatment of colon cancer: From old drugs to new hope. *International Journal of Pharmaceutics* 514(1): 24-40.

Koveitypour, Z., Panahi, F., Vakilian, M., Peymani, M., Seyed Forootan, F., Nasr Esfahani, M.H. & Ghaedi, K. 2019. Signaling pathways involved in colorectal cancer progression. *Cell and Bioscience* 9(1): 1-14.

Kumari, S. & Kondapi, A.K. 2017. Lactoferrin nanoparticle mediated targeted delivery of 5-fluorouracil for enhanced therapeutic efficacy. *International Journal of Biological Macromolecules* 95: 232-237.

Kwon, Y.W., Jo, H.S., Bae, S., Seo, Y., Song, P., Song, M. & Yoon, J.H. 2021. Application of Proteomics in Cancer: Recent Trends and Approaches for Biomarkers Discovery. *Frontiers in medicine* 8: 747333.

Lauth, V., Maas, M. & Rezwan, K. 2017. An evaluation of colloidal and crystalline properties of CaCO3 nanoparticles for biological applications. *Materials Science and Engineering C* 78: 305-314.

Lee, G., Joung, J.Y., Cho, J.H., Son, C.G. & Lee, N. 2018. Overcoming P-Glycoprotein-Mediated Multidrug Resistance in Colorectal Cancer: Potential Reversal Agents among Herbal Medicines. *Evidence-based Complementary and Alternative Medicine* 2018: 3412074.

Lei, X., Lv, X., Liu, M., Yang, Z., Ji, M., Guo, X. & Dong, W. 2012. Thymoquinone inhibits growth and augments 5-fluorouracil-induced apoptosis in gastric cancer cells both in vitro and in vivo. *Biochemical and Biophysical Research Communications* 417(2): 864-868.

Li, W., Zhang, H., Assaraf, Y.G., Zhao, K., Xu, X., Xie, J., Yang, D.H. & Chen, Z.S. 2016. Overcoming ABC transporter-mediated multidrug resistance: Molecular mechanisms and novel therapeutic drug strategies. *Drug resistance updates: reviews and commentaries in antimicrobial and anticancer chemotherapy* 27: 14-29.

Lôbo, G.C.N.B., Paiva, K.L.R., Silva, A.L.G., Simões, M.M., Báo, S.N. & Radicchi, M.A. 2021. Nanocarriers used in drug delivery to enhance immune system in cancer therapy. *Pharmaceutics* 13(8): 1167.

Ma, J., Zhang, Y., Deng, H., Liu, Y., Lei, X., He, P. & Dong, W. 2020. Thymoquinone inhibits the proliferation and invasion of esophageal cancer cells by disrupting the AKT/GSK-3β/Wnt signaling pathway via PTEN upregulation. *Phytotherapy Research* 34(12): 3388-3399.

Madani, F., Kazemi, S., Shirafkan, F., Lotfi, M., Hosseini, S.M. & Moghadamnia, A.A. 2023. Thymoquinone protects against 5-Fluorouracil-induced mucositis by NF-κβ and HIF-1 mechanisms in mice. *Journal of Biochemical and Molecular Toxicology* 37(9): e23405.

Maeda, K., Kang, S.M., Sawada, T., Nishiguchi, Y., Yashiro, M., Ogawa, Y., Ohira, M., Ishikawa, T. & Chung, K.H.Y. 2002. Expression of intercellular adhesion molecule-1 and prognosis in colorectal cancer. *Oncology Reports* 9(3): 511-514.

Maheswaran, R., Shanmugavel, B.P. 2022. A Critical Review of the Role of Carbon Nanotubes in the Progress of Next-Generation Electronic Applications. *Journal of Electronic Materials* 51: 2786-2800.

Makaremi, S., Ganji, A., Ghazavi, A. & Mosayebi, G. 2021. Inhibition of tumor growth in CT-26 colorectal cancer-bearing mice with alcoholic extracts of Curcuma longa and Rosmarinus officinalis. *Gene Reports* 22: 101006.

Maleki Dizaj, S., Barzegar-Jalali, M., Zarrintan, M.H., Adibkia, K. & Lotfipour, F. 2015. Calcium carbonate nanoparticles as cancer drug delivery system. *Expert Opinion on Drug Delivery* 12(10): 1649–1660.

Malki, A., Elruz, R.A., Gupta, I., Allouch, A., Vranic, S. & Al Moustafa, A.E. 2020. Molecular Mechanisms of Colon Cancer Progression and Metastasis: Recent Insights and Advancements. *International Journal of Molecular Sciences* 22(1): 130.

Manabile, M.A., Hull, R., Khanyile, R., Molefi, T., Damane, B.P., Mongan, N.P., Bates, D.O. & Dlamini, Z. 2023. Alternative Splicing Events and Their Clinical Significance in Colorectal Cancer: Targeted Therapeutic Opportunities. *Cancers* 15(15): 3999.

Mao, R., Krautscheid, P., Graham, R. P., Ganguly, A., Shankar, S., Ferber, M., & Hegde, M. 2021. Genetic testing for inherited colorectal cancer and polyposis, 2021 revision: A technical standard of the American College of Medical Genetics and Genomics (ACMG). *Genetics in Medicine* 23(10): 1807-1817.

Meena, D., Vimala, K. & Kannan, S. 2022. Combined Delivery of DOX and Kaempferol using PEGylated Gold Nanoparticles to Target Colon Cancer. *Journal of Cluster Science* 33(1): 173-187.

Mehta, G., Hsiao, A.Y., Ingram, M., Luker, G.D. & Takayama, S. 2012. Opportunities and challenges for use of tumor spheroids as models to test drug delivery and efficacy. *Journal of Controlled Release* 164(2): 192-204.

Meyers, B.M., Cosby, R., Quereshy, F. & Jonker, D. 2017. Adjuvant Chemotherapy for Stage II and III Colon Cancer Following Complete Resection: A Cancer Care Ontario Systematic Review. *Clinical Oncology* 29(7): 459-465.

Miguel, T. P., Laurienzo, C. E., Faria, E. F., Sarri, A. J., Castro, I. Q., Affonso Júnior, R. J., Andrade, C., & Vieira, A. 2020. Chemoradiation for cervical cancer treatment portends high risk of pelvic floor dysfunction. *PLoS ONE* 15(6): e0234389.

Milczarek, M., Mielczarek, L., Lubelska, K., Dąbrowska, A., Chilmonczyk, Z., Matosiuk, D. & Wiktorska, K. 2018. In vitro evaluation of sulforaphane and a natural analog as potent inducers of 5-fluorouracil anticancer activity. *Molecules* 23(11): 3040.

Minkowicz, L., Dagan, A., Uvarov, V. & Benny, O. 2021. Controlling calcium carbonate particle morphology, size, and molecular order using silicate. *Materials* 14(13): 3525.

Mishra, B. & Chaurasia, S. 2017. Design of novel chemotherapeutic delivery systems for colon cancer therapy based on oral polymeric nanoparticles. *Therapeutic Delivery* 8(1): 29-47.

Mo, R. & Gu, Z. 2016. Tumor microenvironment and intracellular signal-activated nanomaterials for anticancer drug delivery. *Materials Today* 19(5): 274-283.

Mokhtari, R.B., Homayouni, T.S., Baluch, N., Morgatskaya, E., Kumar, S., Das, B. & Yeger, H. 2017. Combination therapy in combating cancer. *Oncotarget* 8(23): 38022-38043.

Mukhopadhyay, S., Veroniaina, H., Chimombe, T., Han, L., Zhenghong, W. & Xiaole, Q. 2019. Synthesis and compatibility evaluation of versatile mesoporous silica nanoparticles with red blood cells: an overview. *RSC Advances* 9(61): 35566-35578.

Naeem, M., Awan, U.A., Subhan, F., Cao, J., Hlaing, S.P., Lee, J., Im, E., Jung, Y. & Yoo, J.W. 2020. Advances in colon-targeted nano-drug delivery systems: challenges and solutions. *Archives of Pharmacal Research* 43(1): 153-169.

Nath, S. & Devi, G.R. 2016. Three-dimensional culture systems in cancer research: Focus on tumor spheroid model. *Pharmacology & Therapeutics* 163: 94-108.

National Cancer Institute. 2020. Drugs Approved for Colon and Rectal Cancer. https://www.cancer.gov/about-cancer/treatment/drugs/colorectal [3 May 2022].

Newman, A.C. & Maddocks, O.D.K. 2017. One-carbon metabolism in cancer. *British Journal of Cancer* 116(12): 1499-1504.

Nikolova, M.P. & Chavali, M.S. 2020. Metal oxide nanoparticles as biomedical materials. *Biomimetics* 5(2): 27.

Niroumand, U., Firouzabadi, N., Goshtasbi, G., Hassani, B., & Ghasemiyeh, P. 2023. The effect of size, morphology and surface properties of mesoporous silica nanoparticles on pharmacokinetic aspects and potential toxicity concerns. *Frontiers in Materials* 10: 1189463.

Ntungwe N, E., Domínguez-Martín, E. M., Roberto, A., Tavares, J., Isca, V. M. S., Pereira, P., Cebola, M.-J., & Rijo, P. 2020. Artemia species: An Important Tool to Screen General Toxicity Samples. *Current Pharmaceutical Design* 26(24): 2892-2908.

O'Brien, J., Hayder, H., Zayed, Y. & Peng, C. 2018. Overview of microRNA biogenesis, mechanisms of actions, and circulation. *Frontiers in endocrinology* 9: 402.

O'Keefe, S.J.D. 2016. Diet, microorganisms and their metabolites, and colon cancer. *Nature Reviews Gastroenterology and Hepatology* 13(12): 691-706.

Opattova, A., Horak, J., Vodenkova, S., Kostovcikova, K., Cumova, A., Macinga, P., Galanova, N., Rejhova, A., Vodickova, L., Kozics, K., Turnovcova, K., Hucl, T., Sliva, D. & Vodicka, P. 2019. Ganoderma Lucidum induces oxidative DNA damage and enhances the effect of 5-Fluorouracil in colorectal cancer in vitro and in vivo. *Mutation Research/Genetic Toxicology and Environmental Mutagenesis* 845: 403065.

Pai, R.K. & Pillai, S. 2008. Nanoparticles of amorphous calcium carbonate by miniemulsion: Synthesis and mechanism. *CrystEngComm* 10(7): 865-872.

Pan, G., Jia, T. ting, Huang, Q. xia, Qiu, Y. yan, Xu, J., Yin, P. hao & Liu, T. 2017. Mesoporous silica nanoparticles (MSNs)-based organic/inorganic hybrid nanocarriers loading 5-Fluorouracil for the treatment of colon cancer with improved anticancer efficacy. *Colloids and Surfaces B: Biointerfaces* 159: 375-385.

Pan, Y. B., Maeda, Y., Wilson, A., Glynne-Jones, R., & Vaizey, C. J. 2018. Late gastrointestinal toxicity after radiotherapy for anal cancer: a systematic literature review. *Acta Oncologica* 57(11): 1427-1437.

Park, G., Song, N.Y., Kim, D.H., Lee, S.J. & Chun, K.S. 2021. Thymoquinone suppresses migration of human renal carcinoma caki-1 cells through inhibition of the pge2-mediated activation of the ep2 receptor pathway. *Biomolecules and Therapeutics* 29(1): 64.

Patriarca, E.J., Cermola, F., D'Aniello, C., Fico, A., Guardiola, O., De Cesare, D. & Minchiotti, G. 2021. The Multifaceted Roles of Proline in Cell Behavior. *Frontiers in cell and developmental biology* 9: 728576.

Pavitra, E., Dariya, B., Srivani, G., Kang, S.M., Alam, A., Sudhir, P.R., Kamal, M.A., Raju, G.S.R., Han, Y.K., Lakkakula, B.V.K.S., Nagaraju, G.P. & Huh, Y.S. 2021. Engineered nanoparticles for imaging and drug delivery in colorectal cancer. *Seminars in Cancer Biology* 69: 293-306.

Perez-Potti, A., Rodríguez-Pérez, M., Polo, E., Pelaz, B. & del Pino, P. 2023. Nanoparticle-based immunotherapeutics: From the properties of nanocores to the differential effects of administration routes. *Advanced drug delivery reviews* 197: 114829.

Persano, F., Nobile, C., Piccirillo, C., Gigli, G. & Leporatti, S. 2022. Monodisperse and Nanometric-Sized Calcium Carbonate Particles Synthesis Optimization. *Nanomaterials* 12(9): 1494.

Phua, C.Y.H., Teoh, Z.L., Goh, B.H., Yap, W.H. & Tang, Y.Q. 2021. Triangulating the pharmacological properties of thymoquinone in regulating reactive oxygen species, inflammation, and cancer: Therapeutic applications and mechanistic pathways. *Life Sciences* 287: 120120.

Pinheiro, S.K.D.P., Lima, A.K.M., Miguel, T.B.A.R., Filho, A.G.S., Ferreira, O.P., Pontes, M.D.S., Grillo, R. & Miguel, E.D.C. 2023. Assessing toxicity mechanism of silver nanoparticles by using brine shrimp (Artemia salina) as model. *Chemosphere* 347: 140673.

Piotrowska, M., Swierczynski, M., Fichna, J. & Piechota-Polanczyk, A. 2021. The Nrf2 in the pathophysiology of the intestine: Molecular mechanisms and therapeutic implications for inflammatory bowel diseases. *Pharmacological Research* 163: 105243.

Popova, V., Poletaeva, Y., Pyshnaya, I., Pyshnyi, D. & Dmitrienko, E. 2021. Designing pH-dependent systems based on nanoscale calcium carbonate for the delivery of an antitumor drug. *Nanomaterials* 11(11): 2794.

Rajabi, S., Ramazani, A., Hamidi, M. & Naji, T. 2015. Artemia salina as a model organism in toxicity assessment of nanoparticles. *DARU: Journal of Pharmaceutical Sciences* 23(1): 20.

Rathore, C., Upadhyay, N., Kaundal, R., Dwivedi, R.P., Rahatekar, S., John, A., Dua, K., Tambuwala, M.M., Jain, S., Chaudari, D. & Negi, P. 2020. Enhanced oral bioavailability and hepatoprotective activity of thymoquinone in the form of phospholipidic nano-constructs. *Expert Opinion on Drug Delivery* 17(2): 237-253.

Redondo-Blanco, S., Fernández, J., Gutiérrez-del-Río, I., Villar, C.J. & Lombó, F. 2017. New insights toward colorectal cancer chemotherapy using natural bioactive compounds. *Frontiers in Pharmacology* 8: 109.

Rejhová, A., Opattová, A., Čumová, A., Slíva, D. & Vodička, P. 2018. Natural compounds and combination therapy in colorectal cancer treatment. *European Journal of Medicinal Chemistry* 144: 582-594.

Render, D., Samuel, T., King, H., Vig, M., Jeelani, S., Babu, R.J. & Rangari, V. 2016. Biomaterial-Derived Calcium Carbonate Nanoparticles for Enteric Drug Delivery. *Journal of Nanomaterials* 2016: 3170248.

Rosenblum, D., Joshi, N., Tao, W., Karp, J.M. & Peer, D. 2018. Progress and challenges towards targeted delivery of cancer therapeutics. *Nature Communications* 9(1): 1-12.

Sæbø, I.P., Bjørås, M., Franzyk, H., Helgesen, E. & Booth, J.A. 2023. Optimization of the Hemolysis Assay for the Assessment of Cytotoxicity. *International Journal of Molecular Sciences* 24(3): 2914.

Saeidnia, S., Manayi, A. & Abdollahi, M. 2016. From in vitro Experiments to in vivo and Clinical Studies; Pros and Cons. *Current Drug Discovery Technologies* 12(4): 218-224.

Safavi, M.S., Shojaosadati, S.A., Dorkoosh, F.A., Jo, H.J., Kwon, Y., Lee, K.C., Yang, H.G., Park, E.J. & Na, D.H. 2017. The synthesis of tamoxifen-loaded albumin nanoparticles by homogenizers: Optimization and in vitro characterization. *Journal of Drug Delivery Science and Technology* 41: 20-30.

Sahu, T., Ratre, Y.K., Chauhan, S., Bhaskar, L.V.K.S., Nair, M.P. & Verma, H.K. 2021. Nanotechnology based drug delivery system: Current strategies and emerging therapeutic potential for medical science. *Journal of Drug Delivery Science and Technology* 63: 102487.

Said, A.H., Raufman, J.P. & Xie, G. 2014. The Role of Matrix Metalloproteinases in Colorectal Cancer. *Cancers 2014, Vol. 6, Pages 366-375* 6(1): 366-375.

Saito, R. de F., Andrade, L.N. de S., Bustos, S.O. & Chammas, R. 2022. Phosphatidylcholine-Derived Lipid Mediators: The Crosstalk Between Cancer Cells and Immune Cells. *Frontiers in immunology* 13: 768606.

Salmani, J.M.M., Asghar, S., Lv, H. & Zhou, J. 2014. Aqueous solubility and degradation kinetics of the phytochemical anticancer thymoquinone; probing the effects of solvents, pH and light. *Molecules* 19(5): 5925-5939.

Santandreu, F.M., Valle, A., Oliver, J. & Roca, P. 2011. Resveratrol potentiates the cytotoxic oxidative stress induced by chemotherapy in human colon cancer cells. *Cellular Physiology and Biochemistry* 28(2): 219-228.

Sargheini, J., Ataie, A., Salili, S.M. & Hoseinion, A.A. 2012. One-step facile synthesis of CaCO3 nanoparticles via mechano-chemical route. *Powder Technology* 219: 72-77.

Sato, K., Masuda, T., Hu, Q., Tobo, T., Kidogami, S., Ogawa, Y., Saito, T., Nambara, S., Komatsu, H., Hirata, H., Sakimura, S., Uchi, R., Hayashi, N., Iguchi, T., Eguchi, H., Ito, S., Nakagawa, T. & Mimori, K. 2017. Phosphoserine phosphatase is a novel prognostic biomarker on chromosome 7 in colorectal cancer. *Anticancer Research* 37(5): 2365-2371.

Schmidt, D.R., Patel, R., Kirsch, D.G., Lewis, C.A., Vander Heiden, M.G. & Locasale, J.W. 2021. Metabolomics in cancer research and emerging applications in clinical oncology. *CA: A Cancer Journal for Clinicians* 71(4): 333-358.

Schwarz, D.S. & Blower, M.D. 2016. The endoplasmic reticulum: Structure, function and response to cellular signaling. *Cellular and molecular life sciences* 73(1): 79-94.

Senapati, S., Mahanta, A.K., Kumar, S. & Maiti, P. 2018. Controlled drug delivery vehicles for cancer treatment and their performance. *Signal Transduction and Targeted Therapy* 3(1): 7.

Sethy, C., & Kundu, C. N. 2021. 5-Fluorouracil (5-FU) resistance and the new strategy to enhance the sensitivity against cancer: Implication of DNA repair inhibition. *Biomedicine & Pharmacotherapy* 137: 111285.

Sette, C. & Paronetto, M.P. 2022. Somatic Mutations in Core Spliceosome Components Promote Tumorigenesis and Generate an Exploitable Vulnerability in Human Cancer. *Cancers* 14(7): 1827.

Ševčík, R., Pérez-Estébanez, M., Viani, A., Šašek, P. & Mácová, P. 2015. Characterization of vaterite synthesized at various temperatures and stirring velocities without use of additives. *Powder Technology* 284: 265-271.

Sharma, N., Madan, P. & Lin, S. 2016. Effect of process and formulation variables on the preparation of parenteral paclitaxel-loaded biodegradable polymeric nanoparticles: A co-surfactant study. *Asian Journal of Pharmaceutical Sciences* 11(3): 404-416.

Shi, H., Li, L., Zhang, L., Wang, T., Wang, C., Zhu, D. & Su, Z. 2015. Designed preparation of polyacrylic acid/calcium carbonate nanoparticles with high doxorubicin payload for liver cancer chemotherapy. *CrystEngComm* 17(26): 4768-4773.

Shi, J., Kantoff, P.W., Wooster, R. & Farokhzad, O.C. 2017. Cancer nanomedicine: Progress, challenges and opportunities. *Nature reviews. Cancer* 17(1): 20-37.

Sivanand, S. & Vander Heiden, M.G. 2020. Emerging Roles for Branched-Chain Amino Acid Metabolism in Cancer. *Cancer cell* 37(2): 147-156.

Solmonson, A. & DeBerardinis, R.J. 2018. Lipoic acid metabolism and mitochondrial redox regulation. *The Journal of biological chemistry* 293(20): 7522-7530.

Srivastava, P., Hira, S.K., Srivastava, D.N., Gupta, U., Sen, P., Singh, R.A. & Manna, P.P. 2017. Protease-Responsive Targeted Delivery of Doxorubicin from Bilirubin-BSA-Capped Mesoporous Silica Nanoparticles against Colon Cancer. *ACS Biomaterials Science and Engineering* 3(12): 3376-3385.

Stephanos, J.J. & Addison, A.W. 2017. Vibrational Rotational Spectroscopy. *Electrons, Atoms, and Molecules in Inorganic Chemistry*: 505-584.

Sulaiman, G.M., Waheeb, H.M., Jabir, M.S., Khazaal, S.H., Dewir, Y.H. & Naidoo, Y. 2020. Hesperidin Loaded on Gold Nanoparticles as a Drug Delivery System for a Successful Biocompatible, Anti-Cancer, Anti-Inflammatory and Phagocytosis Inducer Model. *Scientific Reports* 10(1): 1-16.

Sun, L., Chen, Y., Zhou, Y., Guo, D., Fan, Y., Guo, F., Zheng, Y. & Chen, W. 2017. Preparation of 5-fluorouracil-loaded chitosan nanoparticles and study of the sustained release in vitro and in vivo. *Asian Journal of Pharmaceutical Sciences* 12(5): 418-423.

Sung, Y., Yoon, I., Han, J.M. & Kim, S. 2022. Functional and pathologic association of aminoacyl-tRNA synthetases with cancer. *Experimental & molecular medicine* 54(5): 553-566.

Tadano, T., Zhu, R., Muroga, Y., Hoshi, T., Sasaki, D., Yano, S. & Sawaguchi, T. 2014. A new mechanism for the silica nanoparticle dispersion-agglomeration transition in a poly (methyl methacrylate)/silica hybrid suspension. *Polymer Journal* 46(6): 342-348.

Taha, M.M.E., Sheikh, B.Y., Salim, L.Z.A., Mohan, S., Khan, A., Kamalidehghan, B., Ahmadipour, F. & Abdelwahab, S.I. 2016. Thymoquinone induces apoptosis and increase ROS in ovarian cancer cell line. *Cellular and Molecular Biology* 62(6): 97-101.

Tang, J., Lam, G. T., Brooks, R. D., Miles, M., Useckaite, Z., Johnson, I. R., Ung, B. S. Y., Martini, C., Karageorgos, L., Hickey, S. M., Selemidis, S., Hopkins, A. M., Rowland, A., Vather, R., O'Leary, J. J., Brooks, D. A., Caruso, M. C., & Logan, J. M. 2024. Exploring the role of sporadic BRAF and KRAS mutations during colorectal cancer pathogenesis: A spotlight on the contribution of the endosome-lysosome system. *Cancer Letters* 585: 216639.

Tang, Z., Yuan, S., Hu, Y., Zhang, H., Wu, W., Zeng, Z., Yang, J., Yun, J., Xu, R. & Huang, P. 2012. Over-expression of GAPDH in human colorectal carcinoma as a preferred target of 3-bromopyruvate propyl ester. *Journal of Bioenergetics and Biomembranes* 44(1): 117-125.

Testa, U., Pelosi, E., & Castelli, G. 2018. Colorectal Cancer: Genetic Abnormalities, Tumor Progression, Tumor Heterogeneity, Clonal Evolution and Tumor-Initiating Cells. *Medical Sciences* 6(2): 31.

Tiwari, A., Saraf, S., Jain, A., Panda, P.K., Verma, A. & Jain, S.K. 2020. Basics to advances in nanotherapy of colorectal cancer. *Drug Delivery and Translational Research* 10(2): 319-338.

Trushina, D.B., Borodina, T.N., Belyakov, S. & Antipina, M.N. 2022. Calcium carbonate vaterite particles for drug delivery: Advances and challenges. *Materials Today Advances* 14: 100214.

Vergaro, V., Pisano, I., Grisorio, R., Baldassarre, F., Mallamaci, R., Santoro, A., Suranna, G.P., Papadia, P., Fanizzi, F.P. & Ciccarella, G. 2019. CaCO3 as an environmentally friendly renewable material for drug delivery systems: Uptake of HSA-CaCO3 nanocrystals conjugates in cancer cell lines. *Materials* 12(9): 1481.

Vodenkova, S., Buchler, T., Cervena, K., Veskrnova, V., Vodicka, P. & Vymetalkova, V. 2020. 5-fluorouracil and other fluoropyrimidines in colorectal cancer: Past, present and future. *Pharmacology & Therapeutics* 206: 107447.

Wahab, S., Alshahrani, M.Y., Ahmad, M.F. & Abbas, H. 2021. Current trends and future perspectives of nanomedicine for the management of colon cancer. *European Journal of Pharmacology* 910: 174464.

Wang, F., Chen, L., Nie, M. & Li, Z. 2024. Integrative analysis of causal associations between neurodegenerative diseases and colorectal cancer. *Heliyon* 10(15): e35432.

Wang, J., Li, B., Qiu, L., Qiao, X. & Yang, H. 2022. Dendrimer-based drug delivery systems: history, challenges, and latest developments. *Journal of Biological Engineering* 16: 18.

Wang, J., Yu, X., Cao, X., Tan, L., Jia, B., Chen, R. & Li, J. 2023. GAPDH: A common housekeeping gene with an oncogenic role in pan-cancer. *Computational and Structural Biotechnology Journal* 21: 4056-4069.

Wang, N., Yang, L., Dai, J., Wu, Y., Zhang, R., Jia, X. & Liu, C. 2021a. 5-FU inhibits migration and invasion of CRC cells through PI3K/AKT pathway regulated by MARCH1. *Cell Biology International* 45(2): 368-381.

Wang, Q., Zhu, G., Lin, C., Lin, P., Chen, H., He, R., Huang, Y., Yang, S. & Ye, J. 2021b. Vimentin affects colorectal cancer proliferation, invasion, and migration via regulated by activator protein 1. *Journal of Cellular Physiology* 236(11): 7591-7604.

Wang, X., Ye, Y., Wu, X., Smyth, J.R., Yang, Y., Zhang, Z. & Wang, Z. 2019. High-temperature Raman and FTIR study of aragonite-group carbonates. *Physics and Chemistry of Minerals* 46(1): 51-62.

Wathoni, N., Nguyen, A.N., Rusdin, A., Umar, A.K., Mohammed, A.F.A., Motoyama, K., Joni, I.M. & Muchtaridi, M. 2020. Enteric-coated strategies in colorectal cancer nanoparticle drug delivery system. *Drug Design, Development and Therapy* 14: 4387-4405.

Wehrmeister, U., Soldati, A.L., Jacob, D.E., Häger, T. & Hofmeister, W. 2010. Raman spectroscopy of synthetic, geological and biological vaterite: A Raman spectroscopic study. *Journal of Raman Spectroscopy* 41(2): 193-201.

Weng, W. & Goel, A. 2022. Curcumin and colorectal cancer: An update and current perspective on this natural medicine. *Seminars in Cancer Biology* 80: 73-86.

Williamson, J.M. & Lyons, D.A. 2018. Myelin dynamics throughout life: An ever-changing landscape? *Frontiers in Cellular Neuroscience* 12: 424.

Wong, T.L., Che, N. & Ma, S. 2017. Reprogramming of central carbon metabolism in cancer stem cells. *Biochimica et biophysica acta-Molecular basis of disease* 1863(7): 1728-1738.

World Health Organization. 2024. The Global Cancer Observatory: Cancer Today. https://gco.iarc.who.int/media/globocan/factsheets/cancers/41-colorectum-fact-sheet.pdf [10 April 2024].

Wu, G.X., Ding, J. & Xue, J.M. 2008. Synthesis of calcium carbonate capsules in water-in-oil-in-water double emulsions. *Journal of Materials Research* 23(1): 140-149.

Xie, J., Wang, J., Chen, H., Shen, W., Sinko, P.J., Dong, H., Zhao, R., Lu, Y., Zhu, Y. & Jia, L. 2015. Multivalent Conjugation of Antibody to Dendrimers for the Enhanced Capture and Regulation on Colon Cancer Cells. *Scientific Reports* 5: 9445.

Xie, X., Li, Y., Lian, S., Lu, Y. & Jia, L. 2022. Cancer metastasis chemoprevention prevents circulating tumour cells from germination. *Signal Transduction and Targeted Therapy* 7(1): 341.

Xie, X., Mahmood, S.R., Gjorgjieva, T. & Percipalle, P. 2020. Emerging roles of cytoskeletal proteins in regulating gene expression and genome organization during differentiation. *Nucleus* 11(1): 53-65.

Xu, D., Jin, T., Song, L., Zhu, N., Han, L. & Hong, H. 2023a. Synthesis of stable calcium carbonate nanoparticles for pH-responsive controlled drug release. *Materials Letters* 333: 133635.

Xu, E., Ji, B., Jin, K. & Chen, Y. 2023b. Branched-chain amino acids catabolism and cancer progression: focus on therapeutic interventions. *Frontiers in oncology* 13: 1220638.

Xu, H., Jia, Z., Liu, F., Li, J., Huang, Y., Jiang, Y., Pu, P., Shang, T., Tang, P., Zhou, Y., Yang, Y., Su, J. & Liu, J. 2023c. Biomarkers and experimental models for cancer immunology investigation. *MedComm* 4(6): e437.

Yakubova, A.A., Mitusova, K.A., Darwish, A., Rogova, A., Ageev, E.I., Brodskaia, A., Muslimov, A.R., Zyuzin, M. V. & Timin, A.S. 2023. Calcium carbonate nanoparticles tumor delivery for combined chemo-photodynamic therapy: Comparison of local and systemic administration. *Journal of Controlled Release* 359: 400-414.

Yan, Y., Wang, R., Hu, Y., Sun, R., Song, T., Shi, X. & Yin, S. 2018. Stacking of doxorubicin on folic acid-targeted multiwalled carbon nanotubes for in vivo chemotherapy of tumors. *Drug Delivery* 25(1): 1607-1616.

Yang, A., Huang, Z., Zhu, Y., Han, Y. & Tong, Z. 2021. Preparation of nano-sized calcium carbonate in solution mixing process. *Journal of Crystal Growth* 571: 126247.

Yang, T., Wan, Z., Liu, Z., Li, H., Wang, H., Lu, N., Chen, Z., Mei, X. & Ren, X. 2016. In situ mineralization of anticancer drug into calcium carbonate monodisperse nanospheres and their pH-responsive release property. *Materials Science and Engineering C* 63: 384-392.

You, X., Tian, J., Zhang, H., Guo, Y., Yang, J., Zhu, C., Song, M., Wang, P., Liu, Z., Cancilla, J., Lu, W., Glorieux, C., Wen, S., Du, H., Huang, P. & Hu, Y. 2021. Loss of mitochondrial aconitase promotes colorectal cancer progression via SCD1-mediated lipid remodeling. *Molecular Metabolism* 48: 101203.

Yu, J., Wang, L., Xie, X., Yu, H., Xu, J., Ren, J., Zhu, W., Lei, Z. & Lv, L. 2023. Multifunctional Nanoparticles Codelivering Doxorubicin and Amorphous Calcium Carbonate Preloaded with Indocyanine Green for Enhanced Chemo-Photothermal Cancer Therapy. *International Journal of Nanomedicine* 18: 323-337.

Yuan, C., Parekh, H., Allegra, C., George, T.J. & Starr, J.S. 2019. 5-FU induced cardiotoxicity: Case series and review of the literature. *Cardio-Oncology* 5(1): 13.

Zhan, T., Rindtorff, N., & Boutros, M. 2017. Wnt signaling in cancer. *Oncogene* 36(11): 1461-1473.

Zhang, L., Bai, Y. & Yang, Y. 2016. Thymoquinone chemosensitizes colon cancer cells through inhibition of NF-κB. *Oncology Letters* 12(4): 2840-2845.

Zhang, W., Shi, Y., Oyang, L., Cui, S., Li, S., Li, J., Liu, L., Li, Y., Peng, M., Tan, S., Xia, L., Lin, J., Xu, X., Wu, N., Peng, Q., Tang, Y., Luo, X., Liao, Q., Jiang, X. & Zhou, Y. 2024. Endoplasmic reticulum stress–a key guardian in cancer. *Cell Death Discovery* 10(1): 343.

Zhang, Y., Qian, J., Gu, C. & Yang, Y. 2021. Alternative splicing and cancer: a systematic review. *Signal transduction and targeted therapy* 6(1): 78.

Zhao, Y., Bian, Y., Xiao, X., Liu, B., Ding, B., Cheng, Z., Ma, P. & Lin, J. 2022. Tumor Microenvironment-Responsive Cu/CaCO3-Based Nanoregulator for Mitochondrial Homeostasis Disruption-Enhanced Chemodynamic/Sonodynamic Therapy. *Small* 18(38): e2204047.

Zhao, Y., Zheng, Y., Zhu, Y., Ding, K., Zhou, M. & Liu, T. 2023. Co-delivery of gemcitabine and Triapine by calcium carbonate nanoparticles against chemoresistant pancreatic cancer. *International Journal of Pharmaceutics* 636: 122844.

Zheng, M., Mei, Z., Junaid, Md., Tania, M., Fu, J., Chen, H.-C. & Khan, Md.A. 2021. Synergistic Role of Thymoquinone on Anticancer Activity of 5-Fluorouracil in Triple Negative Breast Cancer Cells. *Anti-Cancer Agents in Medicinal Chemistry* 22(6): 1111-1118.

Zheng, T., Hou, D., Leng, W., Li, P. & Wei, W. 2023. Preparation, characterization, and formation mechanism of different biological calcium carbonate (CaCO3) induced by Bacillus mucilaginosus and Bacillus alcalophilus. *Journal of Nanoparticle Research* 25(9): 189.

Zhong, Z.F., Tan, W., Wang, S.P., Qiang, W.A. & Wang, Y.T. 2015. Anti-proliferative activity and cell cycle arrest induced by evodiamine on paclitaxel-sensitive and -resistant human ovarian cancer cells. *Scientific Reports* 5: 16415.

Zhou, F., Li, H., Liu, Y., Deng, H., Rong, J. & Zhao, J. 2023. Hyaluronan derivative decorated calcium carbonate nanoparticle as a potential platform for breast cancer synergistic therapy via blood coagulation and drug delivery. *Journal of Drug Delivery Science and Technology* 83: 104406.

Zhu, L., Cao, J., Chen, G., Xu, Y., Lu, J., Fang, F. & Chen, K. 2016a. Anti-tumor and immunomodulatory activities of an exopolysaccharide from Rhizopus nigricans on CT26 tumor-bearing mice. *International Immunopharmacology* 36: 218-224.

Zhu, W.Q., Wang, J., Guo, X.F., Liu, Z. & Dong, W.G. 2016b. Thymoquinone inhibits proliferation in gastric cancer via the STAT3 pathway in vivo and in vitro. *World Journal of Gastroenterology* 22(16): 4149-4159.

Zhu, Y., Wu, G., Yan, W., Zhan, H. & Sun, P. 2017. miR-146b-5p regulates cell growth, invasion, and metabolism by targeting PDHB in colorectal cancer. *American Journal of Cancer Research* 7(5): 1136-1150.

Zhuravlev, Y.N. & Atuchin, V. V. 2020. Comprehensive density functional theory studies of vibrational spectra of carbonates. *Nanomaterials* 10(11): 2275.

Zorrilla-Veloz, R.I., Stelzer, T. & López-Mejías, V. 2018. Measurement and Correlation of the Solubility of 5-Fluorouracil in Pure and Binary Solvents. *Journal of Chemical and Engineering Data* 63(10): 3809-3817.

BIODATA OF STUDENT

Xi Deng was born on May 27, 1995, in Fuling, Chongqing, China. In 2012, she was successfully admitted to the College of Sciences of Shanghai University, majoring in Mathematics and Applied Mathematics. In 2016, she graduated as an outstanding graduate of Shanghai University with a Bachelor of Science degree. In the same year, she went to the Faculty of Natural, Mathematical and Engineering Sciences of King's College London to pursue a Master of Science degree, majoring in Financial Mathematics, and graduated with distinction in 2017. In 2021, due to her long-term love for nutrition and medicine and in order to realize her academic pursuit, she chose to pursue a Doctor of Philosophy degree at the Institute of Bioscience of Universiti Putra Malaysia, with the support of her parents.

LIST OF PUBLICATIONS

Deng, X., Yang, Z., Han, M., Ismail, N., Esa, N. M., Abdull Razis, A. F., Abu Bakar, M. Z., & Chan, K. W. (2024). Comprehensive Insights into the Combinatorial Uses of Selected Phytochemicals in Colorectal Cancer Prevention and Treatment: Isothiocyanates, Quinones, Carotenoids, and Alkaloids. *Phytotherapy Research*, 39(1), 413-452.

Yang, Z., **Deng, X.**, Yang, Z., Han, M., Chan, K. W., Abdull Razis, A. F., Esa, N. M., Ho, K. L., & Abu Bakar, M. Z. (2024). Polygonum minus: A tropical medicinal herb with vast applications in food, agricultural, and medicinal fields. *Food Bioscience*, 60, 104511.